siam

3rd Annual Meeting of the Bulgarian Section of SIAM
December 22-23, 2008
Sofia

BGSIAM'08

PROCEEDINGS

HOSTED BY THE INSTITUTE OF MATHEMATICS AND INFORMATICS
BULGARIAN ACADEMY OF SCIENCES

3rd Annual Meeting of the Bulgarian Section of SIAM
December 22-23, 2008, Sofia

BGSIAM'08 Proceedings

ISSN: 1313-3357

Printed in Sofia, Bulgaria
Cover design: Boris Staikov
Printing and binding: Demetra Ltd.

PREFACE

The Bulgarian Section of SIAM (BGSIAM) was founded on January 18, 2007 and the accepted Rules of Procedure were officially approved by the SIAM Board of Trustees on July 15, 2007. The activities of BGSIAM follow the general objectives of SIAM, as established in its Certificate of Incorporation.

Realizing the importance of interdisciplinary collaboration and the role that applied mathematics plays in advancing science and technology in industry, we solicit the support of SIAM as the major international organization for Industrial and Applied Mathematics in order to promote the application of mathematics to science, engineering and technology in Republic of Bulgaria.

The 3rd Annual Meeting of BGSIAM (BGSIAM'08) was hosted by the Institute of Mathematics and Informatics, Bulgarian Academy of Sciences, Sofia. It took part on December 22 and 23, 2008. The conference support provided by SIAM is very highly appreciated.

During BGSIAM'08 conference a wide range of problems concerning recent achievements in the field of industrial and applied mathematics were presented and discussed. The meeting provided a forum for exchange of ideas between scientists, who develop and study mathematical methods and algorithms, and researchers, who apply them for solving real life problems.

More than 50 participants from four universities, three institutes of the Bulgarian Academy of Sciences and also from outside the traditional academic departments took part in BGSIAM'08. They represent most of the strongest Bulgarian research groups in the field of industrial and applied mathematics. The involvement of younger researchers was especially encouraged and we are glad to report that 8 from the presented 27 talks were given by Ph.D. students.

LIST OF INVITED LECTURES:

- LUDMIL ZIKATANOV
  Penn State, University Park, PA, USA
  DISCONTINUOUS GALERKIN METHODS AND PRECONDITIONING
- GEORGI POPOV
  University of Nantes, France
  INTEGRAL AND SPECTRAL GEOMETRY OF LIOUVILLE BILLIARD TABLES
- SVETLA NIKOVA
  Catholic University of Leuven, Belgium
  SECRET SHARING SCHEMES AND ERROR CORRECTING CODES

The present volume contains the scientific program of BGSIAM'08 (Part A), extended abstracts of the conference talks (Part B), and the list of participants (Part C). The extended abstracts are ordered alphabetically according to the family names of the first author.

Svetozar Margenov
Chair of BGSIAM Section

Stefka Dimova
Vice-Chair of BGSIAM Section

Angela Slavova
Secretary of BGSIAM Section

Sofia, February 2009

Table of Contents

Part A: Scientific program **1**

Part B: Extended abstracts **5**

Andrey Andreev, Milena Racheva
Non-Conforming Z-type FE for Fourth-Order Problems: Estimates and Application **7**

Roumen Anguelov
Dynamically Consistent Schemes for Epidemiological Models **11**

Gergana Bencheva
Towards Real-Time Data-Driven Computer Simulation of Blood Cells Production and Regulation **15**

Petia Boyanova, Svetozar Margenov
On AMLI Preconditioning of Graph-Laplacians: Properties of the Two-Level Method **19**

Paul Cristea, Valeri Mladenov, Georgi Tsenov, Rodica Tuduce
Prediction of Mycobacterium Tuberculosis (rpoB) Nucleotide Sequences by Using Neural Networks **23**

Ivan Dimov, Rayna Georgieva, Sofiya Ivanovska,
Tzvetan Ostromsky, Zahari Zlatev
Sensitivity Analysis of Air Pollution Models **28**

Rossitza Dodunekova
On Error Detection with Block Codes **32**

Stefka Fidanova, Krasimir Atanasov, Pencho Marinov
Intuitionistic Fuzzy Estimations of the Ant Colony Optimization **33**

Daniela Georgieva, Ivan Stefanov,
Michail Todorov, Stoytcho Yazadjiev
Numerical Investigation of Charged Black Holes in the Scalar-Tensor Theories of Gravity with Massive Scalar Field **37**

Vladimir Gerdjikov, Nikolay Kostov, Tihomir Valchev
Reductions and Soliton Solutions of Nonlinear Evolution Equations on Symmetric Spaces **41**

Ivan Hristov, Stefka Dimova
Dynamics of Multilayered Josephson Junctions **45**

Rossen Ivanov
Integrable Models for Shallow Water Waves **49**

Bosko Jovanovic, Miglena Koleva, Lubin Vulkov
Numerical Solution of Elliptic and Parabolic Problems on Disjoint Domains **53**

Natalia Kolkovska, Radomir Slavchov, Daniela Vasileva
On the Numerical Simulation of Surface Forces Acting on AFM Tip **57**

Milena Kostova, Valerij Djurov
Intelligent Approaches for Radiolocational Monitoring **61**

Nikola Kosturski, Svetozar Margenov, Yavor Vutov
Efficient Solution of μFEM Elasticity Problems in the Case of Almost Incompressible Materials **65**

Mladen Manev
Classification of (28,8,2,3) Superimposed Codes **69**

Svetla Nikova
Secret Sharing Schemes and Error Correcting Codes **71**

Georgi Popov, Peter Topalov
Integral and Spectral Geometry of Liouville Billiard Tables **75**

Angela Slavova, Victoria Ivanova
Travelling Waves in Newell-Whitehead Cellular Neural Networks Model **79**

Michail D. Todorov, Christo I. Christov
On the Solution of the System of ODEs Governing the Polarized Stationary Solutions of CNLSE **83**

Yavor Vutov
Scalability Tests of Two Parallel PCG Solvers on Blue Gene/P **87**

Part C: List of participants **91**

Part A

Scientific program

Monday, December 22	
09:00 - 10:50	**SESSION 1**
Chairman	S. Margenov
09:00 - 09:10	Opening
09:10 - 09:50	Invited Plenary Talk: G. Popov, P. Topalov *Integral and Spectral Geometry of Liouville Billiard Tables*
09:50 - 10:10	R. Anguelov, *Dynamically Consistent Schemes for Epidemiological Models*
10:10 - 10:30	O. Kounchev, *An Optimal Control in Elasticity Theory*
10:30 - 10:50	S. Fidanova, K. Atanasov, P. Marinov, *Intuitionistic Fuzzy Estimations of the Ant Colony Optimization*
Coffee Break	
11:10 - 12:30	**SESSION 2**
Chairman	G. Popov
11:10 - 11:30	A. Slavova, *Cellular Neural Networks' Model of Risk Management*
11:30 - 11:50	M. Kostova, V. Djurov, *Intelligent Approaches for Radiolacational Monitoring*
11:50 - 12:10	A. Slavova, V. Ivanova, *Traveling Waves in Newell-Whitehead Cellular Neural Network Model*
12:10 - 12:30	P. Cristea, V. Mladenov, G. Tsenov, R. Tuduce, *Prediction of Mycobacterium Tuberculosis (rpoB) Nucleotide Sequences by Using Neural Networks*
Lunch Break	
14:00 - 16:00	**SESSION 3**
Chairman	N. Kolkovska
14:00 - 14:40	Invited Plenary Talk: L. Zikatanov, *Discontinuous Galerkin Methods and Preconditioning*
14:40 - 15:00	A. Andreev, M. Racheva, *Non-Conforming Z-type FE for Fourth-Order Problems: Estimates and Application*
15:00 - 15:20	P. Boyanova, S. Margenov, *On AMLI Preconditioning of Graph-Laplacians: Properties of the Two-Level Method*
15:20 - 15:40	N. Kosturski, S. Margenov, Y. Vutov, *Efficient Solution of μ-FEM Elasticity Problems in the Case of Almost Incompressible Materials*
15:40 - 16:00	Y. Vutov, *Scalability Tests of Two Parallel PCG Solvers on Blue Gene/P*
Coffee Break	

Monday, December 22	
16:20 - 18:20	**SESSION 4**
Chairman	K. Georgiev
16:20 - 16:40	G. Nikolov, *Cubature Formulae for the Disk Using Radon Projections*
16:40 - 17:00	B. Jovanovic, M. Koleva, L. Vulkov, *Numerical Solution of Elliptic and Parabolic Problems on Disjoint Domains*
17:00 - 17:20	N. Kolkovska, R. Slavchev, D. Vasileva, *On the Numerical Simulation of Surface Forces Acting on AFM Tip*
17:20 - 17:40	I. Hristov, St. Dimova, *Dynamics of Multilayered Josephson Junctions*
17:40 - 18:00	I. Dimov, R. Georgieva, S. Ivanovska, Tz. Ostromsky, Z. Zlatev, *Sensitivity Analysis of Air Pollution Models*
18:00 - 18:20	G. Bencheva, *Towards Real-Time Data-Driven Computer Simulation of Blood Cells Production and Regulation*
RECEPTION	
Tuesday, December 23	
09:00 - 10:40	**SESSION 5**
Chairman	P. Boyvalenkov
09:00 - 09:40	Invited Plenary Talk: S. Nikova *Secret Sharing Schemes and Error Correcting Codes*
09:40 - 10:00	R. Dodunekova, *On Error Detection with Block Codes*
10:00 - 10:20	I. Landjev, *Codes and Geometries Over Finite Rings*
10:20 - 10:40	M. Manev, *Classification of (28,8,2,3) Superimposed Codes*
Coffee Break	
11:00 - 12:20	**SESSION 6**
Chairman	S. Dimova
11:00 - 11:20	V. Gerdjikov, N. Kostov, T. Valchev, *Reductions and Soliton Solutions of Nonlinear Evolution Equations on Symmetric Spaces*
11:20 - 11:40	R. Ivanov, *Integrable Models for Shallow Water Waves*
11:40 - 12:00	M. Todorov, Ch. Christov, *On the Solution of the System of ODEs Governing the Polarized Stationary Solutions of CNLSE*
12:00 - 12:20	D. Georgieva, I. Stefanov, M. Todorov, S. Yazadjiev, *Numerical Investigation of Charged Black Holes in the Scalar-Tensor Theories of Gravity with Massive Scalar Field*
CLOSING	

Part B

Extended abstracts*

*Arranged alphabetically according to the family name of the first author.

Non-Conforming Z-type FE for Fourth-Order Problems: Estimates and Application

Andrey Andreev, Milena Racheva

We present a new convergence analysis of Zienkiewicz-type (Z-type) non-conforming triangular finite element applied to the fourth-order partial differential equations.
Let Ω be a bounded polygonal domain in $\mathbf{R}^2$ with boundary $\partial\Omega$. Let also $H^m(\Omega)$ be the usual $m-$th order Sobolev space on Ω with a norm $\|\cdot\|_{m,\Omega}$ and a seminorm $|\cdot|_{m,\Omega}$ and $(\cdot,\cdot)$ denote the $L_2(\Omega)-$inner product.
Consider the following fourth-order model problem for $f \in L_2(\Omega)$:

$$\begin{aligned} &\Delta^2 u = f \qquad \text{in } \Omega, \\ &u = \frac{\partial u}{\partial \nu} = 0 \quad \text{on } \partial\Omega, \end{aligned} \tag{1}$$

where $\nu = (\nu_1, \nu_2)$ is the unit outer normal to $\partial\Omega$ and Δ is the standard Laplacian operator.
The weak form of the problem (1) is: find $u \in H_0^2(\Omega)$ such that

$$a(u,v) = (f,v), \quad \forall\ v \in H_0^2(\Omega), \tag{2}$$

where

$$a(u,v) = \int_\Omega \sum_{i,j=1}^{2} \partial_{ij}^2 u\ \partial_{ij}^2 v\, dx \quad \forall\ u, v \in H^2(\Omega).$$

Let τ_h be family of regular finite element partitions of Ω which fulfill standard assumptions. The partitions τ_h consist of triangles K and h is mesh parameter. We can define the finite element space V_h by means of Z-type elements which will be introduced.

The corresponding approximate variational problem of (2) is: find $u_h \in V_h \subset H_0^2(\Omega)$ such that

$$a(u_h, v_h) = (f, v_h), \quad \forall\ v_h \in V_h. \tag{3}$$

As it is well-known, the Zienkiewicz triangle represents a reduced cubic Hermite finite element (see [1, 2]) for which:

- K is a 2-simplex with vertices $a_i,\ 1 \le i \le 3$;
- one possible set of degrees of freedom is (for any test function p):

$$p(a_i),\ 1 \le i \le 3 \ \text{ and } \ Dp(a_i)(a_j - a_i),\ 1 \le i, j \le 3,\ i \ne j.$$

- $P_K \subset P_3(K)$ and $\dim P_K = 9$ (fig. 1).

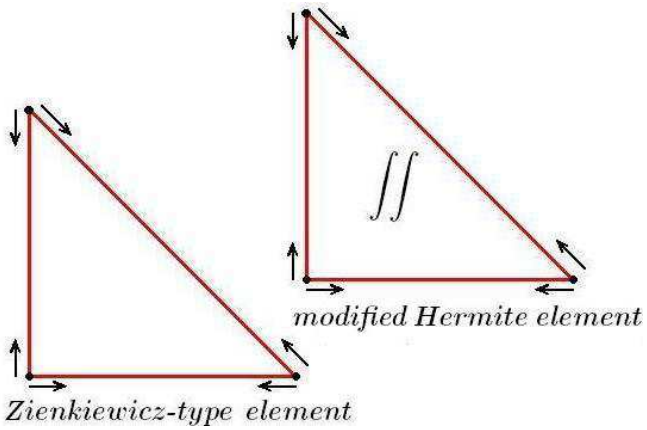

Figure 1:

Some Z-type triangular elements having the same degrees of freedom can be proposed by means of different ways (see, e.q. [2]).
The following properties of Z-type element could be mentioned: *(i)* it is an incomplete and non-conforming C^0-element for fourth-order problems; *(ii)* it uses the degrees of freedom just the same with the Zienkiewicz triangle, but its shape function space is different; *(iii)* it takes values of function and its derivatives at vertices as degrees of freedom and by this the global number of degrees of freedom is an optimal one; *(iv)* it is convergent (applied to 4-order problems) in contrast to Zienkiewicz triangle, which is only convergent in parallel line condition and divergent in general grids.
For any 2-simplex K we define

$$P(K) = P_2(K) + \text{span}\left\{\lambda_i^2\lambda_j - \lambda_i\lambda_j^2,\ 1 \le i < j \le 3\right\},$$

where $\lambda_i,\ i = 1, 2, 3$ are the barycentric coordinates of K. Then we can define the shape function space by $P_3'(K)$.

Lemma 1. *([2], Lemma 1) The set of degrees of freedom is P_K-unisolvent.*

In order to get convergence analysis of the considered element we also consider the Hermite triangle with a suitably modified 10-th degree of freedom, namely, integral value on K is taken instead of the value at the barycenter of K (fig. 1).
Let Π_K denote the interpolation operator corresponding to Z-type finite element partition τ_h and π_h be the interpolation operator related to modified Hermite finite element. Our convergence analysis is based on the estimation of $\Pi_h v - \pi_h v$ for any $v \in H_0^2$ on each element $K \in \tau_h$ [3].
The calculations use the shape functions for both elements and are accomplished on the reference element $(t_1, t_2) \in K = \{t_1, t_2 \ge 0,\ t_1 + t_2 \le 1\}$:

$$\Pi_h v - \pi_h = 60 t_1 t_2 (1 - t_1 - t_2) E_K(v) \le \frac{20}{9}\ E_K(v),$$

where

$$E_K(v) = \left[\frac{1}{3} \sum_{i=1}^{3} v(a_i) - \frac{1}{24} \sum_{\substack{i,j=1 \\ i \neq j}}^{3} Dv(a_i)(a_i - a_j) - \frac{1}{\text{meas}(K)} \int \int_K v \, dt_1 \, dt_2 \right]$$

is error functional of quadrature formula and $E_K(v) = 0$ for $v \in P_2(K)$.
The last estimate is the crutial point of the main result:

Theorem 1. *Let V_h be the finite element space corresponding to nonconforming Z-type element. Then there exists a constant $C = C(\Omega) > 0$, independent of h and such that*

$$\inf_{v_h \in V_h} \sum_{m=0}^{2} h^m |v - v_h|_{m,\Omega} \leq Ch^3 \|v\|_{3,\Omega}, \quad \forall v \in H_0^2(\Omega).$$

Then we can prove the following result:

Theorem 2. *Let $u \in H^3(\Omega) \cap H_0^2(\Omega)$ and $u_h \in V_h$ be the solutions of the problems (2) and (3), respectively. Then there exists a constant $C = C(\Omega) > 0$, independent of h and such that*

$$\|u - u_h\|_{2,\Omega} \leq Ch \|u\|_{3,\Omega}.$$

We apply the previous consideration to the corresponding fourth-order eigenvalue problem. Consider a thin elastic plate corresponding to a bounded domain $\Omega \in \mathbf{R}^2$. If the material is homogeneous and isotropic, the question about the possible small vibrations of the plate leads to the basic eigenvalue equation:

$$\Delta^2 w = \lambda w \quad \text{in } \Omega, \tag{4}$$

subject to some boundary conditions.
The variational EVP takes the form

$$a(w, v) = \lambda(w, v), \quad \forall v \in V \subset H_0^2(\Omega).$$

The finite dimensional analogue of the problem (4) by means of Z-type non-conforming elements is (see [5]):

$$a_h(w_h, v_h) = \lambda_h(w_h, v_h), \quad \forall v_h \in V_h.$$

It is to be noted here that the sesquilinear form a_h is uniformly elliptic:

$$\alpha \|\Delta u\|_{0,\Omega}^2 \leq a_h(u, u), \quad \forall u \in H^2(\Omega).$$

Theorem 3. *Assume the conditions of Theorem 2 are satisfied.*
Then $\lambda_h^{(k)} \longrightarrow \lambda^{(k)}$ $(h \to 0)$, $k = 1, \ldots, N_h$ and for any sequence of normalized eigenfunctions $w_h^{(k)} \in V_h$, $\|w_h^{(k)}\| = 1$, there exist eigenfunctions $w \in H_0^2(\Omega)$ such that

$$\|w_h^{(k)} - w\|_{2,\Omega} \longrightarrow 0 \quad (h \to 0).$$

Moreover, if $w \in H^3(\Omega) \cap H_0^2(\Omega)$*, then*

$$\|w_h^{(k)} - w\|_{2,\Omega} \leq Ch\|w\|_{3,\Omega},$$

$$|\lambda_h^{(k)} - \lambda| \leq Ch^2\|w\|_{3,\Omega}^2.$$

Acknowledgements. This work is partly supported by the Bulgarian NSF Grants VU-MI 202/2006 and DO02-147/2008.

References

[1] Bazaley, G.P., Cheung, Y.K., Irons, B.M., Ziemkiewicz, O.C.: Triangular Elements in Plate Bending - Conforming and Non-conforming Solutions. Proceedings of the Conference on Matrix Methods in Structural Mechanics, Wright Patterson A.F. Base, Ohio, pp. 547-576 (1965)

[2] Wang, M., Shi, Z., Xu, J.: A New Class of Zienkiewicz-type Non-conforming Element in Any Dimensions. Numer. Math. 106 (2007), pp. 335-347

[3] Andreev, A.B., Racheva, M.R.: Optimal Order FEM for a Coupled Eigenvalue Problem on 2-D Overlapping Domains. LNCS, Springer (to appear)

[4] Babuska I., J. Osborn: Eigenvalue Problems. Handbook of Numer. Anal., Vol. II, North-Holland, Amsterdam 1991

[5] Rannacher, R.: Non-conforming Finite Element Methods for Eigenvalue Problems in Linear Plate Theory. Numer. Math. 33 (1979), pp. 23-42

Dynamically Consistent Schemes for Epidemiological Models

Roumen Anguelov

The paper deals with the construction of numerical schemes that faithfully replicate the behavior of dynamical systems modeling the spread of disease. The alignment of the properties of the dynamical system and its numerical discretization is characterized in terms of "topological dynamic consistency" introduced in [2] and described below.

Let $D \subseteq \mathbb{R}^d$, $d \geq 1$ be a given domain and let us assume that the system of differential equations

$$\frac{dy}{dt} = f(y), \quad y(0) = x, \tag{1}$$

where $x \in D$ and $f \in C^0(D, D)$, defines a (positive) dynamical system on D. This means that for every $x \in D$ problem (1) has a unique solution $y = y(x,t) \in D$ for all $t \in [0, \infty)$. For a given $t \in (0, \infty)$, the mapping $S(t) : D \to D$ given by $S(t)(x) \to y(x,t)$ is called the *evolution operator*, and the set

$$\{S(t) : t \in (0, \infty)\} \tag{2}$$

is the well-known *evolution semi-group*. To simplify the matters, we assume here that the maps $S(t)$, $t > 0$, are all topologically equivalent to each other. This is for example the case of Morse-Smale flows with fixed points only. In this respect let us recall that two maps $p : X \to X$ and $q : Y \to Y$, where X and Y are topological spaces, are called *topologically equivalent* if there exists a homeomorphism $\mu : X \to Y$ such that $p \circ \mu = \mu \circ q$.

Suppose that the solution of (1) is approximated on the time grid $\{t_k = kh : k = 0, 1, ...\}$ by a difference equation of the form

$$y_{k+1} = F(h)(y_k) \ , \quad y_0 = x \ , \tag{3}$$

where the maps $F(h) : D \to D$ are defined for every $h > 0$. Hence, for every $h > 0$, the difference equation in (3) defines a discrete dynamical system.

Definition The difference scheme (3) is called *topologically dynamically consistent* with the dynamical system (1), whenever for every $h > 0$ the map $F(h)$ is topologically equivalent to the maps in the set (2). (Thus, the maps $S(t)$ and $F(h)$ are topologically the same for every $t > 0$ and $h > 0$).

The concept of structural stability describes maps $f : X \to X$, which remain essentially the same under small perturbations in the sense that the perturbed map is topologically equivalent to the original one. The underlying function space is typically considered to be $C^r(X, X)$, where often $r = 1$. In practical applications this space may be determined not only by the differentiability of the maps but also by conditions intrinsic to the model. Hence, we formulate the definition of structural stability in the following more general form.

Definition Let $\mathcal{V}$ be a topological space of maps from X to X. A map $f \in \mathcal{V}$ is called $\mathcal{V}$ structurally stable if there exists a neighborhood U of f in the topology of $\mathcal{V}$ such that every map $g \in U$ is topologically equivalent to f.

The notion of structural stability is used for the construction of topologically dynamically consistent schemes in the following way

1. Identify all unstable "features" of the maps $S(t)$, $t > 0$, e.g. nonhyperbolic fixed points, fixed points on the boundary, orbits connecting saddle points, orbits on the boundary, etc. The list needs to be complete so that if these features are removed, all maps $S(t)$ are C^1 structurally stable.

2. Consider the space $\mathcal{V}$ of all maps in $C^1(D, D)$ which have the same unstable features. Then the maps $S(t)$, $t > 0$, are $\mathcal{V}$ structurally stable.

3. Construct a numerical method of the form (3) such that $F(h) \in \mathcal{V}$ and the map $F(h)$ is $\mathcal{V}$ structurally stable for all $h > 0$.

As a model example we consider the classic SIR model, [3], for the spread of disease,

$$\begin{aligned} \frac{ds}{dt} &= b(1-s) - \beta is + \delta r, \\ \frac{di}{dt} &= \beta is - \gamma i - bi, \\ \frac{dr}{dt} &= \gamma i - \delta r - br, \end{aligned} \tag{4}$$

where s is the fraction of susceptibles in the total population, i is the fraction of the infectives and r is the fraction of the recovered. It is easy to see that the system of differential equations (4) defines a (positive) dynamical system on the two-dimensional manifold $M = \{(s, i, r) : s + i + r = 1,\ s \geq 0,\ i \geq 0,\ r \geq 0\}$. Eliminating s we obtain the system (4) in an equivalent form of two equations

$$\begin{aligned} \frac{di}{dt} &= \beta i(1-i-r) - \gamma i - bi, \\ \frac{dr}{dt} &= \gamma i - \delta r - br. \end{aligned} \tag{5}$$

Now, (5) defines a dynamical system on $D = \{(i, r) : i \geq 0\,, r \geq 0\,, i + r \leq 1\}$.
The point $(0, 0)$ is always an equilibrium of (5) and respectively $(1, 0, 0)$ is always an equilibrium of (4). This is the Disease Free Equilibrium (DFE). The system may have another equilibrium, namely,

$$\left(\frac{\delta + b}{\gamma + \delta + b} \left(1 - \frac{1}{\sigma} \right), \frac{\gamma}{\gamma + \delta + b} \left(1 - \frac{1}{\sigma} \right) \right), \tag{6}$$

where $\sigma = \frac{\beta}{\gamma + b}$ is the basic reproduction number. Our concern here are the properties of the dynamical system. The point in (6) is an equilibrium of the dynamical

system whenever it belongs to its domain D, that is, when $\sigma > 1$. It is called an Endemic Equilibrium (EE) since it describes a permanent presence of the disease. Using standard techniques one can establish the following properties:

- The orbit of $(1, 0)$ is always the line segment connecting it to DFE. Denote this line by Γ_1 and the rest of the boundary of D by Γ_2.
- If $\sigma \leq 1$ then DFE is globally asymptotically stable on D.
- If $\sigma > 1$ then EE is stable and attracting with basin of attraction $D \setminus \Gamma_1$ and DFE is a hyperbolic saddle point with Γ_1 being its stable manifold.

It is easy to see that the maps $S(t)$ for the model (5) are not C^1 structurally stable due to the fact that it has a fixed point and an orbit on the boundary of the domain D. However, the maps $S(t)$ are $\mathcal{V}$ structurally stable, where

$$\mathcal{V} = \left\{ g : D \to D : \left| \begin{array}{l} 1)\ g : D \to g(D) \text{ is a diffeomorphism} \\ 2)\ \text{DFE is a fixed point of } g \\ 3)\ \Gamma_1 \text{ is invariant and in the stable manifold of DFE} \end{array} \right. \right\}$$

Now we need to construct a difference scheme of the form (3) with an operator $F(h)$ which is structurally stable with respect to the same space $\mathcal{V}$. To this end we apply the non-standard finite difference method. The following scheme, which uses nonlocal approximation of the nonlinear term, is crafted in such a way that the operator $F(h)$ is $\mathcal{V}$ structurally stable.

$$\begin{array}{rcl} \dfrac{i^{n+1} - i^n}{h} & = & (\beta - b - \beta i^{n+1} - \beta r^{n+1}) i^n - \gamma i^{n+1}, \\ \dfrac{r^{n+1} - r^n}{h} & = & \gamma i^{n+1} - (\delta + b) r^{n+1}. \end{array} \tag{7}$$

Then, as indicated earlier, the topological dynamic consistency of the scheme follows. The numerical results in the figures below are obtained with $\beta = 1$, $b = 0$ and varying values of the parameters γ and δ and the time step size h. Note that $\sigma = \frac{1}{\gamma}$. Figures 1, 2 and 3 represent numerical solutions by the nonstandard method (7). As an indication of what can go wrong if the dynamic consistency is not taken into account the simulation with data as in Figure 3 is repeated by using the second order Runge-Kutta method and the computed solution is given in Figure 4.

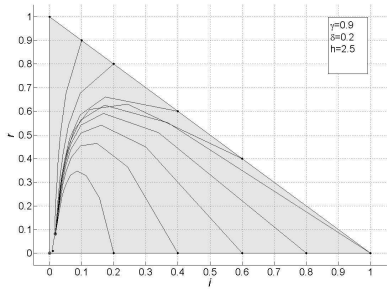

Fig. 1

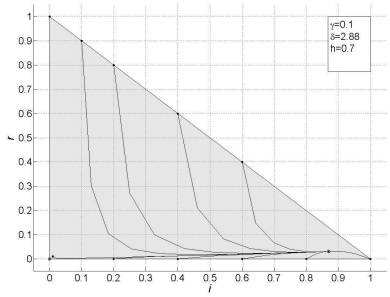

Fig. 2

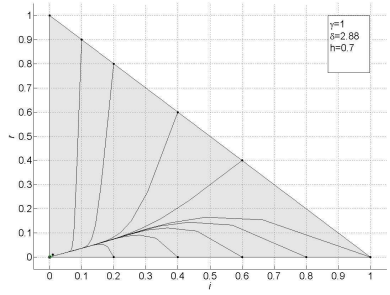

Fig. 3

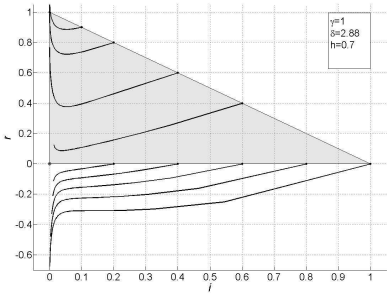

Fig. 4

References

[1] R. Anguelov, J.M-S. Lubuma, Nonstandard finite difference method by nonlocal approximation, *Mathematics and Computers in Simulation* **61**(3-6) (2003), 465–475.

[2] R. Anguelov, J.M.-S. Lubuma and M. Shillor, Dynamically consistent nonstandard finite difference schemes for continuous dynamical systems, AIMS Proceedings Series, to appear (see also University of Pretoria Technical Report UPWT 2008/05).

[3] H.W. Hethcote, The mathematics of infectious disease, *SIAM Rev.* **42** (2000), 599–653.

[4] A. Katok, B. Hasselblatt, *Introduction to the Modern Theory of Dynamical Systems*, Cambridge University Press, New York, 1995.

[5] R.E. Mickens (Ed.), *Applications of Nonstandard Finite Difference Schemes*, World Scientific, Singapore, 2000.

Towards Real-Time Data-Driven Computer Simulation of Blood Cells Production and Regulation

Gergana Bencheva

Motivation. The blood cells (BCs) are produced and regulated during a complex biological process, called *haematopoiesis*. Mature BCs evolve from haematopoietic pluripotent stem cells (HSCs) after a sequence of complex differentiations in the bone marrow. This is possible due to the high self-renewal and differentiation capacity of the HSCs. Each type of BCs is a result of the action of specific proteins, known as *Growth Factors* or *Colony Stimulating Factors* (CSF), at specific moments during the haematopoiesis process. BCs that have not yet matured are called *blast cells*. Simplified diagram of the differentiation stages in haematopoiesis and the main growth

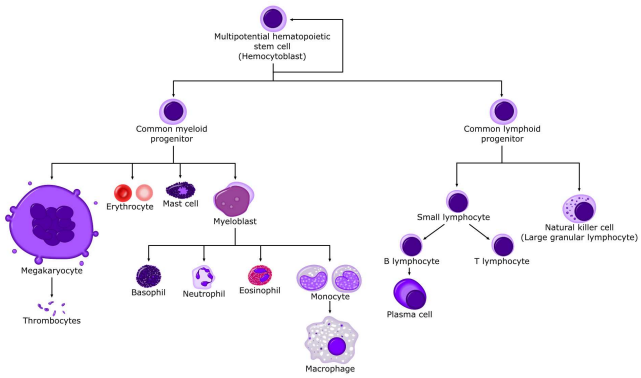

BC type	Vital function	Growth factors
Erythrocyte	Transport oxygen	Erythropoietin
Leukocyte	Fight infections	Granulocyte-CSF, Macrophage-CSF, Granulocyte-Macrophage-CSF, Interleukins
Thrombocyte	Control bleeding	Thrombopoietin

Figure 1: Differentiation stages and growth factors in haematopoiesis.

factors responsible for each of the BC types are shown in Figure 1.
Need for computer simulation. The BCs perform various vital functions like transporting oxygen to tissues, fighting infections and controlling bleeding. Various haematological diseases are characterized by abnormal production of particular BCs (either matured or blast). For example, acute leukaemia occurs when the blast cells replicate themselves uncontrollably and interfere with the production and activity of normal BCs. If undiscovered or left untreated, it can cause death within few weeks or months. The approach "trial-error" is not recommended for dealing with questions related to understanding and predicting of human physiological processes in health and disease.

The computer modelling is especially useful in such cases and gives possibility to: a) understand better the BCs production and regulation processes; b) design nature experiments for validation of hypotheses; c) predict the effect of various treatment options for patients with specific haematological diseases. The current step towards real-time data-driven computer simulation of haematopoiesis aims at tuning of software parameters and comparison of the obtained results with those presented in [1].
Delay differential equations (DDEs) provide an important way of describing the time evolution of biological systems whose rate of change also depends on their configuration at previous time instances. DDEs take part in the mathematical model of CSF mediated haematopoiesis which is proposed in [1] and used in the current investigations. In the bone marrow, HSCs are divided into two groups: proliferating cells and nonproliferating (or quiescent) cells. Their populations at time t are denoted by $P(t) \geq 0$ and $Q(t) \geq 0$ respectively. The population of the circulating mature BCs is denoted by $M(t) \geq 0$ and the growth factor concentration is $E(t) \geq 0$. The following system of stiff nonlinear ordinary DDEs have to be solved

$$\left\{ \begin{array}{rcl} \dfrac{dQ}{dt} & = & -\delta Q(t) - g(Q(t)) - \beta(Q(t), E(t))Q(t) \\ & & +2e^{-\gamma\tau}\beta(Q(t-\tau), E(t-\tau))Q(t-\tau) \\ \dfrac{dM}{dt} & = & -\mu M(t) + g(Q(t)) \\ \dfrac{dE}{dt} & = & -kE(t) + f(M(t)) \end{array} \right. \tag{1}$$

with appropriate initial conditions for $t \in [-\tau, 0]$. The delay τ corresponds to the proliferating phase duration, which is assumed to be constant. The rates at which the proliferating and quiescent cells can die are represented in (1) by the parameters γ and δ respectively. The degradation rates μ and k of the mature BCs and of CSF in the blood are assumed to be positive. Quiescent cells can either be introduced in the proliferating phase with a rate $\beta(Q(t), E(t))$ or differentiate in mature BCs with a rate $g(Q(t))$. The negative feedback control $f(M(t))$ of the bone marrow production on the CSF production acts by the mean of circulating mature BCs: the more circulating BCs are, the less growth factor is produced.
The trivial steady-state of (1) is not a biologically interesting equilibrium since it describes a pathological situation that can only lead to death without appropriate treatment. The existence of nontrivial positive steady-state is ensured (see [1] for details) by the conditions:

$$0 < \delta + g'(0) < \beta\left(0, \frac{f(0)}{k}\right),\ 0 \leq \tau < \tau_{max} := \frac{1}{\gamma}\ln\left(\frac{2\beta\left(0, \frac{f(0)}{k}\right)}{\delta + g'(0) + \beta\left(0, \frac{f(0)}{k}\right)}\right) \tag{2}$$

Computer simulation. Runge-Kutta methods are widely used for numerical solution of systems of ordinary differential equations (see e.g. [3]). Efficient codes for both stiff and non-stiff problems have been developed and made freely available in Internet. Two of them are *DOPRI5*, implementing Dormand and Prince method of

order 5 for non-stiff problems, and *RADAU5*, implementing Runge-Kutta method based on Radau quadrature formula for stiff problems (both downloadable from [4]). When dealing with delays, a special attention should be focused on the so called breaking points (or primary discontinuities), at which the solution possesses only a limited number of derivatives, and remains piecewise regular between two consecutive such points. Locating the breaking points and including them into the mesh is a crucial issue on the numerical integration of DDEs, because any step-by-step method attains its own order of accuracy provided that the solution sought is sufficiently smooth in the current integration interval. The codes *RETARD* and *RADAR5* are modifications of *DOPRI5* and *RADAU5* for the case of DDEs, where the issues of breaking points are taken into account. More information regarding the numerical solution of DDEs can be found e.g. in [2] and references therein.
In the current work, the software parameters of *RETARD* and *RADAR5* are tuned in order to solve (1). It is done with the help of the test data for erythropoiesis presented in [1], where the numerical results are obtained using *dde23*, a Matlab solver for DDEs written by Shampine and Thompson [5].
The coefficient functions for normalized initial conditions $E_0 = 0.5$, $Q_0 = 2$, $M_0 = 5$ and the values of the parameters involved in the model are taken as follows (τ_{max} is computed from (2) with the presented data):

Function		Parameter	Value	Range (day^{-1})
$\beta(E) = \beta_0 \dfrac{E}{1+E}$,	$\beta_0 > 0$	δ	0.01 day^{-1}	0 – 0.09
		G	0.04 day^{-1}	0 – 0.09
$g(Q) = GQ$,	$G > 0$	β_0	0.5 day^{-1}	0.08 – 2.24
		γ	0.2 day^{-1}	0 – 0.9
		μ	0.02 day^{-1}	0.001 – 0.1
$f(M) = \dfrac{a}{1+KM^r}$,	$a, K, r > 0$	k	2.8 day^{-1}	—
		a	6570	—
$\tau \in [0, \tau_{max}), \tau_{max} = 2.99\, days$		K	0.0382	—
		r	7	—

In this case the system is not stiff and the solvers *RETARD*, *RADAR5* and *dde23* produce one and the same results. The obtained solution for three values of the delay τ is presented in Figure 2. The Hopf bifurcation for $\tau = 1.4$ is the reason for the periodic solutions in the second case.
Further steps towards real-time data-driven computer simulation of haematopoiesis include calibration of the model and software tools for: a) leukocytes (each of the 7 types) and thrombocytes on the base of model data, e.g. taken from papers and experiments *in vitro*; b) each of the three BC types on the base of real data from clinical practice, i.e. on the base of patient specific data taken *in vivo*. They require identification of parameters and sensitivity analysis as intermediate steps.

Acknowledgements. This work is partly supported by the Bulgarian NSF Grant DO02-214/2008.

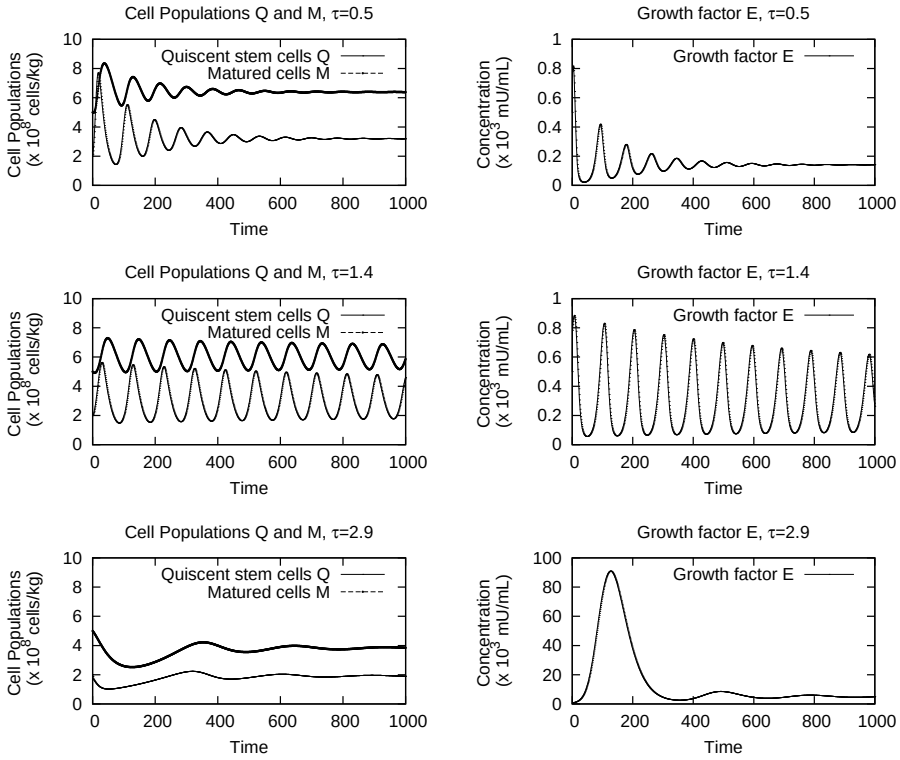

Figure 2: Solution of (1) for three values of the delay $\tau = 0.5, 1.4, 2.9$.

References

[1] M. Adimy, F. Crauste, S. Ruan, Modelling Hematopoiesis Mediated by Growth Factors with Applications to Periodic Hematological Diseases, Bulletin of Mathematical Biology, 68 (8), (2006), 2321-2351.

[2] A. Bellen, N. Guglielmi, S. Maset, Numerical methods for delay models in biomathematics, In: A. Quarteroni, L. Formaggia, A. Veneziani (Eds.) Complex Systems in Biomedicine, Springer-Verlag Italia, Milano 2006, 147-185.

[3] E. Hairer, (S.P. Norsett), G. Wanner, Solving ordinary differential equations I, II, Springer Ser. in Comp. Math., Springer, 2000 (part I), 2002 (part II)

[4] `http://www.unige.ch/~hairer/software.html`

[5] `http://www.radford.edu/$\sim$thompson/webddes/`

On AMLI Preconditioning of Graph-Laplacians: Properties of the Two-Level Method

Petia Boyanova, Svetozar Margenov

We consider a second-order elliptic problem in mixed form that has to be solved as a part of a projection algorithm for unsteady Navier-Stokes equations. The use of Crouzeix-Raviart non-conforming elements for the velocities and piece-wise constants for the pressure provides a locally mass-conservative algorithm (see e.g. [2] and the references therein). Then, the Crouzeix-Raviart mass matrix is diagonal, and the velocity unknowns can be eliminated exactly. The reduced matrix for the pressure is referred to as weighted graph-Laplacian. For a 2-D model problem and uniform mesh of right triangles it corresponds to the T-shaped four point stencil shown in Fig. 1.

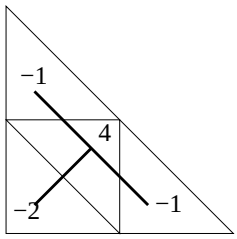

Figure 1: Schur complement four point stencil for the pressure

We study the construction of optimal order preconditioners based on algebraic multilevel iterations (AMLI). The framework for this method was originally proposed in [1]. AMLI is recursive generalization of two-level preconditioners that has optimal behavior due to a proper Schur complement stabilization using Chebyshev polynomials. Regarding a hierarchical 2x2 block partitioning of the system matrix $A^{(k)}$ at level k

$$\widehat{A}^{(k)} = J^{(k)} A^{(k)} {J^{(k)}}^T = \begin{bmatrix} \widehat{A}_{11}^{(k)} & \widehat{A}_{12}^{(k)} \\ \widehat{A}_{21}^{(k)} & \widehat{A}_{22}^{(k)} \end{bmatrix} \begin{matrix} \}\text{degrees of freedom added by refinement} \\ \}\text{coarse mesh degrees of freedom} \end{matrix}$$

the AMLI method is defined as follows: $C^{(0)} = A^{(0)}$ at the coarsest mesh level with index 0;

$$C^{(k)} = {J^{(k)}}^{-1} \begin{bmatrix} \widehat{C}_{11}^{(k)} & 0 \\ \widehat{A}_{21}^{(k)} & \tilde{A}^{(k-1)} \end{bmatrix} \begin{bmatrix} I & {\widehat{C}_{11}^{(k)}}^{-1} \widehat{A}_{12}^{(k)} \\ 0 & I \end{bmatrix} {J^{(k)}}^{-T}$$

at successively refined levels k, where $\widehat{C}_{11}^{(k)}$ are symmetric positive definite approximations of $\widehat{A}_{11}^{(k)}$ that satisfy $\mathbf{v}^t \widehat{A}_{11}^{(k)} \mathbf{v} \le \mathbf{v}^t \widehat{C}_{11}^{(k)} \mathbf{v} \le (1+b) \mathbf{v}^t \widehat{A}_{11}^{(k)} \mathbf{v}$, and $\tilde{A}^{(k-1)^{-1}} = \left[I - p_\beta \left({C^{(k-1)}}^{-1} A^{(k-1)} \right) \right] {A^{(k-1)}}^{-1}$.

The efficiency of the AMLI preconditioner depends on two things. First, the properties of the two-level partitioning that is characterized by the constant γ in the strengthened Cauchy-Bunyakowski-Schwarz (CBS) inequality. Second, the approximations used for solving systems with the pivot blocks.
We define the hierarchical two-level transformations and corresponding 2x2 splittings locally for macroelements associated with the edges of the coarse triangulation. The local restriction of the global transformation matrix for a macroelement with node numbering shown in Fig. 2

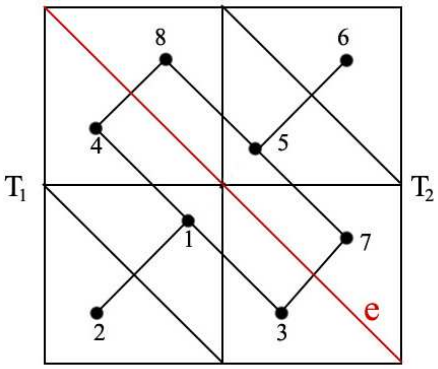

Figure 2: Macroelement of two adjacent coarse triangles with a common hypotenuse

is defined as:

$$J_e = \begin{bmatrix} 1 & p & q & q & & & & \\ 1 & q & p & q & & & & \\ 1 & q & q & p & & & & \\ & & & & 1 & p & q & q \\ & & & & 1 & q & p & q \\ & & & & 1 & q & q & p \\ r & r & r & r & & & & \\ & & & & r & r & r & r \end{bmatrix},$$

where p, q are parameters, and each refined mesh is obtained by dividing the current coarse triangles in four congruent ones by connecting the midpoints of the sides. As shown in [4] this two-level hierarchical partitioning complies with the conditions of the main theorem in AMLI theory (see [1]) when $r = \sqrt{2}/2$. The estimates for the CBS constant: $\gamma^2 \leq 0.73$ for $p = 1$, $q = -0.5$, and $\gamma^2 \leq 0.58$ for $p = 1$, $q = -0.1$, are derived there too.

Table 1: Two-level method, no pivot approximation: number of PCG iterations

	PCG stop criteria	Number of degrees of freedom				
		128	512	2048	8192	32768
$p = 1$,	$\epsilon = 10^{-3}$	4	4	4	4	4
	$\epsilon = 10^{-6}$	7	8	7	8	8
$q = -0.5$	$\epsilon = 10^{-9}$	10	11	11	12	12
$p = 1$,	$\epsilon = 10^{-3}$	4	4	4	4	4
	$\epsilon = 10^{-6}$	6	7	7	7	7
$q = -0.1$	$\epsilon = 10^{-9}$	9	10	10	10	10

Table 2: Two-level method, simple diagonal pivot approximation: PCG iterations

	PCG stop criteria	Number of degrees of freedom				
		128	512	2048	8192	32768
$p = 1$,	$\epsilon = 10^{-3}$	10	10	10	10	10
	$\epsilon = 10^{-6}$	20	21	21	21	21
$q = -0.5$	$\epsilon = 10^{-9}$	30	31	31	31	32
$p = 1$,	$\epsilon = 10^{-3}$	12	12	12	12	12
	$\epsilon = 10^{-6}$	24	24	25	25	24
$q = -0.1$	$\epsilon = 10^{-9}$	35	36	37	37	37

Numerical results for the preconditioned conjugate gradient (PCG) number of iterations for the two-level method with the two considered parameter sets are presented in Table 1. They let us conclude that the proposed hierarchical splitting defines a proper two-level preconditioner. The convergence rate behaves as theoretically expected – it does not depend on the number of unknowns but changes proportionally when different stop criteria are applied. In Table 2 we present results for a two-level method with a simple diagonal pivot block approximation – the computationally less expensive case with respect to solving systems with $\widehat{C}_{11}^{(k)}$. The number of iterations increases substantially but the behaviour is still the same.

The nodes corresponding to the pivot block in the hierarchical splitting can be associated with the edges of the current coarse triangle. This means that an edge has two related nodes. The macroelement pivot block is a dense matrix. There are two things to take in consideration when defining $\widehat{C}_{11}^{(k)}$ – the relative condition number $\kappa(\widehat{C}_{11}^{-1}\widehat{A}_{11})$ and the computational cost for solving systems with $\widehat{C}_{11}^{(k)}$. One approach for approximating $\widehat{A}_{11}$ is to preserve the links along lines with dominating anisotropy. The corresponding pivot block preconditioner connectivity is shown in Fig. 3. The local analysis for an approximation based on this idea leads to the following estimates: $\kappa(\widehat{C}_{11}^{-1}\widehat{A}_{11}) \leq 13.2$ for $p = 1$, $q = -0.5$, and $\kappa(\widehat{C}_{11}^{-1}\widehat{A}_{11}) \leq 46.6$ for $p = 1$, $q = -0.1$. These results, together with those in Table 1 and 2, imply that the hierarchical splitting parameters p and q have substantial influence both on γ and the pivot block

conditioning and should be tuned carefully.

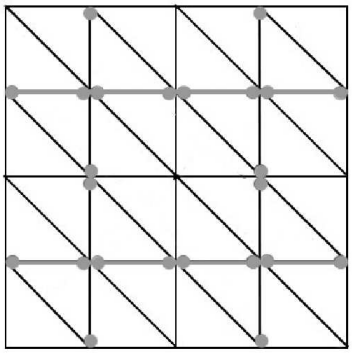

Figure 3: Pivot block preconditioner connectivity

Acknowledgements. This work is partly supported by the Bulgarian NSF Grant DO02-147/2008.

References

[1] O. Axelsson and P.S. Vassilevski, Algebraic multilevel preconditioning methods II, *SIAM J. Numer. Anal.*, 27 (1990), 1569-1590.

[2] B. Bejanov, J. Guermond and P. Minev, A locally *div*-free projection scheme for incompressible flows based on non-conforming finite elements, Int. J. Numer. Meth. Fluids, **49**, 2005, 239-258.

[3] R. Lazarov and S. Margenov, CBS constants for multilevel splitting of graph-Laplacian and application to preconditioning of discontinuous Galerkin systems, *J. Complexity*, **23(4-6)** (2007), 498-515.

[4] P. T. Boyanova and S. D. Margenov, Multilevel Splitting of Weighted Graph-Laplacian Arising in Non-conforming Mixed FEM Elliptic Problems, NAA 2008, LNCS 5434, pp. 216-223, 2009.

Prediction of Mycobacterium Tuberculosis (rpoB) Nucleotide Sequences by Using Neural Networks

Paul Cristea, Valeri Mladenov, Georgi Tsenov, Rodica Tuduce

1 Introduction and background

The conversion of nucleotide sequences into digital signals (GS) [3,6] offers the possibility to apply signal processing methods for the analysis of genomic data. Genomic Signal Analysis (GSA) has been used to analyze large scale features of DNA sequences, at the scale of whole chromosomes, including both coding and non-coding regions. The striking regularities of genomic signals reveal restrictions in the way nucleotides and pairs of nucleotides are distributed along nucleotide sequences. This methodology reveals surprising regularities, both locally and at a global scale [1,3]. Such regularities would be difficult to identify by using only statistical analysis and pattern matching, as currently done for symbolic sequences. The approach is useful for studying large scale features of chromosomes [11,12,16], detect mutations in small and medium genomes such as those of pathogens [2,7,8,9,10], detect exogenous inserts [5] and model some of ribosome functionalities [5,14].
The regularities in the distribution of nucleotides and pairs of nucleotides, reflected in the low values and predictable variation of the nucleotide imbalance (cumulated phase) and nucleotide pair imbalance (unwrapped phase) [3], show that a genome has a multi-level ordered structure. Mutations, such as those in pathogen genomes, tend to mutually compensate, so that overall regularities of the GS are conserved. A consequence of this statistical regularity is that SNPs appear often in correlated groups, sometimes placed at large distances along a nucleotide sequence [9]. The regularity of genomic signals allows using techniques similar to time series prediction [15,17] to estimate the nucleotides in a sequence, when knowing the preceding ones [4,6]. Such experiments have a biologic significance, as they explore the possibility and the theoretic efficiency of error correction in processes like replication, transcription and translation. The paper analyzes the rpoB gene of Mycobacterium tuberculosis by using Feed Forward Neural Network (FFNN), Radial Basis Functions Neural Network (RBFNN) and Elman Neural Network (Elman NN) for prediction of the samples in the structure.

2 Nucleotide representation

As detailed earlier [3] and presented here for convenience, the mapping we are using for nucleotide representation is a one-to-one representation which attaches complex numbers to adenine, cytosine, guanine and thymine nucleotides:

$$A = 1 + j, C = -1 - j, G = -1 + j, T = 1 - j \tag{1}$$

This mapping is unbiased, i.e., introduces no artifacts related to specific assumptions on the types of interaction that characterize the nucleotides. Classes of nucleotides can also be represented in this way, as illustrated in Table 1. The distribution of nucleotides along a sequence is described by the nucleotide imbalance:

$$N = 3(n_G - n_C) + (n_A - n_T) \tag{2}$$

where n_A, n_C, n_G and n_T are the numbers of adenine, cytosine, guanine and thymine nucleotides in the sequence, from the first to the current entry. The distribution of nucleotide pairs is given by the nucleotide pair imbalance:

$$P = n_+ - n_- \tag{3}$$

where n_+ is the number of positive pairs ($A \to G$, $G \to C$, $C \to T$, $T \to A$), and n_- the number of negative pairs ($A \to T$, $T \to C$, $C \to G$, $G \to A$).

TABLE 1: THE DATA SET MAPPING USED FOR DATA PRESENTATION

Class	IUPAC symbol	Complex representation
Adenine	A	[1,1]
Guanine	G	[1,-1]
Cytosine	C	[-1,-1]
Thymine	T	[-1,1]
Week bond	W	[1,0]
Purines	R	[0,1]
Strong bond	S	[-1,0]
Pyrimidines	Y	[0,-1]

3 Mycrobacterium tyrbeculosis and prediction of nucleotide sequences with neural networks.

Mycobacterium tuberculosis is the pathogen that causes tuberculosis. The genome of the H37Rv strain was published in 1998. It's size is about 4 million base pairs, with 3959 genes. 40% of these genes have had their function characterised, with possible function postulated for another 44%. Within the genome there are also 6 pseudogenes. The geneome contains 250 genes involved in fatty acid metabolism, with 39 of these involved in the polyketide metabolism generating the waxy coat. Such large numbers of conserved genes shows the evolutionary importance of the waxy coat to pathogen survival. As shown in [6], the prediction of nucleotide sequences, in a way similar to time series prediction, is also a theoretical investigation of the possibility to use the redundancy in the genomic sequences to correct errors at the level of a ribosome. Similar questions can be formulated about the DNA replication or the transcription to mRNA.

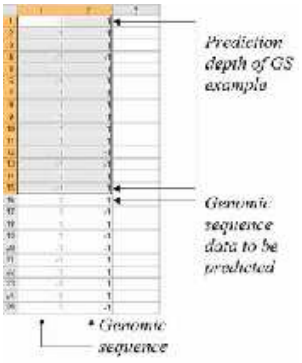

Figure1. Example of digital genomic sequence.

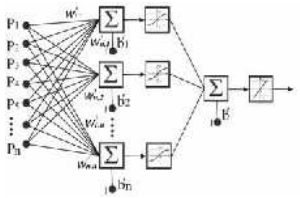

Figure2. The FFNN structure used for time-series prediction.

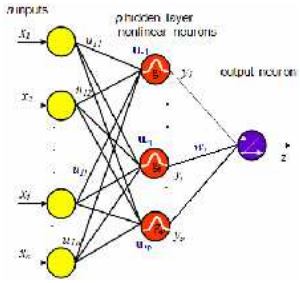

Figure3. The RBNN structure used for time-series prediction.

Data sequenced in 2006 and 2007 for 40 patients with multiple drug resistance have been used. The data structure is shown in Figure2, where the first column is the real and the second column is the imaginary part of the genomic sequence. The set of data was divided in two parts -half for training the ANN's and the second to test their performance (successful prediction rate). To avoid contradictions and conceptual difficulties, the model uses only the information from previous nucleotides (15 in Figure 1). The possible fractional values at the output of the neural network are rounded to integer values. The first ANN we used was a feed-forward neural network (FFNN) with the number of input neurons equalling the prediction depth, one hidden-layer with a number of neurons given by the Oja's rule formula and one output neuron, as shown in Figure 2. The second ANN was a radial basis neural network (RBNN) as the one in Figure 3. The third ANN is a Elman neural network (ELNN) as the one shown in Figure 4. For this ANN the number of the neurons in the hidden layer was determined as for the FFNN by Oja's rule of thumb.

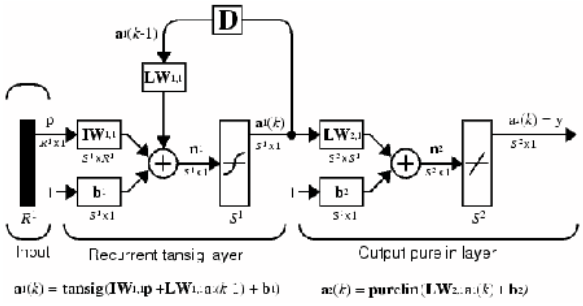

Figure4. The ELNN structure used for time-series prediction

We found (Figure 5) that the prediction rate can reach 90%, compared to 25% for the random case. The optimal length of the prediction depth, that gives maximal prediction rates turned out to be in the 9 to 11 interval.

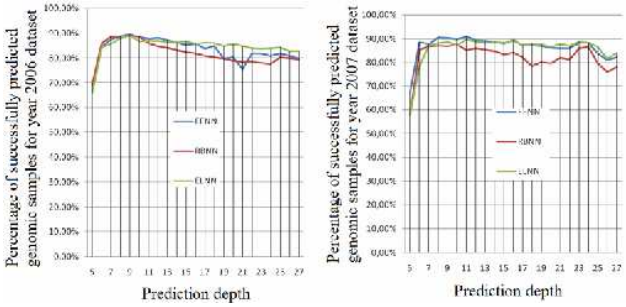

Figure5. The successful prediction rate for different length of the prediction depth

Acknowledgement The work was supported in part by grants from the Ministry of Education and Research of Romania, the CEEX Program contract 50/2005 and CNC-SIS 963-5/2007, the Ministry of Education and Science of Bulgaria, in the framework of the bilateral Scientific, Technological and Innovative Co-operation with Romania - project -08, University "Politehnica" of Bucharest and by the Franqui Research Project ADSI 133 / 2007, ETRO.

References

[1] E.Chargaff, Structure and function of nucleic acids as cell constituents, Fed. Proc., 10, 1951, pp. 654-659.

[2] S.T.Cole, R.Brosch, J.Parkhill, et al., Deciphering the biology of Mycobacterium tuberculosis from the complete genome sequence, Nature, 393 (6685) , 1998, p. 537-544.

[3] P.D.Cristea,Chapter 1, Representation and analysis of DNA sequences, in Genomic Signal Processing and Statistics, E.Daugherty, I. Shmulevich, J. Chen and Z.J. Wang, Eds., EURASIP Book Series on Signal Proc. and Comm., Hindawi Publ. Corp., 2005, pp. 15-65.

[4] P.D.Cristea, V.Mladenov, R.A.Tuduce, G.Tsenov, S.Petrakieva, Prediction of Nucleotide Sequences by using Genomic Signals, NN'08 - 9th WSEAS International Conference on Neural Networks, Sofia, Bulgaria, May 2-4, 2008, pp.107-112.

[5] P.D.Cristea, R.A.Tuduce, Analysis of inserts in prokaryote genomes, Proc. of SPIE, 6859-47, San Jose, CA, USA, January 21-23, 2008, pp. 108.

[6] P.D.Cristea, Rodica Tuduce, I. Nastac, J. Cornelis, R. Deklerck, M. Andrei, Signal Representation and Processing of Nucleotide Sequences, Proc. of IEEE BIBE, Boston, MA, 2007, pp.1214-1219.

[7] P.D.Cristea, Genomic Signal Analysis of Mycobacterium tuberculosis, Proc. of SPIE, vol. 6447, 2007, pp. C-1 - C8.

[8] P.D.Cristea, Pathogen Variability. A Genomic Signal Approach, International Journal of Computers, Communications and Control Vol. I (3), 2006, pp. 25-32.

[9] P.D.Cristea, Genomic Signal Analysis of Pathogen Variability, Progress in Biomedical Optics and Imaging, Proc. of SPIE, vol. 6088, 2006, pp. P1-P12.

[10] P.D.Cristea, R.A.Tuduce, D. Otelea, Study of HIV Variability based on Genomic Signal Analysis of Protease and Reverse Transcriptase Genes, Proc.2005 IEEE EMB, 27th Ann. Conf., Shanghai, China, 2005.

[11] P.D.Cristea,Genomic Signals of Re-Oriented ORFs, EURASIP - Journal on Applied Signal Processing, Special Issue on Genomic Signal Processing, 2004, pp. 132-137.

[12] P.D.Cristea, Large Scale Features in DNA Genomic Signals, Signal Processing, Special Issue on Genomic Signal Processing, ELSEVIER, 83, 2003, pp. 871-888.

[13] H.Demuth, M.Beale, M.Hagan, Neural Network Toolbox 5, User's Guide, The Mathworks, 2007.

[14] M.T.Hagan, H.B.Demuth, M.H.Beale, Neural Network Design, Boston, MA: PWS Publishing, 1996.

[15] I.Nastac, P.D.Cristea, Neuro-Adaptive Forecasting for Nonstationary Sequences, Proc. IEEE-SOFA 2005, pp. 179-186.

[16] NIH - National Centre for Biotechnology Information, National Institute of Health, National Library of Medicine, (NCBI/GenBank), http://www.ncbi.nlm.nih.gov/, 2008.

[17] A.C. Tsakoumis, P. Fessas, V.M. Mladenov, N.E. Mastorakis, Application of Chaotic Time Series for Short-Term Load Prediction, WSEAS Trans. on Systems, 2 (3), 2003, pp. 517-523.

Sensitivity Analysis of Air Pollution Models

Ivan Dimov, Rayna Georgieva, Sofiya Ivanovska,
Tzvetan Ostromsky, Zahari Zlatev

1 Introduction

Environmental security is rapidly becoming a significant topic of present interest all over the world. There are several important questions concerning environmental security: study of rate of dependence of pollutant concentrations on influenced factors, apportioning the output uncertainty to the uncertainty in the input parameters, possibility for a reliable prediction of scenarios when the critical pollutant levels exceed.

Here we present a new mechanism for investigation the sensitivity of the concentration levels of important pollutants (like ozone O_3) due to variation of rates of the involved chemical reactions in a real-life scenario of air pollution transport over Europe with the Unified Danish Eulerian Model (UNI-DEM). Specifying the most important chemical reactions for the model output using **s**ensitivity **a**nalysis (SA) techniques the specialists from various applied fields (chemistry, physics) may obtain valuable information for an improvement of the model and thus it will lead to an increase of reliability and robustness of predictions.

2 The Mathematical Model – UNI-DEM

The mathematical model* [5] gives the possibility to study the concentrations by time of the main types of air pollutants – sulphur pollutants, nitrogen pollutants, ammonia-ammonium, ozone, radicals and hydrocarbons. The model takes into account the major physical processes – advection, diffusion, deposition, emissions, and chemical reactions.

Chemical reactions play a significant role in the model – the equations in the model are coupled through the chemical reactions and both non-linearity and stiffness of the equations are mainly introduced by the chemistry (see [6]). UNI-DEM is one of the models of atmospheric chemistry, where the chemical processes are taken into account in a very accurate way. The chemical scheme used in the model is the condensed CBM-IV (Carbon Bond Mechanism, [5]). It includes 35 pollutants and 116 chemical reactions. The scheme is suitable and adequate to study cases of high concentrations of chemical species.

*UNI-DEM has been developed at the Danish National Environmental Research Institute (http://www2.dmu.dk/AtmosphericEnvironment/DEM/).

3 Sobol' Global Sensitivity Study Concept

It is assumed that the mathematical model can be presented as a model function of non-correlated input parameters with a joint probability density function. The indicator measuring the importance of the influence of a given input parameter (normalised between 0 and 1) is defined as a ratio of the variance of the conditional expectation of the model function with respect to a given input parameter and the total variance according to the model function. This indicator is named *first-order sensitivity index* by Sobol' [2] or *correlation ratio* by McKay. The *total sensitivity index* provides a measure of the total effect of a given parameter onto the model output variability.

The Sobol' method is one of the most often used variance-based methods [2]. An important advantage of this method is that it allows to compute not only the first-order indices, but also indices of a higher order in a way similar to the computation of the main effects, the total sensitivity index can be calculated with just one Monte Carlo integral per factor. The Sobol' method for global SA applied here is based on a decomposition of an integrable model function f in the d-dimensional factor space into terms of increasing dimensionality. This representation is unique under certain condition about its terms. The total variance of the model output is partitioned into partial variances [2] (ANOVA-representation, [3]) in the analogous way as the model function. The main sensitivity measures introduced in the Sobol' approach represent ratios between the corresponding partial variances and total variance (Sobol' global sensitivity indices, [2, 3]). The basic assumption underlying the so called High Dimensional Model Representation is that the major features of the model functions describing typical real-live problems can be shown by low-order subsets of inputs – constants, terms of first and second order. This means that one can use low-order indices only, but should be able to control the contribution of higher order terms.

The mathematical treatment of the problem of providing global sensitivity analysis consists in evaluating total sensitivity indices (in particular Sobol' global sensitivity indices of corresponding order). It leads to computing multidimensional integrals (from the mathematical representation of variances) using Monte Carlo technique (according to Sobol' approach), where the integrand is an square integrable function in the corresponding domain. The computational cost (in terms of model runs) for estimating all first-order and total sensitivity indices using Sobol' approach is proportional to the sample size and the number of input parameters. It makes this approach one of the most efficient variance-based methods from the point of view of its computational complexity.

Two approaches for evaluating *small* sensitivity indices (to avoid loss of accuracy because the analyzed database comes under this case) have been applied - reducing of the mean value (proposed by I.M. Sobol', 1990) and a combined approach (between approach of reducing of the mean value and correlated sampling) suggested in [4]. It should be noted that the variance of the second approach is smaller than the first one under certain conditions specified in a proposition about the variances of the corresponding estimators that has been proven in [4].

Table 1: First-order S_1, S_2, S_3 and total sensitivity indices $S^{tot}_{x_1}, S^{tot}_{x_2}, S^{tot}_{x_3}$ of input parameters obtained using different approaches for sensitivity analysis.

approach / estimated quantity	Standard (Sobol')		Approaches for small indices	
			red. of the m.v.	combined
	x ∈ [0.1; 2.0]	x ∈ [0.6; 1.4]	x ∈ [0.6; 1.4]	x ∈ [0.6; 1.4]
integrand $g(\mathrm{x})$	$f(\mathrm{x})$	$f(\mathrm{x})$	$f(\mathrm{x}) - c$	$f(\mathrm{x}) - c$
$c \sim f_0 = \int f(\mathrm{x})\mathrm{dx}$	–	–	0.51737	0.51737
$g_0 = \int g(\mathrm{x})\mathrm{dx}$	0.51520	0.51634	0.25145	0.25145
total variance **D**	0.26181	0.26446	0.07061	0.00530
S_1	0.26386	0.26530	0.27354	0.52979
S_2	0.26447	0.26359	0.26713	0.46142
S_3	0.25348	0.25209	0.22406	0.00222
$S^{tot}_{x_1}$	0.41592	0.41841	0.44195	0.53615
$S^{tot}_{x_2}$	0.41667	0.41627	0.43395	0.46791
$S^{tot}_{x_3}$	0.40281	0.40170	0.37938	0.00252

4 Discussion of Numerical Results

The idea of sensitivity tests with UNI-DEM performed in a previous study [1] is based on the computation of standard deviations and skewness of the pollutants concentrations under consideration.

For the present sensitivity study of the concentrations of one of the most important pollutants – ozone, a representative summer month (July 1998) has been selected because the concentrations of many chemical species achieve their annual maximum in summer-time. The first stage of present study includes a generation of input data obtained by using UNI-DEM (on SunFire E25000 supercomputer at the Technical University of Denmark) for our procedure of providing SA. The model runs have been done for the chemical rates variations with a fixed set of perturbation factors, where each of them corresponds to a chemical rate among the set of chemical reactions. The input data is a set of average values of pollutant concentrations normalized according to the maximum mean value of the concentration of the corresponding pollutant.

We study numerically how the chemical rate constants (considered to be input parameters) influence the output results (the behavior of the pollutants concentrations) at the second stage of computations. It consists of two steps: *Approximation* and *Computing of Sobol' global sensitivity indices*. Here we use polynomials of third and forth degree as an approximation tool to produce an analytical form of the model function on the basis of the table of values. Our numerical results showed that the squared 2-vector norm is more influenced by the domain than by the degree of the polynomial. Since three chemical reactions have been chosen as the most important for the distribution of ozone concentrations, the domain of integration is a cube. According to Table 1 the results for total sensitivity indices obtained using the combined approach

for small indices are the most reliable – the values of total effects are fully consistent with the expected tendencies according to results obtained on the first stage using UNI-DEM.

A comparison of results obtained using the present scheme for SA (applying the combined approach for small sensitivity indices) and results obtained using the available software tool for SA – R language and environment for statistical computing (http://www.r-project.org/) has been done. The results are close with an exception obtained with the R package using Sobol'& Saltelli approach, where we found a negative value for the total sensitivity index of the 3-rd input which is not acceptable. The reason that one would prefer our approach is that we are able to control the accuracy at each stage of the computations, i.e. at the stage of *approximation of the mesh function* by changing the polynomial degree and *computing total sensitivity indices* by applying the refined technique suitable for computing *small* sensitivity indices.

The obtained results have an important twofold role: for mathematical models verification and/or improvement, and/or for a reliable prediction the effects of high pollution levels (a) on human health and (b) on losses of crops in the agriculture. Most of the results can also be applied when other large-scale mathematical models are used.

5 Acknowledgements

This work is partly supported by the Bulgarian NSF Grant DO 02-215/2008.

References

[1] I. T. Dimov, *Monte Carlo Methods For Applied Scientists*, World Scientific, 2007.

[2] I. M. Sobol', Sensitivity Estimates for Nonlinear Mathematical Models, *Matem. Modelirovanie* **2 (1)** (1990), 112–118 (in Russian); *Mathematical Modeling and Computational Experiment*, Vol. 1 (1993), 407–414 (in English).

[3] I. M. Sobol', Global Sensitivity Indices for Nonlinear Mathematical Models and Their Monte Carlo Estimates, *Mathematics and Computers in Simulation*, Vol. 55 (1-3) (2001), 271–280.

[4] I. Sobol', E. Myshetskaya, Monte Carlo Estimators for Small Sensitivity Indices, *Monte Carlo Methods and Applications*, Vol. 13 (5-6) (2007), 455–465.

[5] Z. Zlatev, *Computer Treatment of Large Air Pollution Models*, KLUWER Academic Publishers, Dorsrecht-Boston-London, 1995.

[6] Z. Zlatev, I. Dimov, K. Georgiev, Modeling the Long-Range Transport of Air Pollutants, *IEEE Computational Science and Engineering*, Vol. 1 (3) (1994), 45–52.

On Error Detection with Block Codes

Rossitza Dodunekova

In error detection with block codes over symmetric memoryless channels the code performance is measured by the probability of undetected error. This probability depends on code characteristics and on ε, the symbol error probability of the channel. When the undetected error probability behaves irregularly with respect to ε, difficulties arise in finding a code appropriate for error detection over a channel with not exactly known symbol error probability. *Good* and *proper* codes are to be preferred in such cases. We present a survey of known methods and techniques for the study of block codes with respect to properness and goodness, together with applications to families of block codes, and some open problems.

Keywords: error detection, block code, proper code, good code.

Intuitionistic Fuzzy Estimations of the Ant Colony Optimization

Stefka Fidanova, Krasimir Atanasov, Pencho Marinov

1 Introduction

Combinatorial optimization is a branch of optimization. Its domain is optimization problems which set of feasible solutions is discrete or can be reduced to a discrete one, and the goal is to find the best possible solution. A combinatorial optimization problem consists of objective function, which needs to be minimized or maximized, and constraints. Examples of optimization problems are Traveling Salesman Problem [5], Vehicle Routing [6], Minimum Spanning Tree [4], Knapsack Problem [3], etc. They are NP-hard problems and in order to obtain solution close to the optimality in reasonable time, metaheuristic methods are used. One of them is Ant Colony Optimization (ACO) [2].

Real ants foraging for food lay down quantities of pheromone (chemical cues) marking the path that they follow. An isolated ant moves essentially at random but an ant encountering a previously laid pheromone will detect it and decide to follow it with high probability and thereby reinforce it with a further quantity of pheromone. The repetition of the above mechanism represents the auto-catalytic behavior of a real ant colony where the more the ants follow a trail, the more attractive that trail becomes. The ACO algorithm uses a colony of artificial ants that behave as cooperative agents in a mathematical space where they are allowed to search and reinforce pathways (solutions) in order to find the optimal ones. The problem is represented by graph and the ants walk on the graph to construct solutions. The solutions are represented by paths in the graph. After the initialization of the pheromone trails, the ants construct feasible solutions, starting from random nodes, and then the pheromone trails are updated. At each step the ants compute a set of feasible moves and select the best one (according to some probabilistic rules) to continue the rest of the tour. The structure of the ACO algorithm is shown by the pseudocode below. The transition probability $p_{i,j}$, to choose the node j when the current node is i, is based on the heuristic information $\eta_{i,j}$ and the pheromone trail level $\tau_{i,j}$ of the move, where $i, j = 1, \ldots, n$.

$$p_{i,j} = \frac{\tau_{i,j}^a \eta_{i,j}^b}{\sum_{k \in Unused} \tau_{i,k}^a \eta_{i,k}^b},$$

where $Unused$ is the set of unused nodes of the graph.

The higher the value of the pheromone and the heuristic information, the more profitable it is to select this move and resume the search. In the beginning, the initial pheromone level is set to a small positive constant value τ_0; later, the ants update this value after completing the construction stage. ACO algorithms adopt different criteria to update the pheromone level.

Ant Colony Optimization
Initialize number of ants;
Initialize the ACO parameters;
while not end-condition **do**
    for k=0 **to** number of ants
        ant k choses start node;
        while solution is not constructed **do**
            ant k selects higher probability node;
        end while
    end for
    Update-pheromone-trails;
end while

Figure 1: Pseudocode for ACO

The pheromone trail update rule is given by:

$$\tau_{i,j} \leftarrow \rho\tau_{i,j} + \Delta\tau_{i,j},$$

where ρ models evaporation in the nature and $\Delta\tau_{i,j}$ is new added pheromone which is proportional to the quality of the solution.
Our novelty is to use Intuitionistic Fuzzy Estimations (IFE see [1]) of start nodes with respect to the quality of the solution and thus to better menage the search process. We offer various start strategies and their combinations.

2 Start Strategies

The known ACO algorithms create a solution starting from random node. But for some problems, especially subset problems, it is important from which node the search process starts. For example if an ant starts from node which does not belong to the optimal solution, probability to construct it is zero. Therefore we offer several start strategies.
Let the graph of the problem has m nodes. We divide the set of nodes on N subsets. There are different ways for dividing. Normally, the graph are randomly enumerated. An example for creating of the subset, without lost of generality, is: the node number one is in the first subset, the node number two ï¿½ in the second subset, etc. the node number N is in the $N-th$ subset, the node number $N+1$ is in the first subset, etc. Thus the number of the nodes in the separate subsets are almost equal. We introduce estimations $D_j(i)$ and $E_j(i)$ of the node subsets, where $i \geq 2$ is the number of the current iteration and $D_j(i)$ and $E_j(i)$ are weight coefficients of $j-th$ node subset $(1 \leq j \leq N)$, which we calculate by the following formulas:

$$D_j(i) = \frac{i.D_j(i-1) + F_j(i)}{i},$$

$$E_j(i) = \frac{i.E_j(i-1) + G_j(i)}{i},$$

where $i \geq 1$ is the current process iteration and for each j $(1 \leq j \leq N)$:

$$F_j(i) = \begin{cases} \frac{f_{j,A}}{n_j} & \text{if } n_j \neq 0 \\ F_j(i-1) & \text{otherwise} \end{cases}, \tag{1}$$

$$G_j(i) = \begin{cases} \frac{g_{j,B}}{n_j} & \text{if } n_j \neq 0 \\ G_j(i-1) & \text{otherwise} \end{cases}, \tag{2}$$

and $f_{j,A}$ is the number of the solutions among the best $A\%$, and $g_{j,B}$ is the number of the solutions among the worst $B\%$, where $A + B \leq 100$, $i \geq 1$ and

$$\sum_{j=1}^{N} n_j = n,$$

where n_j $(1 \leq j \leq N)$ is the number of solutions obtained by ants starting from nodes subset j. Initial values of the weight coefficients are: $D_j(1) = 1$ and $E_j(1) = 0$. Obviously, $F_j(i)$, $G_j(i)$, $F_j(i)$ and $G_j(i) \in [0, 1]$, i.e., they are IFEs.
We try to use the experience of the ants from previous iteration to choose the better starting node. Other authors use this experience only by the pheromone, when the ants construct the solutions. Let us fix threshold E for $E_j(i)$ and D for $D_j(i)$, than we construct several strategies to choose start nod for every ant, the threshold E increase every iteration with $1/i$ where i is the number of the current iteration:

1 If $E_j(i) > E$ then the subset j is forbidden for current iteration and we choose the starting node randomly from $\{j \mid j \text{ is not forbidden}\}$;

2 If $E_j(i) > E$ then the subset j is forbidden for current simulation and we choose the starting node randomly from $\{j \mid j \text{ is not forbidden}\}$;

3 If $E_j(i) > E+$ then the subset j is forbidden for K_1 consecutive iterations and we choose the starting node randomly from $\{j \mid j \text{ is not forbidden}\}$;

4 If $E \geq E_j(i)$ and $D \geq D_j(i)$ for K_2 consecutive iterations, then the subset j is forbidden for current simulation and we choose the starting node randomly from $\{j \mid j \text{ is not forbidden}\}$;

5 Let $r_1 \in [0.5, 1)$ is a random number. Let $r_2 \in [0, 1]$ is a random number. If $r_2 > r_1$ we randomly choose node from subset $\{j \mid D_j(i) > D\}$, otherwise we randomly chose a node from the not forbidden subsets, r_1 is chosen and fixed at the beginning.

6 Let $r_1 \in [0.5, 1)$ is a random number. Let $r_2 \in [0, 1]$ is a random number. If $r_2 > r_1$ we randomly choose node from subset $\{j \mid D_j(i) > D\}$, otherwise we randomly chose a node from the not forbidden subsets, r_1 is chosen at the beginning and increase with r_3 every iteration.

Where $0 \leq K_1 \leq$"number of iterations" is a parameter. If $K_1 = 0$, than strategy 3 is equal to the random choose of the start node. If $K_1 = 1$, than strategy 3 is equal to the strategy 1. If $K_1 =$"maximal number of iterations", than strategy 3 is equal to the strategy 2.
We can use more than one strategy for choosing the start node, but there are strategies which can not be combined. We distribute the strategies into three sets: $St1 = \{strategy1,\ strategy2,\ strategy3\}$, $St2 = \{strategy4\}$ and $St3 = \{strategy5,\ strategy6\}$. The strategies from same set can not be used at once. Thus we can use strategy from one set or combine it with strategies from other sets. Exemplary combinations are ($strategy1$), ($strategy2$; $strategy5$), ($strategy3$; $strategy4$; $strategy6$).
In this paper we address the modelling of the process of ant colony optimization method by using fuzzy estimations, combining six start strategies. So, the start node of each ant depends of the goodness of the respective region. In a future we will focus on parameter settings which manage the starting procedure. We will investigate on influence of the parameters to algorithm performance.

Acknowledgements

This work is partly supported by the Bulgarian NSF Grant VU-MI-204/2006.

References

[1] Atanassov, K., Intuitionistic Fuzzy Sets, Springer, Heidelberg, 1999.

[2] Dorigo M., Gambardella L.M., Ant Colony System: A Cooperative Learning Approach to the Traveling Salesman Problem. IEEE Transactions on Evolutionary Computation 1,53-66,1997.

[3] Fidanova S., Evolutionary Algorithm for Multiple Knapsack Problem, Int. Conference Parallel Problems Solving from Nature, Real World Optimization Using Evolutionary Computing, ISBN No 0-9543481-0-9,Granada, Spain, 2002.

[4] Reiman M., Laumanns M., A Hybrid ACO algorithm for the Capacitated Minimum Spanning Tree Problem, In proc. of First Int. Workshop on Hybrid Metahuristics, Valencia, Spain, 2004, 1-10.

[5] Stutzle T. Dorigo M., ACO Algorithm for the Traveling Salesman Problem, In K. Miettinen, M. Makela, P. Neittaanmaki, J. Periaux eds., Evolutionary Algorithms in Engineering and Computer Science, Wiley, 163-183, 1999.

[6] Zhang T., Wang S., Tian W., Zhang Y., ACO-VRPTWRV: A New Algorithm for the Vehicle Routing Problems with Time Windows and Re-used Vehicles based on Ant Colony Optimization, Sixth International Conference on Intelligent Systems Design and Applications, IEEE press, 2006, 390-395.

Numerical Investigation of Charged Black Holes in the Scalar-Tensor Theories of Gravity with Massive Scalar Field

Daniela Georgieva, Ivan Stefanov,
Michail Todorov, Stoytcho Yazadjiev

Our aim is to study numerically Born-Infeld black holes in the Scalar-tensor theories (STT) of gravity with massive scalar field.
Scalar-tensor theories of gravity are a generalization of General Relativity [1]. In STT the gravitational interaction is described by two fields – one scalar field φ, and one tensor field, namely, the metric $g_{\mu\nu}, \mu, \nu = 0, 1, 2, 3$. In the Einstein frame the action of STT has the form

$$S = \frac{1}{16\pi G_*}\int d^4x\sqrt{-g}\left(\mathcal{R} - 2g^{\mu\nu}\partial_\mu\varphi\partial_\nu\varphi - 4V(\varphi)\right) + S_m[\Psi_m; \mathcal{A}^2(\varphi)g_{\mu\nu}] \qquad (1)$$

where $\mathcal{R}$ is the Ricci scalar curvature with respect to the metric $g_{\mu\nu}$, G_* is the bare gravitational constant and S_m is the action of the matter fields. The function $V(\varphi)$ is the potential of the scalar field φ. For numerical calculations we will take the potential in the form $V(\varphi) = \frac{1}{2}m_*^2\varphi^2$ where m_* is the mass of the scalar field.
We will be searching for static, spherically symmetric, asymptotically flat black holes. In this case the metric can be written in the form

$$ds^2 = g_{\mu\nu}dx^\mu dx^\nu = -f(r)e^{-2\delta(r)}dt^2 + \frac{dr^2}{f(r)} + r^2\left(d\theta^2 + \sin^2\theta d\phi^2\right),$$

with $f(r) = 1 - m(r)/r$, r – the radial coordinate, and $m(r)$ – the local gravitational mass.
We will study magnetically charged black holes with Born-Infeld electrodynamics described by the Lagrangian*[2]

$$L(X) = 2\left(1 - \sqrt{1+X}\right),$$

where $X = [r\mathcal{A}(\varphi)]^{-4}P^2/2$, and P is the magnetic charge of the black hole.
The action (1) in case of static, spherically symmetric space-time yields the following system of ordinary differential equations (ODE)

$$\frac{d\delta}{dr} = -r\left(\frac{d\varphi}{dr}\right)^2, \qquad (2)$$

$$\frac{dm}{dr} = r^2\left[\frac{1}{2}f\left(\frac{d\varphi}{dr}\right)^2 + V(\varphi) - \mathcal{A}(\varphi)^4 L(X)\right], \qquad (3)$$

$$\frac{d}{dr}\left(r^2 f\frac{d\varphi}{dr}\right) = r^2\left\{\frac{dV}{d\varphi} - 4\alpha(\varphi)\mathcal{A}^4(\varphi)\left[L - X\partial_X L(X)\right] - rf\left(\frac{d\varphi}{dr}\right)^3\right\}. \qquad (4)$$

*We use dimensionless quantities.

where $\partial_X = \frac{\partial}{\partial X}$ and $\alpha(\varphi) = \frac{d \ln \mathcal{A}(\varphi)}{d\varphi}$. For numerical investigation we will take the function $\mathcal{A}(\varphi)$ in the form $\mathcal{A}(\varphi) = e^{\alpha\varphi}$, where $\alpha > 0$. Hence, in this case, $\alpha(\varphi) = \alpha = \text{const}$.
The positive zeros of the metric function $f(r)$ correspond to the inner horizons of the black hole, and the greatest of them – to the event horizon. The massive scalar field admits the presence of inner horizons and extremal solutions: $f(r) = f'(r) = 0$.
We aim at obtaining solutions that describe asymptotically flat black holes. We split the problem in two sub-problems – in the exterior and in the interior region of the black hole. For the exterior region we can formulate a boundary-value problem (BVP) for (2)-(4) with the boundary conditions

$$f(r_H) = 0,$$

on the event horizon $r = r_H$ and

$$\lim_{r\to\infty} m(r) = M, \quad \lim_{r\to\infty} \delta(r) = \lim_{r\to\infty} \varphi(r) = 0,$$

at infinity, where M is the mass of the black hole. Since the exterior solutions can be continued inwards we can formulate an initial-value problem (IVP) for the interior region.
The problem in the exterior domain is a BVP with free left-hand boundary [4]. Apart from the unknown functions $\delta(r)$, $m(r)$ and $\varphi(r)$ the field equations also include one unknown parameter, namely the event horizon $r = r_H$. Since the radius r_H is *a priori* an unknown quantity we introduce a new shifted variable $x = r - r_H$. As a result the domain $r \in [r_H, \infty)$ maps to the domain with a fixed left boundary $x \in [0, \infty)$. After this transformation the event horizon $r = r_H$ takes part in explicit form in the ODEs. In this way, the so formulated BVP can be considered as nonlinear problem with a spectral parameter r_H. For the location of the event horizon the following condition is used

$$\left(\frac{df}{dr}\cdot\frac{d\varphi}{dr}\right)\Big|_{r=r_H} = \left\{\frac{dV(\varphi)}{d\varphi} + 4\alpha(\varphi)\mathcal{A}^4(\varphi)[X\partial_X L(X) - L(X)]\right\}\Big|_{r=r_H}.$$

It describes the requirement that the event horizon must be regular point for the sought functions.
For the numerical treating of the above posed BVP the Continuous Analogue of Newton Method (CANM) is used [3]. After an appropriate linearization the original BVP is rendered to solving two vector BVPs with regard to increments of the functions $\delta(r)$, $m(r)$, and $\varphi(r)$. The linear ODE systems are solved numerically by means of collocation scheme of fourth order of approximation. The corresponding matrix has an almost block-diagonal structure.
A IVP for the field equations (2)-(4) can be formulated in the interior region $r < r_H$ *a posteriori*. Since the values of the functions and their derivatives on the event horizon are already obtained from the exterior problem the sought functions can be continued inwards. The event horizon, however, is a singular point for the equation of the scalar field (4). The coefficient $r^2 f$ in front of the leading derivative φ'' in the equation

for the scalar field turns to zero on r_H (because $f(r_H) \equiv 0$) and the equation loses its order. So, to pose a regular IVP we shift the initial point r_H by small enough $\varepsilon > 0$ and choose for initial point $r_H - \varepsilon$ instead r_H. On the other hand the functions in question are smooth in the interval $(r_H - \varepsilon, r_H)$ and hence the following series expansions hold

$$
\begin{aligned}
m(r_H - \varepsilon) &= m(r_H) - m'(r_H)\varepsilon + o(\varepsilon^2), \\
\delta(r_H - \varepsilon) &= \delta(r_H) - \delta'(r_H)\varepsilon + o(\varepsilon^2), \\
\varphi(r_H - \varepsilon) &= \varphi(r_H) - \varphi'(r_H)\varepsilon + o(\varepsilon^2).
\end{aligned}
$$

A similar shift is made also at the every inner horizon (if such is reached). The latter admits an algorithmic sequence of IVPs for finding possible inner horizons. For the numerical treating of the above posed IVP again CANM is used.

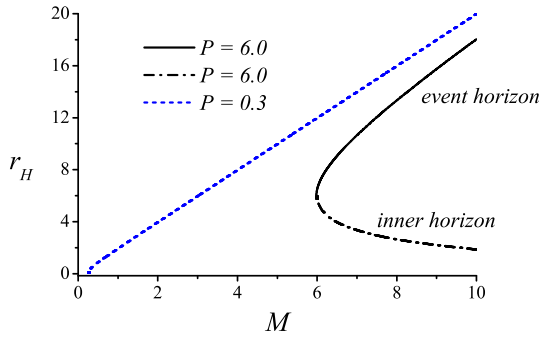

Figure 1: The radii of the horizons of black holes as function of the mass M.

In Figure 1 the $M - r_H$ relation is presented for $\alpha = 0.01$, $m_*^2 = 0.8$. On this figure two graphs are plotted – one for $P = 0.3$ (for small values of P) and one more for $P = 6.0$ (for big values of P). In the former case the black holes have a single non-degenerate horizon. In the latter case for masses in the interval $M \in [5.9804, 21.1]$ the black holes have two regular horizons. The two horizons merge and an extremal black hole occurs at $M = 5.9804$ when $P/M \approx 1$. For masses $M > 21.1$ we observe black holes with one horizon. The functions $f(r)$, $\delta(r)$ and $\varphi(r)$ for the solutions with two horizons and one degenerated horizon are given in Figure 2. The results are presented for values of the parameters $\alpha = 0.01, m_*^2 = 0.8, P = 6.0$ and two different masses of the black hole $M = 5.9804$ and $M = 8.0$. The radius of the extremal black hole is designated with "◯" while the two radii of the solution with $M = 8.0$ are designated with "×"-es. We can see that $\delta(r)$ has an inflexion point in the extremum of $\varphi(r)$.
As a result of the numerical investigation, the structure of the charged black holes coupled to non-linear electrodynamics in STT with massive scalar field inside the event horizon was studied.

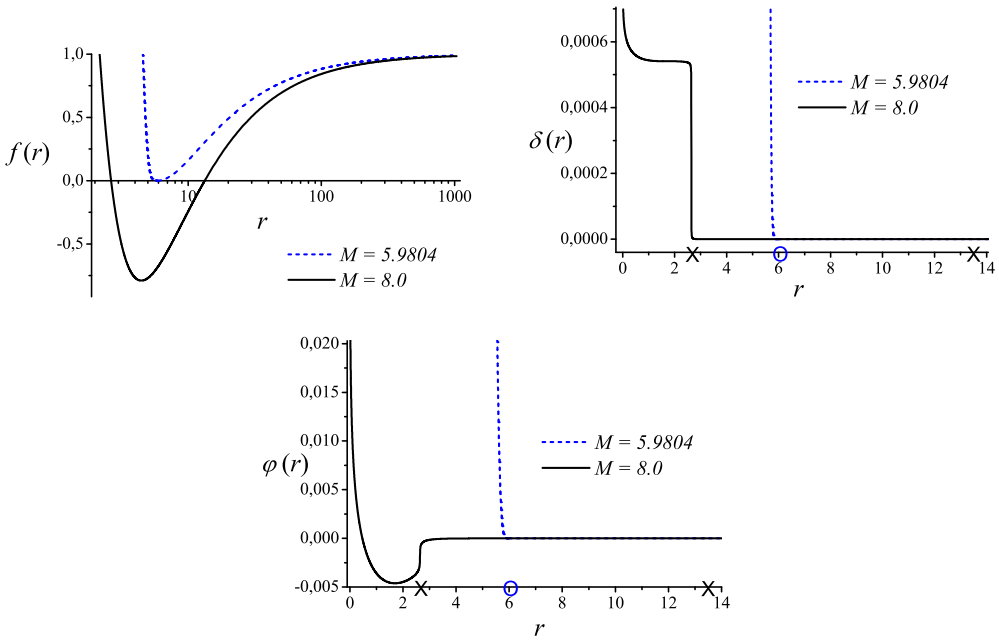

Figure 2: Solutions $f(r)$, $\delta(r)$, $\varphi(r)$ for $\alpha = 0.01, m_*^2 = 0.8, P = 6.0$.

References

[1] C. Will, *Theory and Experiment in Gravitational Physics*, Cambrige University Press (1934).

[2] M. Born and L. Infeld, Proc. R. Soc. London **A143**, 410 (1934).

[3] M. K. Gavurin, Izvestia VUZ, *Matematika* **14**(6), 18–31 (1958) (in Russian) (see also *Math.Rev.* **25**(2), #1380 (1958)).

[4] I. Stefanov, S. Yazadjiev and M. Todorov, *Phys. Rev.* **D 75**, 084036 (2007).

Reductions and Soliton Solutions of Nonlinear Evolution Equations on Symmetric Spaces

Vladimir Gerdjikov, Nikolay Kostov, Tihomir Valchev

Many integrable partial differential equations possessing a Lax pair are obtained after imposing an additional algebraic constraint called reduction [1] on its Lax operators. A well known example is the classical nonlinear Schrödinger equation (NLS)

$$iu_t + u_{xx} + 2|u|^2 u = 0, \tag{1}$$

whose scattering problem is Zakharov-Shabat's system

$$L\psi \equiv (i\partial_x + q(x,t) - \lambda\sigma_3)\,\psi(x,t,\lambda) = 0, \tag{2}$$

where

$$q(x,t) = \begin{pmatrix} 0 & u^*(x,t) \\ u(x,t) & 0 \end{pmatrix}, \qquad \sigma_3 = \begin{pmatrix} 1 & 0 \\ 0 & -1 \end{pmatrix}. \tag{3}$$

Since the off-diagonal elements are complex conjugated the potential is $\mathbb{Z}_2$-reduced. Another example is provided by the modified Korteweg-de Vries equation (mKdV)

$$\mathbf{u}_t + \mathbf{u}_{xxx} + 6\mathbf{u}^2\mathbf{u}_x = 0. \tag{4}$$

Its scattering problem is the Zakharov-Shabat system (2) too but in this case the function u is purely imaginary $u = i\mathbf{u}$. In this case there are two $\mathbb{Z}_2$ reductions acting simultaneously. From spectral point of view each reduction imposes symmetries on the spectral data of L, and, in particular, on its discrete eigenvalues. For the Lax operator associated with NLS they come in complex conjugated $\lambda_k^{\pm} = \mu_k \pm i\nu_k$, $\nu_k > 0$. In the case of mKdV we have an additional symmetry which means, that if $\lambda_k^{\pm}$ is an eigenvalue then $-\lambda_k^{\pm}$ is also an eigenvalue. Therefore we have two different groups of eigenvalues: "doublets" of two imaginary eigenvalues $\{\pm i\nu_k\}_{k=1}^n$ and quadruplets of four eigenvalues $\{\pm(\mu_k + i\nu_k), \pm(\mu_k - i\nu_k)\}_{k=1}^n$. Soliton solutions are tightly connected with the discrete part of spectrum of L — the group velocities of solitons are expressed by the real and imaginary parts of the discrete eigenvalues. Since mKdV has two types of eigenvalues it is natural to expect that it allows for two types of soliton solutions: doublet solitons associated with 2 eigenvalues and quadruplets — with 4 eigenvalues. This situation resembles that of the sin-Gordon equation which possesses topological solitons and breathers.

Our purpose is twofold: i) to demonstrate how one can obtain multicomponent generalizations of NLS and mKdV, and ii) to explain how their soliton solutions can be found. All equations under consideration are related to symmetric spaces of the series **BD.I** according to Cartan's classification [2]. This relation is realized by the corresponding Lax representation. To clarify this suppose that it is given a symmetric space G/K where G is simple complex Lie group and K is its subgroup. There exists a splitting (grading) of the corresponding Lie algebra $\mathfrak{g}$ in the form

$$\mathfrak{g} = \mathfrak{k} + m, \qquad [\mathfrak{k}, \mathfrak{k}] \in \mathfrak{k}, \qquad [\mathfrak{k}, m] \in m, \qquad [m, m] \in \mathfrak{k}, \tag{5}$$

where the subalgebra $\mathfrak{k}$ corresponds to the subgroup K and m is the complement of $\mathfrak{k}$ to $\mathfrak{g}$, see [2, 3] for more details. There is an element J of the Cartan subalgebra $\mathfrak{h} \in \mathfrak{g}$ such that

$$\mathfrak{k} = \{X \in \mathfrak{g}; [J, X] = 0\}.$$

Thus we can associate with any Lax operator of the form

$$L = i\partial_x + q(x,t) - \lambda J, \qquad \lim_{|x|\to\infty} q(x,t) = 0$$

a symmetric space G/K by simply choosing $q \in m$.
For example, the following system of coupled mKdV equations [4]:

$$\begin{aligned} q_{2,t} + q_{2,xxx} - 3(q_2 q_3)_x q_3 + 3q_3 q_2^* q_{3,x} - 6q_2^2 q_{2,x} = 0, \\ q_{3,t} + q_{3,xxx} + 3|q_2|_x^2 q_3 - 3(q_2 q_3)_x q_2 - 3(q_2^* q_3)_x q_2^* - 3q_3^2 q_{3,x} = 0. \end{aligned}$$

represents the compatibility condition for generic Lax pair of the type

$$L = i\partial_x + q - \lambda J, \tag{6}$$

$$M = i\partial_t + V_0(x,t) + V_1(x,t)\lambda + q(x,t)\lambda^2 - \lambda^3 J, \tag{7}$$

$$V_1 = i\mathrm{ad}_J \partial_x q + \frac{1}{2}\left[\mathrm{ad}_J q, q\right], \qquad V_0 = -\partial_{xx}^2 q + \frac{1}{2}\left[\mathrm{ad}_J q, [\mathrm{ad}_J q, q]\right] + i\left[\partial_x q, q\right].$$

Since

$$J = \mathrm{diag}\,(1,0,0,0,-1), \qquad q = \begin{pmatrix} 0 & q_2 & q_3 & q_4 & 0 \\ p_2 & 0 & 0 & 0 & q_4 \\ q_3 & 0 & 0 & 0 & -q_3 \\ q_4 & 0 & 0 & 0 & q_2 \\ 0 & p_4 & -p_3 & p_2 & 0 \end{pmatrix}, \tag{8}$$

this Lax representation is related to the symmetric space $SO(5)/SO(2) \times SO(3)$. In order to derive the system above one has to impose the additional constraints

$$p_k = q_k \qquad k = 2,3,4; \qquad q_4 = -q_2^*, \qquad q_3 = -q_3^*, \qquad p_4 = -p_2^*, \qquad p_3 = -p_3^*.$$

In order to realize our second puspose we make use of Zakharov-Shabat's dressing technique [5]. A basic requirement which we stress on is that the dressing procedure has to be compatible with the presence of reductions. The idea of the dressing method consists in finding a solution q of a nonlinear problem startingfrom a known one q_0 by taking into account the existence of Lax representation. This is done by "dressing" a fundamental solution ψ_0 of the auxiliary Zakharov-Shabat's system

$$L_0\psi_0 = i\partial_x\psi_0 + (q_0 - \lambda J)\psi_0 = 0 \tag{9}$$

with a factor g as follows

$$\psi_0 \mapsto \psi = g\psi_0.$$

It is assumed that ψ is a fundamental solution Zakharov-Shabat's system

$$L\psi = i\partial_x\psi + (q - \lambda J)\psi = 0 \tag{10}$$

with a potential q to be found. We use dressing factors which are meromorphic functions on λ, for example

$$g = \mathbb{1} + \frac{A}{\lambda - \lambda^+} + \frac{B}{\lambda - \lambda^-}, \tag{11}$$

where the poles λ^+ and λ^- belong to the upper and lower halves of the complex λ-plane. A more detailed analysis is required to show how q can be obtained from q_0 and the residues A and B. The residues in their turn depend on the so-called fundamental analytic solutions χ_0^+ and χ_0^- (see [6, 7] for a definition and a construction of these quantities) of the initial linear problem. The poles of g are discrete eigenvalues of the Lax operator L.

We apply the dressing procedure on the already dressed solution and thus obtain another solution and so on. In particular, when $q_0 \equiv 0$ the dressed solution is called 1-soliton solution.

In the case under consideration there exist two essentially different types of soliton solutions: doublet solitons (2 eigenvalues $\pm i\nu$ of L) and quadruplet solitons (4 eigenvalues $\pm\lambda^+, \pm(\lambda^+)^*$ of L). The doublet soliton is obtained by applying a dressing procedure with a 2-poles factor in the form (11). It reads

$$\begin{aligned} q_2(x,t) &= \frac{-i\nu e^{i\delta_0}}{\cosh 2\nu(x - ut - \xi_0) + \mathcal{C}} \left(e^{-\nu(x-ut-\xi_0)}\mathcal{F}_2 + e^{\nu(x-ut-\xi_0)}\mathcal{F}_4\right), \\ q_3(x,t) &= \frac{2i\nu\mathcal{F}_3 e^{i\delta_0}\sinh\nu(x - ut - \xi_0)}{\cosh 2\nu(x - ut - \xi_0) + \mathcal{C}}, \qquad \mathcal{C} = \frac{2\mathrm{Re}\,(\mathcal{F}_2\mathcal{F}_4^*) + |\mathcal{F}_3|^2}{2}, \end{aligned}$$

where

$$\mathcal{F}_k = \frac{F_{0,k}}{\sqrt{|F_{0,1}||F_{0,5}|}}, \quad \xi_0 = \frac{1}{2\nu}\ln\frac{|F_{0,1}|}{|F_{0,5}|}, \quad u = \nu^2, \quad \delta_0 = \frac{l\pi}{2}.$$

In order to calculate the corresponding quadruplet soliton we use the dressing factor

$$g(x,\lambda) = \mathbb{1} + \frac{A(x)}{\lambda - \lambda^+} - \frac{KSA^*(x)SK}{\lambda + (\lambda^+)^*} - \frac{SA(x)S}{\lambda + \lambda^+} + \frac{KA^*(x)K}{\lambda - (\lambda^+)^*}.$$

The result reads

$$
\begin{aligned}
q_2 &= \frac{2\sqrt{|F_{0,1}F_{0,2}F_{0,4}F_{0,5}|}}{|a|^2+b^2-c^2}\left\{a^*\cosh(\phi_{\rm R}^- - i\phi_{\rm I}^-) - b[\cosh(\phi_{\rm R}^- + i\phi_{\rm I}^+)\right.\\
&+ \left.\cosh(\phi_{\rm R}^+ - i\phi_{\rm I}^-)] - a\cosh(\phi_{\rm R}^+ + i\phi_{\rm I}^+) + c[\cosh(\phi_{\rm R}^+ + i\phi_{\rm I}^-) - \cosh(\phi_{\rm R}^- - i\phi_{\rm I}^+)]\right\},\\
q_3 &= \frac{2i\sqrt{|F_{0,1}F_{0,5}|}}{|a|^2+b^2-c^2}{\rm Im}\left\{(b+c)\sinh(\phi_{\rm R}+i\phi_{\rm I}) - a^*\sinh(\phi_{\rm R}-i\phi_{\rm I})\right\}F_{0,3},\\
a &= \frac{|F_{0,1}F_{0,5}|}{\mu+i\nu}(\cosh 2(\phi_{\rm R}-i\phi_{\rm I}) + \mathcal{C}_a), \quad \mathcal{C}_a = \frac{F_{0,2}^2+F_{0,3}^2+F_{0,4}^2}{2|F_{0,1}F_{0,5}|},\\
b &= \frac{i|F_{0,1}F_{0,5}|}{\nu}(\cosh 2\phi_{\rm R} + \mathcal{C}_b), \quad \mathcal{C}_b = \frac{2{\rm Re}\,(F_{0,2}^*F_{0,4}) + |F_{0,3}|^2}{2|F_{0,1}F_{0,5}|},\\
c &= \frac{|F_{0,1}F_{0,5}|}{\mu}(\mathcal{C}_c - \cos 2\phi_{\rm I}), \quad \mathcal{C}_c = \frac{(|F_{0,2}|^2+|F_{0,4}|^2) - |F_{0,3}|^2}{2|F_{0,1}F_{0,5}|},\\
\phi_{\rm R} &= \nu\,(x-ut-\xi_0)\,, \qquad \phi_{\rm I} = \mu\,(x-vt-\arg F_{0,5}/\mu)\\
\phi_{\rm R}^{\pm} &= \phi_{\rm R} \pm \frac{1}{2}\ln(|F_{0,2}|/|F_{0,4}|), \qquad \phi_{\rm I}^{\pm} = \phi_{\rm I} \pm \arg F_{0,4}.
\end{aligned}
$$

Similar treatment can be applied to equations of NLS type associated with other types of symmetric space. The difference is in the form of M operator.

Acknowledgements

One of us (T. I. V.) acknowledges support from the European Operational programm HRD, contract BGO051PO001/07/3.3-02/53 with the Bulgarian Ministry of Education.

References

[1] A. Mikhailov, *Physica D* **3**, 73–117 (1981).

[2] S. Helgason, *Differential Geometry, Lie Groups and Symmetric Spaces*, (Academic Press, Toronto, 1978).

[3] A. Fordy, P. Kulish, *Commun. Math. Phys.* **89**, 427–443 (1983).

[4] Gerdjikov V., Kaup D., Kostov N., Valchev T., *J. Phys. A: Math. Theor.* **41**, 36 pages (2008).

[5] V. Zakharov, A. Shabat, *Funkts. Anal. Prilozhen.* **13**, 13–22 (1979) (In Russian).

[6] A. Shabat, *Diff. Equations* **15**, 1824–1834 (1979) (In Russian).

[7] V. Gerdjikov, *Contemporary Math.* **301** (2002).

Dynamics of Multilayered Josephson Junctions

Ivan Hristov, Stefka Dimova

Introduction

Stacks of long Josephson Junctions (JJs) were intensively studied during the past years. In these systems both nonlinearity and interaction between subsystems play an important role. Such structures make it possible to state and study new physical effects that do not occur in single JJs. One of the most interesting experimental results for two stacked JJs found in resent years is the so-called current locking (CL). The essence of this phenomenon is as follows: there exists a range of the external magnetic field where the different junctions switch to dynamic state simultaneously when the external current exceeds some critical value. It was shown by means of numerical simulation [2] that experimentally found CL for two stacked JJs can be obtained and well explained in the framework of inductive coupling model [1]. In this work we show that the transient process of switching from static to dynamic state in symmetric three stacked JJs depends on the way of increasing the external current.

Mathematical model

The dynamics of the magnetic flux $\varphi(x,t) = (\varphi_1(x,t), \ldots, \varphi_N(x,t))^T$ in geometrically symmetric N stacked JJs is described by the following system of perturbed sine-Gordon equations [1]:

$$\varphi_{tt} + \alpha\varphi_t + J + \Gamma = L^{-1}\varphi_{xx}, \tag{1}$$

where α is the dissipation coefficient, $J = (\sin\varphi_1, \sin\varphi_2, \ldots, \sin\varphi_N)^T$ is the vector of the Josephson current density, $\Gamma = \gamma\,(1,1,\ldots,1)^T$ is the vector of the external current density and $L = \text{tridiag}\,(1,s,1)$, ($-0.5 < s \leq 0$ for arbitrary N).
In this work we consider stacks of overlap geometry placed in external magnetic field h_e, therefore the system (1) should be solved together with the boundary conditions:

$$\varphi_x(-\ell) = \varphi_x(\ell) = H, \tag{2}$$

where H is the vector $H = h_e\,(1,1,\ldots,1)^T$.
The existence of Josephson current generates a specific magnetic flux. When the external current is less then some critical value the junctions are in static state. In order to obtain precise initial values to close the problem (1), (2) and to make a correspondence between the loss of stability of a possible static distribution of the magnetic flux and switching to dynamic state, we solve numerically the static problem, i.e., the system of equations with time independent fluxes. To study the global stability of a possible static solution the following Sturm-Liouville problem

(SLP) is generated:

$$-L^{-1}u_{xx} + Q(x)u = \lambda\, u, \tag{3a}$$

$$u_x(\pm l) = 0, \qquad \int_{-l}^{l} \langle u, u\rangle\, dx - 1 = 0, \tag{3b}$$

where $Q(x) = J_z'(\varphi(x))$. This is equivalent to study the positive definiteness of the second variation of the potential energy of the system. The minimal eigenvalue λ_{min} determines the stability of the distribution under consideration. A minimal eigenvalue equal to zero means a bifurcation caused by change of some parameter, in our case – the external current γ.

Numerical method

The simplest generalizable model of stacked JJs is the case of three stacked JJs because it takes into account the different behavior of the interior and exterior junctions. The numerical results presented here are for the particular case of three stacked JJs.
In order to solve the mentioned above static nonlinear boundary value problem we use an iterative algorithm [5], based on the continuous analog of Newton's method (CAMN) [3]. CANM gives a linearized boundary value problem at each iteration step. The linear boundary value problem is solved numerically by means of Galerkin finite element method (FEM) and quadratic finite elements. FEM is used also to reduce the SLP (3) to a linear algebraic problem whose few smallest eigenvalues and the corresponding eigenfunctions are found by the subspace iteration method [4]. To test the accuracy of the above methods we have used the method of Runge by computing the solutions on sequence of embedded meshes. The numerous experiments made show a super-convergence of order four for both the static problem and SLP.
For symmetric three stacked JJs we consider solutions, which components φ^{ex} for the exterior junctions are of the same type. In this case we reduce the system of three equations to a system of two equations (φ^{in} is the component of the solution in the interior junction):

$$a_{11}\varphi^{ex}_{xx} + a_{12}\varphi^{in}_{xx} = \varphi^{ex}_{tt} + \alpha\varphi^{ex}_{t} + \sin\varphi^{ex} + \gamma \tag{4}$$

$$a_{21}\varphi^{ex}_{xx} + a_{22}\varphi^{in}_{xx} = \varphi^{in}_{tt} + \alpha\varphi^{in}_{t} + \sin\varphi^{in} + \gamma, \tag{5}$$

where $a_{11} = a_{22} = 1/(1-2s^2),\ a_{12} = -s/(1-2s^2),\ a_{21} = -2s/(1-2s^2)$.
To solve the system (4), (5) we use an implicit difference scheme. The difference equations corresponding to equation (4) are:

$$0.5a_{11}\delta\hat{y}^{ex}_{k-1} - (1 + a_{11}\delta + 0.5\alpha\tau)\hat{y}^{ex}_{k} + 0.5a_{11}\delta\hat{y}^{ex}_{k+1} = -2y^{ex}_{k} +$$

$$(1-0.5\alpha\tau)\check{y}^{ex}_{k} - 0.5a_{11}\delta(\check{y}^{ex}_{k-1} - 2\check{y}^{ex}_{k} + \check{y}^{ex}_{k+1}) - a_{12}\delta(y^{in}_{k-1} - 2y^{in}_{k} + y^{in}_{k+1}) + \tau^2(\sin y^{ex}_{k} + \gamma)$$

Here h and τ are the steps in space and time respectively, $\delta = (\tau/h)^2$. To check the numerical stability and the order of accuracy we have made computations for fixed time level and embedded meshes in space. The results show second order of convergence in space and time.

Numerical results

We briefly discuss the numerical result. For "small" values of the external magnetic field h_e and below the critical current γ_{cr} all the junctions are in Meissner state. In order to verify the critical current found by solving the SLP (3) and to analyze the transient process of switching to dynamic state we excite the solution in four different ways (Fig.1). Excitation $\gamma_1(t)$ is under γ_{cr}. Excitations $\gamma_3(t)$ and $\gamma_4(t)$ are above γ_{cr}, they have the same final value, but they differ in slope. Excitation $\gamma_2(t)$ is above γ_{cr}, it has the same slope as $\gamma_4(t)$, but lower final value.

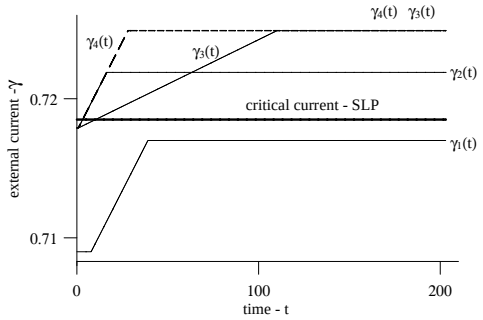

Figure 1: Increasing the external current in different ways in vicinity of the critical current of Meissner type solution at $h_e = 0.5$ for $2l = 10$, $\alpha = 0.1$, $S = -0.3$

As we have expected, for excitation $\gamma_1(t)$ all the junctions remain in Meissner state. The numerical experiments confirmed also our expectation that if γ_{cr} is some how exceeded, at least one of the junctions will switch to dynamic state. For excitation $\gamma_4(t)$ all three junctions switch to resistive state (Fig.2,3) (a kind of dynamic state). For $\gamma_2(t)$ and $\gamma_3(t)$ only the interior junction switches to resistive state (Fig.4,5). In all these cases the transient process starts with penetration of fluxons in the interior junction, i.e., the interior junction drives the transient process. In the case $\gamma_4(t)$ the switching of the interior junction to resistive state triggers the switching of the exterior ones, while in the cases $\gamma_2(t)$ and $\gamma_3(t)$ it does not.

Conclusions

A perfect agreement between the results found by solving the Sturm-Liouville problem and those found by solving the dynamic problem is established. The numerical simulation shows that the switching from static to dynamic state in symmetric three stacked JJs strongly depends on the way of increasing the external current.

Acknowledgments. This work is supported by Sofia University Scientific foundation under Grant No 135/2008.

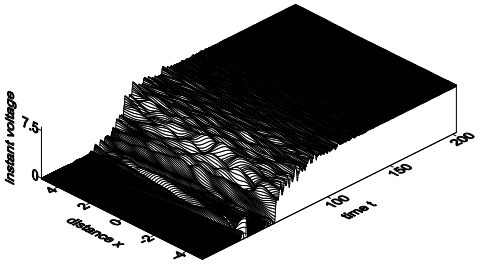

Figure 2: $\gamma_4(t)$, instant voltage φ_t^{ex}

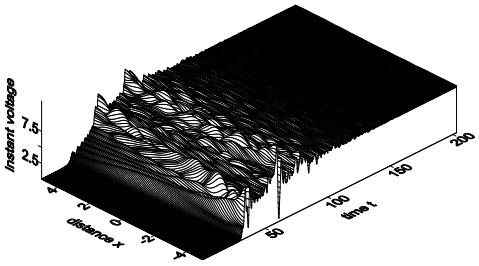

Figure 3: $\gamma_4(t)$, instant voltage φ_t^{in}

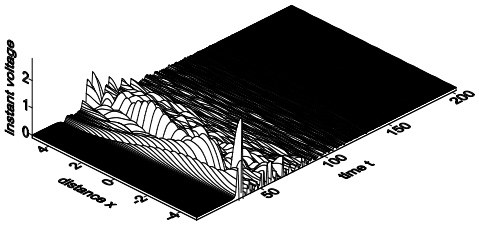

Figure 4: $\gamma_2(t)$, instant voltage φ_t^{ex}

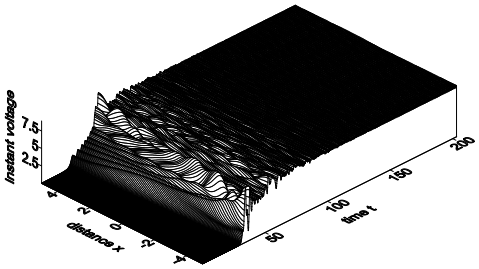

Figure 5: $\gamma_2(t)$, instant voltage φ_t^{in}

References

[1] S. Sakai, P. Bodin, N.F. Pedersen, Fluxons in thin-film superconductor-insulator superlattices, J. Appl. Phys., v. **73**, No. 5, 1993, pp. 2411 – 2418.

[2] E. Goldobin, A.V. Ustinov, Current locking in magnetically coupled long Josephson junctions, Phys. Rev. B, 59 (17), 1999, pp. 11532–11538.

[3] I. V. Puzynin *et al.*, Methods of computational physics for investigation of models of complex physical systems, Particals & Nucley **38**, 1 (2007), Dubna.

[4] K.J. Bathe and E. Wilson, Numerical Methods in Finite Element Analisis, Prentice Hall, Englewood Cliffs, 1976.

[5] I. Hristov, S. Dimova, T. Boyadjiev, Stability and Bifurcation of the Magnetic Flux, NAA 2008, Bound States in Stacked Josephson Junctions. LNCS, v. **5434**, 2009, pp. 224 – 232.

Integrable Models for Shallow Water Waves

Rossen Ivanov

The motion of inviscid fluid with a constant density ρ is described by the Euler's equations:

$$\begin{aligned} \frac{\partial \mathbf{v}}{\partial t} + (\mathbf{v}\cdot\nabla)\mathbf{v} &= -\frac{1}{\rho}\nabla P + \mathbf{g}, \\ \nabla\cdot\mathbf{v} &= 0, \end{aligned}$$

where $\mathbf{v}(x,y,z,t)$ is the velocity of the fluid at the point (x,y,z) at the time t, P is the pressure in the fluid, $\mathbf{g}=(0,0,-g)$ is the constant Earth's gravity acceleration. Consider now a motion of a shallow water over a flat bottom, which is located at $z=0$. We assume that the motion is in the x-direction, and that the physical variables do not depend on y. Let h be the mean level of the water and let $\eta(x,t)$ describes the shape of the water surface, i.e. the deviation from the average level. The pressure is

$$P = P_A + \rho g(h-z) + p(x,z,t),$$

where P_A is the constant atmospheric pressure, and p is a pressure variable, measuring the deviation from the hydrostatic pressure distribution.
On the surface $z=h+\eta$, $P=P_A$ and therefore $p=\eta\rho g$. Taking $\mathbf{v}\equiv(u,0,w)$ we can write the kinematic condition on the surface as [1]

$$w = \frac{\partial\eta}{\partial t} + u\frac{\partial\eta}{\partial x} \qquad \text{on} \qquad z=h+\eta.$$

Finally, there is no horizontal velocity at the bottom, thus $w=0$ on $z=0$. Let us introduce now dimensionless parameters $\varepsilon=a/h$ and $\delta=h/\lambda$, where a is the typical amplitude of the wave and λ is the typical wavelength of the wave. Now we can introduce dimensionless quantities, according to the magnitude of the physical quantities, see [1, 2] for details: $x\to\lambda x$, $z\to zh$, $t\to\frac{\lambda}{\sqrt{gh}}t$, $\eta\to a\eta$, $u\to\varepsilon\sqrt{gh}u$, $w\to\varepsilon\delta\sqrt{gh}w$, $p\to\varepsilon\rho gh$. This scaling is due to the observation that both w and p are proportional to ε i.e. the wave amplitude, since at undisturbed surface ($\varepsilon=0$) both $w=0$ and $p=0$. The system in the new, dimensionless variables is

$$\begin{aligned} u_t + \varepsilon(uu_x + wu_z) &= -p_x, \\ \delta^2(w_t + \varepsilon(uw_x + ww_z)) &= -p_z, \\ u_x + w_z &= 0, \\ w = \eta_t + \varepsilon u\eta_x, \quad p=\eta, \qquad \text{on} \qquad z &= 1+\varepsilon\eta, \\ w = 0 \qquad \text{on} \qquad z &= 0. \end{aligned}$$

We present now a derivation of the relevant form of the Green-Naghdi (GN) equations [3], which follows directly from the above system. We assume that u is not a

function of z, an approximation valid for the leading-order problem. This assumption is equivalent to the simplifying approximation used by Green and Naghdi (namely, that w is linear in z in a single-layer model). Thus we have $w = -zu_x$, which satisfies $u_x + w_z = 0$ and the bottom condition. The second equation gives

$$p = \eta - \frac{1}{2}\delta^2[(1+\varepsilon\eta)^2 - z^2](u_{xt} + \epsilon u u_x - \epsilon u_x^2),$$

which satisfies the pressure condition at the surface. This expression for p is now used in the first equation, which is then integrated over all z to give

$$u_t + \varepsilon u u_x + \eta_x = \frac{\delta^2/3}{1+\varepsilon\eta}[(1+\varepsilon\eta)^3(u_{xt} + \varepsilon u u_{xx} - \varepsilon u_x^2)]_x,$$

The first order in the small parameters is

$$u_t - \frac{\delta^2}{3}u_{xxt} + \varepsilon u u_x + \eta_x = 0.$$

The condition on the surface gives

$$\eta_t + [(u(1+\varepsilon\eta)]_x = 0.$$

One can demonstrate that the Green-Naghdi system can be related to the following two component Camassa-Holm system (CH2) in the first order with respect to ε and δ^2 [4]:

$$\begin{aligned} m_t + 2u_x m + u m_x + \rho\rho_x &= 0, \\ \rho_t + (u\rho)_x &= 0 \end{aligned}$$

where $m = u - u_{xx}$. This system appears originally in [5] and its mathematical properties have been studied further in many works.
The Camassa-Holm equation [6] can be obtained via the obvious reduction $\rho \equiv 0$. The system is integrable, it can be written as a compatibility condition of two linear systems (Lax pair) with a spectral parameter ζ:

$$\begin{aligned} \Psi_{xx} &= \Big(-\zeta^2\rho^2 + \zeta m + \frac{1}{4}\Big)\Psi, \\ \Psi_t &= \Big(\frac{1}{2\zeta} - u\Big)\Psi_x + \frac{1}{2}u_x\Psi. \end{aligned}$$

The system is also bi-Hamiltonian. The first Poisson bracket is

$$\{A,B\} = -\int \Big[\frac{\delta A}{\delta m}(m\partial + \partial m)\frac{\delta B}{\delta m} + \frac{\delta A}{\delta m}\rho\partial\frac{\delta B}{\delta \rho} + \frac{\delta A}{\delta \rho}\partial\rho\frac{\delta B}{\delta m}\Big]\mathrm{d}x$$

for the Hamiltonian $H = \frac{1}{2}\int(um + \rho^2)\mathrm{d}x$; The second Poisson bracket is

$$\{A,B\}_2 = -\int \Big[\frac{\delta A}{\delta m}(\partial - \partial^3)\frac{\delta B}{\delta m} + \frac{\delta A}{\delta \rho}\partial\frac{\delta B}{\delta \rho}\Big]\mathrm{d}x$$

for the Hamiltonian $H_2 = \frac{1}{2}\int(u\rho^2 + u^3 + uu_x^2)\mathrm{d}x$.
It has two Casimirs: $\int \rho \mathrm{d}x$ and $\int m \mathrm{d}x$.
Let us define

$$\rho = 1 + \frac{1}{2}\varepsilon\eta - \frac{1}{8}\varepsilon^2(u^2 + \eta^2).$$

The expansion of ρ^2 in the same order of ε is $\rho^2 = 1 + \varepsilon\eta - \frac{1}{4}\varepsilon^2 u^2$.
With this definition it is straightforward to write it in the form

$$\left(u - \frac{\delta^2}{3}u_{xx}\right)_t + \frac{3}{2}\varepsilon u u_x + \frac{1}{\varepsilon}(\rho^2)_x = 0$$

or, introducing the variable $m = u - \frac{1}{3}\delta^2 u_{xx}$, in the same order (i.e. neglecting terms of order $\varepsilon\delta^2$)

$$m_t + \varepsilon m u_x + \frac{1}{2}\varepsilon u m_x + \frac{1}{\varepsilon}(\rho^2)_x = 0.$$

Next, using the fact that in linear approximation $u_t \approx -\eta_x$, $\eta_t \approx -u_x$, we have

$$\rho_t = \frac{1}{2}\varepsilon\eta_t + \frac{1}{4}\varepsilon^2(\eta u)_x.$$

With these expressions for ρ and ρ_t the second GN equation can be written as

$$\rho_t + \frac{\varepsilon}{2}(\rho u)_x = 0.$$

The rescaling $u \to \frac{2}{\varepsilon}u$, $x \to \frac{\delta}{\sqrt{3}}\ x$, $t \to \frac{\delta}{\sqrt{3}}t$ in GN equations gives the CH2 system.
The case with $-\rho\rho_x$ term, which is considered in the most previous works on the system, corresponds to a situation in which the gravity acceleration points upwards.
Concerning the occurrences of peakons, it was established that the only peakons of the CH2 system arise when $\rho \equiv 0$ and $u(x,t) = c\,e^{-|x-ct|}$ for some wave speed $c \neq 0$.
Wave breaking is the only way that singularities arise in smooth solutions to the system and that for the occurrence of breaking waves it is not necessary to require that $\rho \equiv 0$, see [4]. The travelling waves and the peakon solutions of the CH2 system are also discussed in [4].
The Kaup - Boussinesq system is another integrable system matching the GN equation to the first order of the small parameters ε, δ. The first GN equation can be written as

$$V_t + \varepsilon V V_x + \eta_x = 0 \quad \text{where} \quad V = u - \frac{\delta^2}{3}u_{xx},$$

The second GN equation - first order in ε, δ:

$$\eta_t + V_x + \frac{\delta^3}{3}V_{xxx} + \varepsilon(\eta V)_x = 0$$

rescaling and shift in η leads to the Kaup - Boussinesq system

$$\begin{aligned} V_t + VV_x + \eta_x &= 0 \\ \eta_t + V_{xxx} + (\eta V)_x &= 0, \end{aligned}$$

which is integrable, with Lax pair

$$\begin{aligned} \Psi_{xx} &= \Big((\zeta - \frac{1}{2}V)^2 - \eta\Big)\Psi, \\ \Psi_t &= -(\zeta + \frac{1}{2}V)\Psi_x + \frac{1}{4}V_x\Psi. \end{aligned}$$

References

[1] R.S. Johnson, *A modern introduction to the mathematical theory of water waves*, Cambridge: Cambridge University Press (1997).

[2] R.S. Johnson, Camassa-Holm, Korteweg-de Vries and related models for water waves. *J. Fluid. Mech.* **457** (2002) 63.

[3] A.E. Green and P.M. Naghdi, A derivation of equations for wave propagation in water of variable depth. *J. Fluid Mech.* **78** (1976) 237-246.

[4] A. Constantin and R. Ivanov, On an integrable two-component Camassa-Holm shallow water system, *Phys. Lett. A*, **372** (2008) 7129–7132.

[5] P. Olver and P. Rosenau, Tri-Hamiltonian duality between solitons and solitary-wave solutions having compact support, *Phys. Rev. E* **53** (1996) 1900.

[6] R. Camassa and D.D. Holm, An integrable shallow water equation with peaked solitons, *Phys. Rev. Lett.* **71** (1993) 1661.

Numerical Solution of Elliptic and Parabolic Problems on Disjoint Domains

Bosko Jovanovic, Miglena Koleva, Lubin Vulkov

1. Introduction. Let $\Omega_1, \ldots, \Omega_m$ are *disjoint* bounded domains in $R^N (N = 1, 2, 3)$, separated from each other by a transparent medium Ω_0, see for example Figure 1. A stationary heat process in a system of black bodies $\Omega_i, i = 1, \ldots, m$ with *different materials* properties is described by the elliptic problem [1, 2, 8]

$$(\mathbf{E}) \qquad \begin{array}{c} Lu \equiv -\mathrm{div}(A(x,u)\nabla u = f(x,u),\ x \in \Omega_i,\ i = 1, 2, \ldots, m, \\ (A(x,u)\nabla u, n(x)) + H(u) = \int_{\partial\Omega} h(u(\xi))\varphi(\xi, x)d\sigma(\xi) + g(x),\ x \in \partial\Omega, \end{array}$$

where for the matrix A (*ellipticity*): $k|\xi| \leq (A(x,u)\xi, \xi)\ \ \forall\, \xi \in R^N,\ k = const > 0$. Existence and uniqueness of positive weak and strong solutions for $1D$ and $2D$ problems are reported in [1]. We also discuss the following parabolic problem [2],

$$(\mathbf{P}) \qquad \begin{array}{c} \rho\frac{\partial u}{\partial t} + Lu = f(x,t,u),\ (x,t) \in Q_T = \Omega \times (0,t), \\ (A(x,t,\nabla u), n(x)) + H(u(x,t)) = \int_{\partial\Omega} h(u(\xi,t))\varphi(\xi,x,t)d\sigma(\xi) + y(x,t), \\ (x,t) \in S \equiv \partial\Omega \times (0,T);\quad u(x,0) = u_0(x),\ x \in \Omega. \end{array}$$

The problems (E) and (P) concern heat exchange that is a significant factor in modern technology. In this field of industrial applications, for example crystal growth, has motivated a lot of mathematical work on this topic. Here we discuss a simple physical model of system $\Omega = \Omega_1 \cup \Omega_2$ (see Fig. 1) where $\Omega_1 = (a_1, b_1) \times (c_1, d_1)$ and $\Omega_2 = (d_2, b_2) \times (c_2, d_2)$, that in fact is a union of two disjoint, conductive and opaque domains in R^2 surrounded by a transparent medium Ω_0. They represent opaque bodies with different material properties. We assume that all material are grey materials, see [2]. Therefore, radiation only needs to be considered at the surface of the bodies $\Omega_1, \Omega_2 : \partial Rad = \partial\Omega_1 \cup \partial\Omega_2$. To this aim, a kernel $w : \partial\Omega_{Rad} \times \partial\Omega_{Rad} \to R$ the so called *view factor*, is introduced by

$$w(\xi,\eta) = \begin{cases} \frac{(n(\xi),\eta-\xi)(n(\eta),\xi-\eta)}{b_N(\xi-\eta)^{N+1}} & if [\xi,\eta] \cap \Omega = \emptyset \\ 0 & if [\xi,\eta] \cap \Omega = \emptyset, \end{cases}$$

where $b_N = \mathrm{mes}S_{N-1}/(N-1)$, S_{N-1} is the unit sphere in R^{N-1}, in particular $b_2 = 2, b_3 = \pi$. The problem of radioactive transfer was first considered by A. Tikhonov in [8]. He proved the unique solvability in "small" of the IBVP for the heat equation $\partial u/\partial u = \triangle u$. The next problem considers heat transfer in a wall consisting of two parallel layers (Ω_1 and Ω_2) enclosing an air cave (Ω_0) , see again Fig. 1 for a cross section. The cavity is neither ventilated, nor heated. At the surfaces Γ_{10} and Γ_{20} heat is transferred by convection from the layers to the air, which is assumed to be at an a priori unknown temperature $T(t)$, uniformly throughout the cavity. The radiation between the surfaces of the cavity is neglected. At parts Γ_i of the "outer"

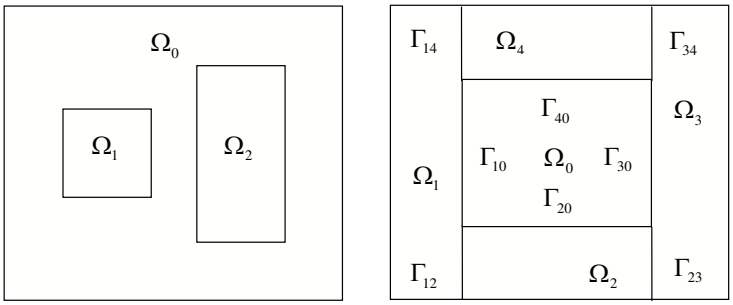

Figure 1: Domain Ω

boundary of $\Omega_i, i = 1, 2, \ldots$ there is a convective heat transfer to the surrounding medium at temperature zero, while at the complementary parts Γ_i' of that outer boundary the temperature is kept at the value zero. The initial temperature of the layers is given.

The $2D$ mathematical problem reads: find the functions $u_i(x, y, t)$, for $(x, y) \in \Omega_i (i = 1, 2)$, which obey the heat conduction equations (1), along with radiation boundary conditions (2), (3), zero Dirichlet outer boundary conditions and some initial conditions at assumptions (4)-(6).

There exist different physically important extensions of the above model problems that could be treated theoretically in a similar way. For example, the composite structure shown in Figure 1 (right), where the rectangles $\Omega_1, \ldots, \Omega_4$ enclose the rectangle Ω_0, corresponds to problem of type (1)-(5) with radiation boundary conditions

$$p_1(b_1, y)\frac{\partial u_1}{\partial x}(b_1, y, t) = h^{10}(u_1 - T) \text{ on } \Gamma_{i0},$$

$$-p_2(a_2, y)\frac{\partial u_2}{\partial x}(a_2, y, t) = h^{20}(u_2 - T) \text{ on } \Gamma_{20},\ T(t) = \frac{\int_{\Gamma_{10}} h^{10}u_1 ds + \int_{\Gamma_{20}} h^{20}u_2 ds}{\int_{\Gamma_{10}} h^{10} ds + \int_{\Gamma_{20}} h^{20} ds},$$

with some jump (interface) conditions

$$u_i|_{\Gamma_{ij}} - u_j|_{\Gamma_{ji}} = 0,\ \ p_i\frac{\partial u_i}{\partial x}|_{\Gamma_{ij}} - p_j\frac{\partial u_j}{\partial x}|_{\Gamma_{ij}} = 0,\ \ i < j,\ \ i, j = 1, 2, 3, 4.$$

Numerical results of problems of the type described are obtained in the papers [3]-[7].

2. Iterative Processes. At appropriate nonlinearities $f(\cdot, u)$, $H(u)$ and $h(u)$, the problems (E), (P) could be solved numerically by iterative processes, based on the theory of lower (upper) solutions. Let us consider the iterative process for problem

(P):

$$\rho(x)\frac{\partial u^{n+1}}{\partial t} - \mathrm{div}(A(x)\nabla u^{n+1}) = f(x,t,u^n),$$

(**L**)

$$(A(x)\nabla u^{n+1}, n(x)) + z(x,u_{n+1},u^n) = \int_{\partial\Omega} h(u_n(\xi))\varphi(\xi,x)d\sigma(\xi) + g(x,t).$$

Such a process is characterized by the choice of the function z and the initial guess $u^0(x)$. The unknown function $u(x,t)$ has the physical meaning of absolute temperature, $f(x,t)$ and $g(x,t)$ are heat source and flux densities, $H(x,u) = r(x,u) + h(u)$, $r(u)$, characterizes convective heat transfer while $h(u) = \sigma_0(u)^3 u$ at $u > 0$ is the surface radiation flux density and corresponds to Stefan-Boltzmann radiation law. Let $u \in H_2^1(\Omega)$ and $H(u) \in L_1(\partial\Omega)$. On the space $v = H_2^1(\Omega) \cap L_\infty(\Omega)$ We define the linear functionals $A(t,u), B(t,u)$ and $J(t)$ setting:

$$\langle A(t,u),v)\rangle_\Omega = \int_\Omega (A(x,t)\nabla u, \nabla v)dx,\ \langle J(t),v)\rangle = (f(t),v)_\Omega + (g(t),v)_{\partial\Omega},$$
$$\langle B(t,u),v)\rangle = \int_{\partial\Omega} uvd\sigma - \int\int_{\partial\Omega\times\partial\Omega} u(\xi)\varphi(\xi,x)v(x)d\sigma(\xi)d\sigma(x).$$

Lower (upper) solution is defined as a function u for which the integral inequality

$$-\int_0^T (\rho u(t),v)_\Omega \frac{d}{dt}\eta(t) + \int_0^T \langle A(t,u),v\rangle > \eta(t)dt \underset{(\geq)}{\leq} (\rho u^0,v)_\Omega + \int_0^T \langle J(t),v\rangle\eta(t)\eta(0)$$

is valid for all V and all $\eta \in C^\infty[0,T]$ such that $\eta(T) = 0$. In a work in progress of the authors, existence of minimal and maximal solutions, convergence for sequences lower and upper solutions and construction of function $z(x,u_{n+1},u_n)$ are studied.

3. A Linear Model Problem. As a model linear problem, corresponding to (L), we consider the following initial-boundary-value problem (IBVP): Find functions $u_i(x,y,t)$ in $\Omega_i \equiv (a_i,b_i)\times(c,d)$, $i = 1,2$; $t > 0$ that satisfy the system of parabolic equations

$$\frac{\partial u_i}{\partial t} - \frac{\partial}{\partial x}\left(p_i(x,y)\frac{\partial u_i}{\partial x}\right) - \frac{\partial}{\partial y}\left(q_i(x,y)\frac{\partial u_i}{\partial y}\right) + r_i(x,y)u_i = f_i(x,y,t),\ i = 1,2, \quad (1)$$

the nonlocal interface conditions

$$p_1(b_1,y)\frac{\partial u_1}{\partial x}(b_1,y,t) + \alpha_1(y)u_1(b_1,y,t) = \int_{c_1}^{d_1} \beta_1(y,y')u_2(a_2,y',t)\,\mathrm{d}y', \quad (2)$$

$$-p_2(a_2,y)\frac{\partial u_2}{\partial x}(a_2,y,t) + \alpha_2(y)u_2(a_2,y,t) = \int_{c_2}^{d_2} \beta_2(y,y')u_1(b_1,y',t)\,\mathrm{d}y', \quad (3)$$

with outer zero Dirichlet boundary conditions and given initial conditions. Throughout the paper we assume that the input data satisfy the usual regularity and ellipticity conditions

$$p_i(x,y),\ q_i(x,y),\ r_i(x,y) \in L_\infty(\Omega_i), \quad i = 1,2, \quad (4)$$

$$0 < p_{i0} \leq p_i(x,y), \quad 0 < q_{i0} \leq q_i(x,y), \quad 0 \leq r_i(x,y) \quad \text{a.e. in } \Omega_i, \quad i = 1,2 \quad (5)$$

and

$$\alpha_i \in L_\infty(c_i, d_i), \quad \beta_i \in L_\infty\left((c_1, d_1) \times (c_2, d_2)\right), \quad i = 1, 2. \tag{6}$$

In real physical problems (see [1, 2]) we also have $\alpha_i > 0\,, \quad \beta_i > 0, \quad i = 1, 2.$
In a new paper of the authors, well posedness of this problem in the space

$$W(0,T) = \{u|\ u \in L_2((0,T), H_0^1), \frac{\partial u}{\partial t} \in L_2((0,T), H^{-1})\}$$

is established. Also, results for the rate of convergence of difference schemes are obtained.

Acknowledgement. The research of the first author was supported by the Ministry of Science of Republic of Serbia under project # 144005A. The research of the second and the third authors was supported by the Bulgarian Fund for Science under the Project Bg-Sk-203.

References

[1] A. A. Amosov, Global solvability of a nonlinear nonstationary problem with a nonlocal boundary condition of radiative heat transfer type, Diff. Eqns. 41 (2005) 96-109.

[2] P. -E. Druet, Weak solutions to a time-dependent heat equation with nonlocal radiation condition and right hand side $L^p (p \geq 1)$. WIAS Preprint 1253 (2008).

[3] B. S. Jovanović, L. G. Vulkov, Numerical solution of a parabolic transmission problem, IMA J. Numer. Anal. (2009) (to appear).

[4] B. S. Jovanović, L. G. Vulkov, Numerical solution of a hyperbolic transmission problem, Comp. Meth. in Appl. Math. 4, N 4 (2009) 374 - 385.

[5] B. S. Jovanović, L. G. Vulkov, Finite difference approximations for some interface problems with variable coefficients, Appl. Numer. Math. 59 (2009) 349 - 372.

[6] M. Koleva, Finite element solution of boundary value problems with nonlocal Jump Conditions, J. of Math. Modl. and Anal. 13, N 3 (2008) 383-400.

[7] M. Koleva, L. Vukov, A two-grid approximation of an interface problem for the nonlinear Poisson-Boltzmann equation, Lect. Notes in Comp. Sci. 5434 (2009) 369-376.

[8] A. N. Tikhonov, On functional equations of the Volterrra type and their applications to someproblems of mathematical physics, Byull. Mosk. Gos. Univ., Ser. Mat. Mekh. 1, N 8 (1938) 1-25.

On the Numerical Simulation of Surface Forces Acting on AFM Tip

Natalia Kolkovska, Radomir Slavchov, Daniela Vasileva

AFM is a powerful tool for probing the surface double layer and surface electric properties as a whole. It was used to test the surface charge densities of dielectric surfaces, cell membranes and others [1]. The interpretation of AFM measurements is, however, hindered by the complexity of surface forces acting between the AFM tip and the analyzed surface. Main components of these forces are

1. the electrostatic forces due to effects from the overlapping of the AFM tip and the investigated surface double layers;
2. the image forces due to the tip low dielectric permittivity, which also deforms the double layers.

Most AFM tips carry little or no surface charge densities, so the second effect is presumably of greater importance. The image forces for macroscopic objects are due to differences in bulk dielectric permittivities of the interacting bodies in the system investigated. However, when the sizes of the objects and the distances between them becomes of the order of nanometers, as a general rule, it is not only the bulk but also the surface properties which govern the behaviour of this microscopic system. Therefore, one can expect at such small distances, the surface dielectric properties to play a significant role.

This work is giving a detailed analysis of this statement. The main question it is trying to answer is, can surface dielectric permittivities of tip-water and water-dielectric give a strong addition to the image force pulling the AFM tip toward the dielectric surface investigated. The surface dielectric permittivity was introduced in [2], and it was shown that it may rise additional surface image forces in case of charges at small distances to dielectric interfaces [3].

Mathematical model. In the case of an AFM tip, probing a dielectric, three subdomains are considered – the AFM tip, water and dielectric (see Fig.1). We suppose that the AFM tip is a cone with a spherical end, and the problem is axisymmetric. Then if cylindrical coordinates (r, ϕ, z) are used, the equation for the potential $\varphi(r, z)$ in each subdomain is

$$\nabla^2\varphi = \frac{1}{r}\frac{\partial}{\partial r} r \frac{\partial \varphi}{\partial r} + \frac{\partial^2 \varphi}{\partial^2 z} = k^2 \varphi,$$

where k is the reciprocal Debye length of the corresponding medium.

There are two interface surfaces – tip-water and water-dielectric. On each of them the surface dielectric permittivities are modifying the conditions of the Gauss law: the displacement field jump at each surface is given by

$$D_N^+ - D_N^- + \boldsymbol{\nabla^s} \cdot \boldsymbol{D^s} = \rho^s,$$

where

$$D_N^{\pm} = -\varepsilon^{\pm} \boldsymbol{n} \cdot \boldsymbol{\nabla} \varphi^{\pm} = -\varepsilon^{\pm} \frac{1}{\sqrt{1 + {z_s'}^2}} \left(\frac{\partial \varphi^{\pm}}{\partial z} - z_s' \frac{\partial \varphi^{\pm}}{\partial r} \right),$$

$$\boldsymbol{\nabla^s} \cdot \boldsymbol{D^s} = -\frac{\varepsilon^s}{r\sqrt{1 + {z_s'}^2}} \frac{d}{dr} \left(\frac{r}{\sqrt{1 + {z_s'}^2}} \frac{d\varphi^s}{dr} \right),$$

the surface is defined by $z = z_s(r)$, $\varphi^s(r) := \varphi(r, z_s(r)) = \varphi^+(r, z_s(r)) = \varphi^-(r, z_s(r))$ is the restriction of the potential over the surface, $\varepsilon^+, \varepsilon^-, \varepsilon^s$ are non-negative constants, and ρ may be a constant or a function of φ.
On the water-dielectric surface $z_s' = 0$ and the corresponding interface condition becomes

$$-\varepsilon^+ \frac{\partial \varphi^+}{\partial z} + \varepsilon^- \frac{\partial \varphi^-}{\partial z} - \varepsilon^s \frac{1}{r} \frac{d}{dr} r \frac{d\varphi^s}{dr} = \rho^s.$$

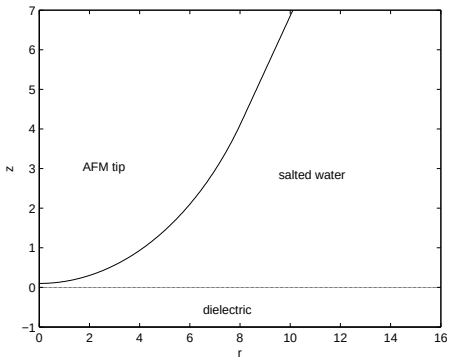

Fig.1

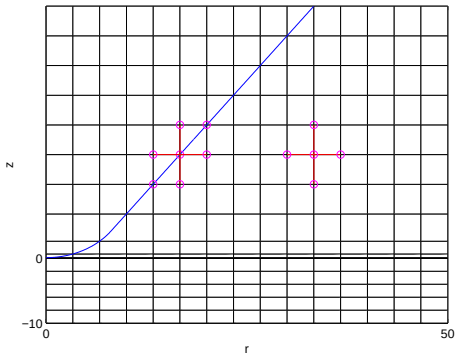

Fig.2

Numerical method. The finite difference method on a non-uniform grid, aligned with both interfaces, is used (see Fig.2). The main peculiarities of the difference scheme are

- In the subdomains, standard 5-points stencils are used (see [4] for approximation in cylindrical coordinates);
- on the interfaces, first order approximation for normal derivatives is used, i.e., the grid points, included in the standard 5-points stencils;
- in order to approximate the "surface" part $\boldsymbol{\nabla^s} \cdot \boldsymbol{D^s}$ in the interface conditions, we use two additional points – the neigbours, lying on the surface (see Fig.2);
- in order to approximate the equations on the left boundary ($r = 0$) we use that $\lim\limits_{r \to 0} \dfrac{\partial \varphi(r,z)}{r} = \dfrac{\partial^2 \varphi(0,z)}{\partial r^2}$ (see [4]) and then the natural symmetric boundary condition is imposed;
- on the bottom and the right boundaries the exact solution of the problem without the AFM tip is used;

- on the top boundary $\frac{\partial \varphi}{\partial \tau} = 0$ is imposed, where τ is tangential to the AFM tip surface.

The linear system obtained after discretisation, is solved using ILU preconditioned BiCGStab method.

Results. Let the end of the tip be a sphere with a radius 10 nm, $k = 0$, $\varepsilon = 2$ nm in the AFM tip subdomain, $k = 0.07\,\mathrm{nm}^{-1}$, $\varepsilon = 80$ nm in the water, $k = 0$, $\varepsilon = 2$ nm in the dielectric.

Example 1. Let the distance between the tip and the dielectric be 0.1 nm. First we solve a problem neglecting the surface dielectric permittivities, i.e., $\varepsilon^s = 0$, $\rho = 0$ on the tip-water surface, $\varepsilon^s = 0$, $\rho = 0.224\,\mathrm{V/nm}$ on the water-dielectric surface. After that we consider two cases, where the surface dielectric permittivities on both interfaces are set to $\varepsilon^s = 10$ nm and $\varepsilon^s = 100$ nm correspondingly. In Table 1 we compare results for the maximum of the potential (it is on the dielectric surface – at $(r, z) = (0, 0)$), obtained on a sequence of embedded grids ($l = 0, 1, 2, \ldots, 5$ denotes the number of the grid, starting from the coarsest, presented in Fig.2, with $16 \times 21 = 336$ grid points). The factor

$$\alpha = \log_2 \frac{\varphi_{l-1} - \varphi_{l-2}}{\varphi_l - \varphi_{l-1}}$$

shows first order of convergence. In the last row of the table the value of φ, obtained by extrapolation from the last two levels, is given. It is seen that the surface dielectric permittivities influence essentially the potential, and the difference between the solutions without and with accounting for the surface dielectric permittivities is greater for greater values of ε^s.

Table 1

		$\varepsilon^s = 0$			$\varepsilon^s = 10$ nm			$\varepsilon^s = 100$ nm		
l	#points	$\varphi(0,0)$	$\varphi_{l-1} - \varphi_l$	α	$\varphi(0,0)$	$\varphi_{l-1} - \varphi_l$	α	$\varphi(0,0)$	$\varphi_{l-1} - \varphi_l$	α
0	336	1.36e-1			9.69e-2			6.46e-2		
1	1271	1.05e-1	3.09e-2		8.65e-2	1.04e-2		6.14e-2	3.26e-3	
2	4941	9.67e-2	8.31e-3	1.9	8.27e-2	3.81e-3	1.5	6.00e-2	1.34e-3	1.3
3	19481	9.34e-2	3.22e-3	1.4	8.09e-2	1.81e-3	1.1	5.93e-2	6.77e-4	1.0
4	77361	9.19e-2	1.53e-3	1.1	8.00e-2	8.94e-4	1.0	5.90e-2	3.37e-4	1.0
5	308321	9.11e-2	7.52e-4	1.0	7.96e-2	4.43e-4	1.0	5.88e-2	1.66e-4	1.0
extrapolated		9.04e-2			7.91e-2			5.87e-2		

Example 2. Let the distance between the tip and dielectric be 1 nm, and all other parameters be as in Example 1. The results shown in Table 2 confirm the first order of convergence of the solutions. The surface dielectric permittivities influence the potential, but as the distance between the tip and dielectric is larger, the influence is weaker.

Table.2

		$\varepsilon^s = 0$			$\varepsilon^s = 10\,\mathrm{nm}$			$\varepsilon^s = 100\,\mathrm{nm}$		
l	#points	$\varphi(0,0)$	$\varphi_{l-1} - \varphi_l$	α	$\varphi(0,0)$	$\varphi_{l-1} - \varphi_l$	α	$\varphi(0,0)$	$\varphi_{l-1} - \varphi_l$	α
0	336	7.71e-2			7.33e-2			5.95e-2		
1	1271	7.11e-2	6.32e-3		6.80e-2	5.24e-3		5.67e-2	2.80e-3	
2	4961	6.84e-2	2.38e-3	1.4	6.60e-2	2.06e-3	1.4	5.56e-2	1.14e-3	1.3
3	19481	6.72e-2	1.14e-3	1.1	6.50e-2	1.01e-3	1.0	5.50e-2	5.73e-4	1.0
4	77361	6.67e-2	5.65e-4	1.0	6.45e-2	5.03e-4	1.0	5.47e-2	2.87e-4	1.0
5	308321	6.64e-2	2.80e-4	1.0	6.42e-2	2.50e-4	1.0	5.46e-2	1.43e-4	1.0
extrapolated		6.61e-2			6.40e-2			5.45e-2		

Conclusion. The results show that the surface dielectric permittivities influence essentially the potential, and so the image forces acting at the AFM tip and dielectric surfaces. This influence is stronger when the distance between the AFM tip and the dielectric surface is smaller.
Future work includes

- Testing other shapes for the end of the AFM tip;
- Comparison with experiments;
- Second order approximation;
- Applying immersed interface method or finite element method;
- Solving 3D problems – the tip is usually a pyramid;
- Local refinement;
- Fast solvers for the linear system;
- Simulating moving tip and moving membrane.

References

[1] Sachs, F.: Probing the double layer: Effect of image forces on AFM. Biophysical J. 91(2), 2006, L14-L15.

[2] Badeaux: Bedeaux, D., Vlieger, J.: Optical properties of surfaces. London: Imperial College Press, 2001.

[3] Slavchov, R: On the theory of the charged heterogeneous surfaces. Electric interactions in Langmuir monolayers and semiconductor surfaces. PhD Thesis, Sofia 2008.

[4] Samarskii, A.A.: The Theory of Difference Schemes, Moskva, Nauka, 1977 (in Russian), English translation CRC Press, 2001, 786 p.

Intelligent Approaches for Radiolocational Monitoring

Milena Kostova, Valerij Djurov

1 Introduction

The radiolocational monitoring (RM) performs exploration, watching and recognition of dynamic objects, in order to ensure control of the civil aviation, air terrorist attack prevention, and in a military situation, helping the anti-aircraft defence (AAD). The implementation of RM is made by radiolocational stations (RS) with phased antenna grid (PAG), working with complicated, wide band, coherent signals. In the modern RS are set the principals of radioholography are set. According to the geometrical theory of Keler‘s diffraction, and the radiolocational model of Dilano, the object is being presented as a combination of shining elementary transmitters, found in a different kinematic condition over the surface of the monitored object. In most cases the coherent RS working in S, X and K frequency band (according to NATO‘s standards), give a possibility for the reception of high quality radioholograms. A number of various methods and means for reconstruction of holograms exist, leading to 2D images (radioholographic images). The images received through the processing of complex radioholograms registered at ground monitoring radiolocational stations, are distinguished with their specific features. They have an outline character, and its quality depends on the parameters of the sound (out) monitoring impulse and from the implementation (construction) of the observed object (coating, shape, trajectory parameters).
With the development of the modern nanotechnologies are created a number of preconditions for the construction of new materials, which have new properties and qualities. The electrical and magnetic constants are being changed; the reflection coefficient; the ferrite properties of the materials. This calls for developing methods and algorithms for recognition of objects with complicated geometry, but with standard technical accomplishment, and also of dynamic objects with a low efficiency reflection surface (Stealth technologies, meta-materials, cold plasma coating). In the modern developments on the basis of the aperture synthesis in the classic modern RS with a high allowing ability with a step changing of the frequency in packets, a realization of a high quality monitoring even in some objects with non-standard accomplishment is possible. Generally speaking, the radioholographic methods cannot always lead to a receiving of an image of the object. This calls for an implementation of other signs of recognition, which to add the great number of signs connected with the silhouette of the object. One approach is the using of the polarisation as a reason of a radioholographic recognition, i.e. the negative reflection coefficients are possible only over the horizontal or vertical (line).
No matter the approach for the RM, the input data have a fuzzy and inaccurate character. This leads to the usage of ”intelligent” modules to the systems for RM, which to process data in real time from objects with a complicated geometry and

non-standard technology.

2 Intelligent block for recognition of dynamic objects with a standard and non-standard technology of implementation

It is being proposed a mathematical model of a block for the recognition of a dynamic object with an application of forms of artificial intelligence (expert system (ES), fuzzy logic (FL), cellular neural network (CNN), probability neural network (PNN). The intelligent block consists of two modules and a module for the recognition of dynamic objects with a complicated geometry and standard implementation, and a module for the recognition of dynamic objects with non-standard implementation technology. The block is made on the principals of ES. The quality of the radiohologram is being determined by the level of the reflected signals entering in the reception trac.t (At the information is being lead to the module for processing of objects with a standard implementation. At ¡ the information is being lead to the module for processing of objects with a non-standard implementation.

2.1 An intelligent block for the recognition of a dynamic object with a standard technology

The application of radioholographic approaches at the recognition of dynamic objects with a complicated geometry, but traditional technological implementation leads to a receiving of a radioholographic image with a good quality. The image is being put over an additional processing, connected with filtration of the common noise background, and impulse noise, receiving a b/w image and taking a contour of the object. An intelligent module is being synthesized for processing and recognition of a radioholographic image, which consists a cellular neural network in the quality of a digital filter with masks MERIAN and DIFFUS. The segmentation is made with an adaptive threshold level defining itself by Otsu‘s method. The outline is extracted by a gradient operator according to Roberts method. The module consists two classifiers on the basis of fuzzy logic and probability neural network, which can classify 32 types of aircrafts in three classes – specific, military and transport depending on the quantity characteristics of three informative geometric signs: (A, α, L_1). A is the width to length ratio of the object; α - a slope toward the fuselage axis of the straight line connecting the geometrical center and the most distant point of one of the wing, L_1 – the difference "geometric middle – geometric center". The module makes an additional classification of the transport aircrafts in seven groups An with 2,4 and 6 engines, Boeing with 2 and 4 engines and Airbus with 2 and 4 engines, depending on the quantity characteristic of the forth geometrical sign – L_2 (wing length). The classifier on the fuzzy logic basis for military aircrafts achieves 60% correct classification and it does not classify 40%, and for transport aircrafts achieves 100% correct classification. Three of the correctly classified transport aircrafts recognizes as other

type. The classifier on the basis of probability neural network for military aircrafts achieves 95% correct classification. One aircraft is classified incorrectly. It is achieved a 100% correct classification of transport aircrafts. Three of the correctly classified aircrafts are been recognized as another type.

2.2 Recognition of a dynamic object with a non-standard technology

2.2.1 Common characteristics of non-standard technologies

- Stealth technologies
A Stealth implementation is a combination of measures for realization of a form of coating with an aim for reducing of the radiolocational visibility of the objects on the radar.
- Metamaterial technologies
The main ability of the metamaterial technologies is the inclusion of precious materials – gold and silver in the composition of articles for causing a negative reflection coefficient. The distance and sizes of the gold and silver are influenced by the length of the wave, which sounds (out) the object
- Plasma coating
The usage of plasma coating is very important for the reduction of the radiolocational reflection in a wide frequency range of 20Hz – 20GHz. In an exact volume is made a cloud of highly concentrated concentric charges, which are moving chaotically but they are subordinated in some order.

2.2.2 An expert system for the recognition of a dynamic object with a non-standard technology

The low level of reflected signal requires confronting of the polarization vertically A_V and horizontally A_H. Depending the correlation $\frac{A_H}{A_V}$ is being determined the specification of the non-standard technology.
At $|\frac{A_H}{A_V}| \geq 0,3$ the object is with a metamaterial implementation. The reading of such objects is made by changing the polarisation, which changes around 30% vertically towards horizontally and reverse. The coefficient of depolarisation δ_p is also being reviewed. Expert knowledge is needed for substantiation and analysis of diffraction and absorption of waves resonant to short waves in a dielectric medium. In this case is possible a recognition of the object through its one dimension radiohologram.
If $|\frac{A_H}{A_V}| < 0,3$ the object could be with a plasma or Stealth implementation. The approach requires a multi frequency reading on the reflected signals with a step $\Delta\lambda = 1cm$. If $A_i = \sqrt{A_H^2 + A_V^2}$ for λ_i and $\sum_{i=1}^{n} \sqrt{A_H^2 + A_V^2} \geq \sigma_{lim}$ we have got an object with Stealth implementation.
At linear frequency changing sound (out) signal for Stealth objects implementation is possible to be seen contour outlines, giving the possibility for processing and analysis of the objects. The expert knowledge for the types of Stealth technologies are connected with a reverse aperture synthesis, theory of FAR, complex signals, multi

frequency sound (out) impulses etc. At high allowing ability of the sound (out) signal (0.3 - 0.5m) can be reported multiple reflertion points of the surface of the aircraft (object). If we note, that a STEALTH implementation is a type of "flying wing", it is enough to be readed only points of parts of the object, as at statistical processed data are established the regression models for an object type "flying wing" at certain angles of azimuth place at the change of the angle over azimuth with a certain length of the sound (out) signal λ.
If $\sum_{i=1}^{n} \sqrt{A_H^2 + A_V^2} < \sigma_{lim}$ we have got an object with a plasma coating. The reflected signals from the monitored object at deposition give a spot, which could be processed with algorithms on the basis of the fractal theory. This approach gives a possibility of indirect defining of the size of the object through the number of reiterations of the own kind's fractal structures. It could be said, that the disorder is in a defined stability connected with the movement of the observed object. The changes of the atractor is connected with the speed of the dynamic object.

Efficient Solution of μFEM Elasticity Problems in the Case of Almost Incompressible Materials

Nikola Kosturski, Svetozar Margenov, Yavor Vutov

The presented study is motivated by the development of methods, algorithms, and software tools for μFE (micro finite element) simulation of human bones. The voxel representation of the bone micro structure is obtained from a high resolution computer tomography (CT) image.

Linear elasticity models at micro and macro levels are applied. The reference volume element (RVE) has a strongly heterogeneous micro structure composed of solid and fluid phases (see Figure 1). Here, we consider a model of the RVE in which the fluid phase is treated as an almost incompressible elastic material.

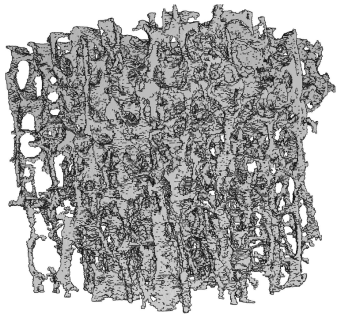

Figure 1: Structure of a human bone

Let $\Omega \subset \mathbb{R}^3$ be a bounded domain with boundary $\Gamma = \Gamma_D \cup \Gamma_N = \partial\Omega$ and $\mathbf{u} = (u_1, u_2, u_3)$ the *displacements* in Ω. The components of the *small strain tensor* are

$$\varepsilon_{ij} = \frac{1}{2}\left(\frac{\partial u_i}{\partial x_j} + \frac{\partial u_j}{\partial x_i}\right), \quad 1 \le i, j \le 3$$

and the components of the *Cauchy stress tensor* are

$$\sigma_{ij} = \lambda\left(\sum_{k=1}^{3} \varepsilon_{kk}\right)\delta_{ij} + 2\mu\varepsilon_{ij}, \quad 1 \le i, j \le 3.$$

Here λ and μ are the Lamé coefficients, which can be expressed by the elasticity modulus E and the Poisson ratio $\nu \in (0, 0.5)$ as follows

$$\lambda = \frac{E\nu}{(1+\nu)(1-2\nu)}, \quad \mu = \frac{E}{2+2\nu}.$$

Now, we can introduce the Lamé's *system of linear elasticity* (see, e.g., [1])

$$\sum_{j=1}^{3} \frac{\partial \sigma_{ij}}{\partial x_j} + f_i = 0, \quad i = 1, 2, 3 \tag{1}$$

equipped with boundary conditions

$$\begin{aligned} u_i(\mathbf{x}) &= g_i(\mathbf{x}), \quad \mathbf{x} \in \Gamma_D \subset \partial\Omega, \\ \textstyle\sum_{j=1}^{3} \sigma_{ij}(\mathbf{x}) n_j(\mathbf{x}) &= h_i(\mathbf{x}), \quad \mathbf{x} \in \Gamma_N \subset \partial\Omega. \end{aligned}$$

The *weak formulation* of (1) can be written in the form (see, e.g., [2]): for a given $\mathbf{f}$ find $\mathbf{u}$ such that for each $\mathbf{v}$

$$a(\mathbf{u},\mathbf{v}) = -\int_\Omega (\mathbf{f},\mathbf{v})dx + \int_{\Gamma_N} (\mathbf{h},\mathbf{v})dx.$$

Crouzeix–Raviart (C.–R.) nonconforming linear finite elements are used to discretize the Lamé system of elasticity. Let us note that the C.–R. elements (after a proper modification of the related bilinear form) provide a locking-free approximation of almost incompressible elasticity problems.
The bilinear form a can be written as

$$a(\mathbf{u},\mathbf{v}) = \int_\Omega (Cd(\mathbf{u}), d(\mathbf{v})) = \int_\Omega (C^* d(\mathbf{u}), d(\mathbf{v})) = a^*(\mathbf{u},\mathbf{v}), \tag{2}$$

where

$$d(\mathbf{u}) = \left(\frac{\partial u_1}{\partial x_1}, \frac{\partial u_1}{\partial x_2}, \frac{\partial u_1}{\partial x_3}, \frac{\partial u_2}{\partial x_1}, \frac{\partial u_2}{\partial x_2}, \frac{\partial u_2}{\partial x_3}, \frac{\partial u_3}{\partial x_1}, \frac{\partial u_3}{\partial x_2}, \frac{\partial u_3}{\partial x_3}\right)^T$$

and the matrices C and C^* are

$$C = \begin{bmatrix} \lambda+2\mu & 0 & 0 & 0 & \lambda & 0 & 0 & 0 & \lambda \\ 0 & \mu & 0 & \mu & 0 & 0 & 0 & 0 & 0 \\ 0 & 0 & \mu & 0 & 0 & 0 & \mu & 0 & 0 \\ 0 & \mu & 0 & \mu & 0 & 0 & 0 & 0 & 0 \\ \lambda & 0 & 0 & 0 & \lambda+2\mu & 0 & 0 & 0 & \lambda \\ 0 & 0 & 0 & 0 & 0 & \mu & 0 & \mu & 0 \\ 0 & 0 & \mu & 0 & 0 & 0 & \mu & 0 & 0 \\ 0 & 0 & 0 & 0 & 0 & \mu & 0 & \mu & 0 \\ \lambda & 0 & 0 & 0 & \lambda & 0 & 0 & 0 & \lambda+2\mu \end{bmatrix},$$

$$C^* = \begin{bmatrix} \lambda+2\mu & 0 & 0 & 0 & \lambda+\mu & 0 & 0 & 0 & \lambda+\mu \\ 0 & \mu & 0 & 0 & 0 & 0 & 0 & 0 & 0 \\ 0 & 0 & \mu & 0 & 0 & 0 & 0 & 0 & 0 \\ 0 & 0 & 0 & \mu & 0 & 0 & 0 & 0 & 0 \\ \lambda+\mu & 0 & 0 & 0 & \lambda+2\mu & 0 & 0 & 0 & \lambda+\mu \\ 0 & 0 & 0 & 0 & 0 & \mu & 0 & 0 & 0 \\ 0 & 0 & 0 & 0 & 0 & 0 & \mu & 0 & 0 \\ 0 & 0 & 0 & 0 & 0 & 0 & 0 & \mu & 0 \\ \lambda+\mu & 0 & 0 & 0 & \lambda+\mu & 0 & 0 & 0 & \lambda+2\mu \end{bmatrix}.$$

Let us note, that the equality (2) holds when the condition

$$\int_\Omega \frac{\partial u_i}{\partial x_j}\frac{\partial u_j}{\partial x_i}dx = \int_\Omega \frac{\partial u_i}{\partial x_i}\frac{\partial u_j}{\partial x_j}dx$$

is fulfilled. More details can be found in [2]. This is known to be the case when the boundary value problem has pure Dirichlet boundary conditions. However, the

same modification of the bilinear form holds true for RVE with constant Dirichlet boundary conditions on the normal displacements, which is exactly the case of the applied numerical upscaling scheme.
The following numerical tests illustrate the robustness (locking-free approximation) of the C.–R. FEM approximation in the case of almost incompressible materials. We consider a simple model problem in the unit cube $[0,1]^3$ with Dirichlet boundary conditions on the whole boundary and a given exact solution $u_1(x,y,z) = x^3 + \sin(y+z)$, $u_2(x,y,z) = y^3 + z^2 - \sin(x-z)$, $u_3(x,y,z) = x^2 + z^3 + \sin(x-y)$. The relative stopping criterion for the Preconditioned Conjugate Gradient (PCG) method is

$$\mathbf{r}_k^T C^{-1} \mathbf{r}_k \leq \varepsilon^2 \mathbf{r}_0^T C^{-1} \mathbf{r}_0, \quad \varepsilon = 10^{-6}. \tag{3}$$

Table 1: Relative error on a fixed $32 \times 32 \times 32$ mesh for $\nu \to 0.5$

ν	$\|\mathbf{r}\|_\infty$	$\|\mathbf{f}\|_\infty$	$\|\mathbf{r}\|_\infty / \|\mathbf{f}\|_\infty$
0.4	0.033733	214407	1.57331E-7
0.49	0.052206	1381450	3.77904E-8
0.499	0.551943	13125600	4.20509E-8
0.4999	5.551980	1.31E+008	4.24652E-8
0.49999	55.552900	1.31E+009	4.25009E-8

The results, given in Table 1, fully confirm the locking-free property of the applied FEM discretization.
Now, let us turn our attention to the applied numerical upscaling scheme. Our goal is to replace the complex heterogeneous structure of the RVE with a homogenized material and to determine the corresponding elasticity parameters. For this purpose we consider a boundary value problem with normal zero displacements on five of the faces of the cube and a small nonzero normal displacement on the sixth face (see Figure 2). As we already mentioned, the modified bilinear form can be used in combination with the applied boundary conditions.

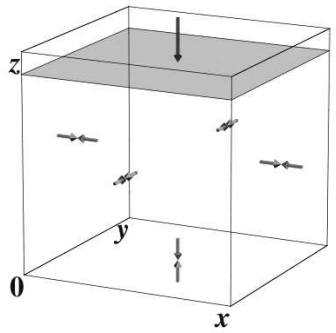

Figure 2: Upscaling problem boundary conditions

Here, we suppose that the stress and the strain tensors of the homogenized cube have zero shear components, and therefore the following relation between the homogenized normal stress and strain components holds:

$$\begin{bmatrix} \sigma_x \\ \sigma_y \\ \sigma_z \end{bmatrix} = \frac{E(1-\nu)}{(1+\nu)(1-2\nu)} \begin{bmatrix} 1 & \frac{\nu}{1-\nu} & \frac{\nu}{1-\nu} \\ \frac{\nu}{1-\nu} & 1 & \frac{\nu}{1-\nu} \\ \frac{\nu}{1-\nu} & \frac{\nu}{1-\nu} & 1 \end{bmatrix} \begin{bmatrix} \varepsilon_x \\ \varepsilon_y \\ \varepsilon_z \end{bmatrix}.$$

The nonzero constant displacements are applied in the z direction, and therefore

$\varepsilon_x = \varepsilon_y = 0$ and

$$\sigma_x = \sigma_y = \frac{E\nu}{(1+\nu)(1-2\nu)}\varepsilon_z \quad \text{and} \quad \sigma_z = \frac{E(1-\nu)}{(1+\nu)(1-2\nu)}\varepsilon_z.$$

From these relations we can directly calculate the homogenized elasticity coefficients as follows:

$$\nu = \frac{1}{1+p}, \quad E = \frac{(1+\nu)(1-2\nu)}{1-\nu}r,$$

where

$$p = \frac{\sigma_z}{\sigma_x} = \frac{\sigma_z}{\sigma_y}, \quad r = \frac{\sigma_z}{\varepsilon_z}.$$

Finally, we present some preliminary numerical results on the performance of the used linear solver. BoomerAMG is used to precondition the linear system. BoomerAMG is a parallel algebraic multigrid implementation from the package Hypre, developed in LLNL, Livermore [3]. The PCG stopping criterion is (3) with $\varepsilon = 10^{-3}$.

Table 2: Numbers of PCG iterations for the upscaling problem

Mesh \ ν	0.4	0.49	0.499	0.4999	0.49999
$16 \times 16 \times 16$	8	10	18	17	9
$32 \times 32 \times 32$	9	11	18	20	11
$64 \times 64 \times 64$	12	14	23	28	22

The preliminary results, given in Table 2 are subject of possible future improvements. However, the question whether the numbers of iterations can be fully stabilized, with respect to both the Poisson ratio and the problem size remains open up to now.

Acknowledgements. This work is partly supported by the Bulgarian NSF Grants DO02-115/2008 and DO02-147/2008.

References

[1] O. Axelsson, I. Gustafsson: *Iterative methods for the Navier equations of elasticity*, Comp. Meth. Appl. Mech. Engin., **15** (1978), 241–258.

[2] S. Brenner, L. Scott: *The Mathematical Theory of Finite Element Models*, Texts in Applied Mathematics, Springer-Verlag (1994), 217-236.

[3] Lawrence Livermore National Laborary, *Scalable Linear Solvers Project*, `https://computation.llnl.gov/casc/linear_solvers/sls_hypre.html`

Classification of (28,8,2,3) Superimposed Codes

Mladen Manev

Definition 1. *A binary $N \times T$ matrix $C = (c_{ij})$ is called an (N, T, w, r) superimposed code (SIC) if for any pair of subsets $W, R \subset \{1, 2, \ldots, T\}$ such that $|W| = w$, $|R| = r$ and $W \cap R = \varnothing$ there exists a row $i \in \{1, 2, \ldots, N\}$ such that $c_{ij} = 1$ for all $j \in W$ and $c_{ij} = 0$ for all $j \in R$. We say also that C is a (w, r) superimposed code of length N and size T.*

The $(N, T, 1, r)$ superimposed codes was introduced by Kautz and Singleton [2]. A natural generalization of the $(N, T, 1, r)$ superimposed codes was done by Mitchell and Piper [5], which discussed the (N, T, w, r) superimposed codes in a connection with cryptographic problems.
The trivial code is a simple example for an (N, T, w, r) superimposed code. The length N of the trivial code is $\binom{T}{w}$ and its rows are all possible binary vectors of weight w.

Definition 2. *Two (N, T, w, r) superimposed codes are equivalent if one of them can be transformed into the other by a permutation of the rows and a permutation of the columns.*

Let $N(T, w, r)$ be the minimum length of an (N, T, w, r) superimposed code for given values of T, w and r and $T(N, w, r)$ be the maximum size of an (N, T, w, r) superimposed code for given values of N, w and r. (N, T, w, r) superimposed codes of length $N = N(T, w, r)$ or size $T = T(N, w, r)$ are called optimal.
The problem of determining the exact values of $N(T, w, r)$ and $T(N, w, r)$ is completely solved only for $w = r = 1$. According to the Sperner Theorem [6] $T(N, 1, 1) = \binom{N}{\lfloor N/2 \rfloor}$. Kim and Lebedev give the following values of $N(T, 2, 3)$[3].

T	5	6	7	8	9
$N(T, 2, 3)$	10	15	21	$24 - 28$	$26 - 30$

The trivial $(10, 5, 2, 3)$, $(15, 6, 2, 3)$ and $(21, 7, 2, 3)$ superimposed codes are the unique optimal $(10, 5, 2, 3)$, $(15, 6, 2, 3)$ and $(21, 7, 2, 3)$ superimposed codes, respectively. It is proved in [4] that the trivial $(28, 8, 2, 3)$ superimposed code is optimal. In this paper we prove that the trivial (28,8,2,3) superimposed code is the unique optimal (28,8,2,3) superimposed code and that $29 \leqslant N(9, 2, 3) \leqslant 30$.
The results have been obtained using the author's computer programs for the generation of superimposed codes and the program *Q-extension* [1] for code equivalence testing. First we generate all inequivalent $(7, 7, 1, 3)$, $(8, 7, 1, 3)$, $(9, 7, 1, 3)$, $(10, 7, 1, 3)$, $(11, 7, 1, 3)$, $(14, 7, 2, 2)$, $(15, 7, 2, 2)$, $(16, 7, 2, 2)$ and $(22, 7, 2, 3)$ superimposed codes. Then, using the codes obtained, we construct all inequivalent $(28, 8, 2, 3)$ superimposed codes and prove the following theorem:

Theorem 1. *The trivial $(28, 8, 2, 3)$ superimposed code is the unique optimal $(28, 8, 2, 3)$ SIC.*

We try to extend the unique $(28, 8, 2, 3)$ superimposed code to a $(28, 9, 2, 3)$ superimposed code but this is impossible. Therefore:

Theorem 2. $29 \leqslant N(9, 2, 3) \leqslant 30$.

References

[1] I. Bouyukliev, What is Q-extension?, *Serdica J. Computing*, 1, 2007, 115–130.

[2] W.H. Kautz and R.C. Singleton, Nonrandom binary superimposed codes, *IEEE Trans. Inform. Theory*, 10, 1964, 363–377.

[3] H.K. Kim and V.S. Lebedev, On optimal superimposed codes, *J. Combin. Designs*, 12, 2004, 79–91.

[4] M. Manev, Optimality of the trivial (28,8,2,3) superimposed code, *Proc. Eleventh International Workshop on Algebraic and Combinatorial Coding Theory*, Pamporovo, Bulgaria, June 16-22, 2008, 140–143.

[5] C.J. Mitchell and F.C. Piper, Key storage in secure network, *Discrete Applied Mathematics*, vol. 21, 215–228, 1988.

[6] E. Sperner, Ein Satz über Untermengen einer endlichen Menge, *Mathematische Zeitschrift*, 27, 1928, 544–548.

Secret Sharing Schemes and Error Correcting Codes

Svetla Nikova

1 Introduction

The goal of this talk is to present a survey on certain recent developments in the theory of unconditional Multi Party Computation (MPC) and Secret Sharing Schemes (SSS) related to Error Correcting Codes. In 1979 Shamir [1] and Blakley [2] proposed independently *secret sharing schemes* (SSS) as a tool to share a secret between set of participants (players) $P_i,\ 1 \leq i \leq n$. Let $\mathbb{F}$ be a finite field and let the secret $s \in \mathbb{F}$.
Access Structure. Denote the set of all *players* by $\mathcal{P} = \{P_1, \ldots, P_n\}$ and the *dealer* of the scheme by $\mathcal{D}$. Let us call the groups which are allowed to reconstruct the secret *qualified* and the groups which should not be able to obtain any information about the secret *forbidden* (unqualified). The set of qualified groups is denoted by Γ and the set of forbidden groups by Δ. The set Γ is *monotone increasing* and the set Δ is *monotone decreasing*. The tuple (Γ, Δ) is called an *access structure* if $\Gamma \cap \Delta = \emptyset$. If any set is ether in Γ or in Δ (i.e., Γ is equal to Δ^c, the complement of Δ), then it is said that the access structure (Γ, Δ) is *complete* and we denote it just by Γ, in this case the SSS is called *perfect*.
The tuple $(\Gamma^\perp, \Delta^\perp)$ is defined on $\mathcal{P}$ as follows $\Gamma^\perp = \{A : \mathcal{P} \setminus A \in \Delta\}$ and $\Delta^\perp = \{A : \mathcal{P} \setminus A \in \Gamma\}$. Then $(\Gamma^\perp, \Delta^\perp)$ is called the *dual access structure* of (Γ, Δ).
Secret Sharing Schemes. A secret sharing scheme based on an access structure (Γ, Δ) is a pair *(Share, Reconstruct)* of protocols (phases) namely, the *sharing phase*, where dealer $\mathcal{D}$ shares to the players a secret s, and the *reconstruction phase*, where the players try to reconstruct s, such that the following access structure rules hold:

- *Privacy:* The players of any set $B \in \Delta$ learn nothing about the secret s as a result of the sharing phase. Hence we call Δ a privacy structure.
- *Correctness:* The secret s can be computed by any set of players $A \in \Gamma$. Analogous we call Γ a reconstruction structure.

When the size of the share for each participant is equal to the size of the secret we speak about *ideal SSSs* and *ideal access structures*. Linear Secret Sharing Schemes are those SSS which use linear operations.
Error Correcting Codes. Any non-empty subset $\mathcal{C}$ of $\mathbb{F}^n$ is called a code, n is the *length* of the code. Each vector in $\mathcal{C}$ is called *codeword* of $\mathcal{C}$; The *minimum distance* of a code $\mathcal{C}$ is defined as $d_{min} = \min_{\mathbf{a},\mathbf{b}.\in\mathcal{C},\ \mathbf{a}\neq\mathbf{b}} d(\mathbf{a}, \mathbf{b})$; Code $\mathcal{C}$ with minimum distance d_{min} can correct $e \leq \lfloor (d_{min} - 1)/2 \rfloor$ errors. More generally, a code $\mathcal{C}$ can correct b errors and c erasures as long as $2b + c < d_{min}$. A linear code $\mathcal{C}$ can be described by its *generator matrix* G or by its *parity check matrix* H.
A code $\mathcal{C}$ is denoted by $[n, k, d]$, where n is the code length, k the dimension and d the minimum distance. The dual of an $[n, k, d]$ code $\mathcal{C}$ is $[n, n-k, d^\perp]$ code $\mathcal{C}^\perp$. Note

that the generator matrix G of the code $\mathcal{C}$ is a parity check matrix of the dual code $\mathcal{C}^{\perp}$ and vice versa the parity check matrix H of $\mathcal{C}$ is a generator matrix for the dual code. In other words $HG^T = GH^T = 0$ holds.
Codes that satisfy the Singleton bound (for an $[n, k, d]$ code: $d \leq n - k + 1$) with equality are called Maximum Distance Separable (MDS) codes, i.e. $[n, k, n + 1 - k]$ codes. Singleton bound can be written in the following equivalent form: $d+d^{\perp} \leq n+2$. Note that the dual of an $[n, k, d]$ MDS code is an $[n, n - k, k + 1]$ MDS code and that any k columns of a generator matrix of MDS code $\mathcal{C}$ are linearly independent.

2 Coding Theoretic Approach to SSS

In 1981, just a few years after the invention of SSS, McEliece and Sarwate [3] have found a fruitful link between SSS and error correcting codes. After that one-to-one relation between threshold SSS and MDS codes has been proven and an approach how to construct ideal SSS from an error-correcting code has been established.
McEliece and Sarwate have reformulated Shamir's scheme in terms of Reed-Solomon codes instead of polynomials. This approach allows the authors to show that the scheme presented in this way has in addition error-correcting properties.
It could be seen that MDS codes (not only Reed-Solomon code) can provide cheating detection to SSS.

Theorem 1. *[3] Consider an $[n + 1, k + 1, d]$ MDS code $\mathcal{C}$ and select at random any codewords $\mathbf{c} = (\mathbf{c}_0, \mathbf{c}_1, \ldots, \mathbf{c}_n)$ with $\mathbf{c}_0 = s$. The dealer gives c_i as a share to participant P_i, $1 \leq i \leq n$.*
If $k + 1 + 2k_a$ or more participants pool together their shares, and at most k_a of these values are incorrect, then the secret s can be recovered correctly and the lying participants can be identified.
If $k + 2k_a$ or less participants pool together their shares, and precisely k_a of these values are incorrect, then the secret s can not be recovered correctly. In fact, each value of s is equally likely.

The general relationship between linear codes and secret sharing schemes has been established by Massey in 1993 [4]. In fact, the coding theoretic approach can be reformulated as the vector space construction introduced by Brickel in 1989 [5]. It has been shown that the coding theoretic approach fully describes the ideal SSS case.
There are two approaches to generate perfectly secure SSS starting from a code:
The first approach uses an $[n, k + 1, d]$ linear code $\overline{\mathcal{C}}$ with generator matrix $\overline{G}$ ($\mathbb{F}^{(k+1)\times n}$). The dealer $\mathcal{D}$ chooses a random information vector $\mathbf{x} \in \mathbb{F}^{k+1}$, subject to $\mathbf{x}_1 = s$ - the secret. He then calculates the codeword $\mathbf{y} = \mathbf{x}\overline{G}$, ($\mathbf{y} \in \mathbb{F}^n$). $\mathcal{D}$ gives $\mathbf{y}_j$ to player P_j to be his share.
The second approach uses an $[n + 1, k + 1, d]$ linear code $\widetilde{\mathcal{C}}$ with generator matrix $\widetilde{G}$ ($\mathbb{F}^{(k+1)\times(n+1)}$). The dealer $\mathcal{D}$ calculates the codeword $\mathbf{y}$ as $\mathbf{y} = \mathbf{x}\widetilde{G}$, ($\mathbf{y} \in \mathbb{F}^{n+1}$), from a random information vector $\mathbf{x} \in \mathbb{F}^{k+1}$, subject to $\mathbf{y}_0 = s$ - the secret. Then $\mathcal{D}$ gives $\mathbf{y}_j$ to player P_j to be his share.

For both constructions a set of shares belonging to group A of players will determine the secret if and only if the first column (or vector ε) is a linear combination of the columns with indices in A. These two approaches for generating SSS are related, in the first approach all the shares form a *complete* codeword of the code, while in the second, all the shares form only part of a codeword. By transforming the matrices of the codes, $\widetilde{G} = (\varepsilon \mid \overline{G})$, the code $\overline{\mathcal{C}}$ can be considered as obtained from the code $\widetilde{\mathcal{C}}$ by *puncturing* i.e. by deleting a coordinate.

3 Generalizing the Coding Theory Approach by Means of Monotone Span Programs

Karchmer and Wigderson [6] introduced in 1993 a linear algebra computational model called *monotone span program* (MSP) to study certain complexity theory problems. In 2000 Cramer et al. [7] have shown that MSPs are in one-to-one correspondence with any general (i.e., non ideal and perfect) SSS. Here is a formal definition for an MSP.

Definition 1. *[6] A* **Monotone Span Program** *(MSP)* $\mathcal{M}$ *is a quadruple* $(\mathbb{F}, M, \varepsilon, \psi)$*, where* $\mathbb{F}$ *is a finite field,* M *is a matrix (with* m *rows and* $d \leq m$ *columns) over* $\mathbb{F}$*,* $\psi : \{1, \ldots, m\} \to \{1, \ldots, n\}$ *is a surjective labeling function and* $\varepsilon = (1, 0, \ldots, 0)^T \in \mathbb{F}^d$ *is called a target vector.*

An MSP is said *to compute* a (complete) access structure Γ when $\varepsilon \in \mathrm{im}(M_A^T) \iff A$ is a member of Γ. It is said that a set A is *accepted* by $\mathcal{M} \iff A \in \Gamma$, otherwise we say A is *rejected* by $\mathcal{M}$.
In 2003 a class of Error-Correcting Codes were proposed [8], which have as a generator matrix an MSP and this approach led to generalized codes called Error-Set Correcting Codes.
For any vector $\mathbf{x}$ the set $\mathcal{P}$ defines a partition by mapping each player P_i to one or more coordinates of the vector. Define $\mathcal{P}$*-support* of vector $\mathbf{x}$: $\sup_{\mathcal{P}}(\mathbf{v}) = \{i : \mathbf{v^i} \neq \mathbf{0}\}$. Obviously $\delta_{\mathcal{P}}(\mathbf{x}, \mathbf{y}) = \sup_{\mathcal{P}}(\mathbf{x} - \mathbf{z})$
The idea is to work in a new metric replacing **Numbers** with **Sets**, i.e. replacing monotone properties defined by numbers into similar properties defined over sets. For any $\mathbf{x}, \mathbf{y} \in \mathbb{F}^N$

$$\begin{aligned} d(\mathbf{x}, \mathbf{y}) = |\{i : \mathbf{x}_i \neq \mathbf{y}_i\}| &\quad \to \quad \delta_{\mathcal{P}}(\mathbf{x}, \mathbf{y}) = \{i : \mathbf{x^i} \neq \mathbf{y^i}\} \\ wt(\mathbf{x}) = |\{i : \mathbf{x}_i \neq 0\}| &\quad \to \quad sup_{\mathcal{P}}(\mathbf{x}) = \{i : \mathbf{x^i} \neq 0\} \end{aligned}$$

We will use $\delta_{\mathcal{P}}(\mathbf{x}, \mathbf{y})$ instead of the Hamming distance and will explore the properties of the so defined space.

Definition 2. *[8] For a code* $\mathcal{C}$ *define the set of* possible (allowed) distances*:* $\Gamma(\mathcal{C}) = \{A : \text{ there exist } \mathbf{a}, \mathbf{b} \text{ in } \mathcal{C}, \ \mathbf{a} \neq \mathbf{b} \text{ such that } \delta_{\mathcal{P}}(\mathbf{a}, \mathbf{b}) \subseteq A\}$*;* forbidden distances*:* $\Delta(\mathcal{C}) = \Gamma(\mathcal{C})^c$*. The so-defined codes are called* error-set correcting codes*.*

Theorem 2. *[8] An error-set correcting code $\mathcal{C}$ with set of forbidden distances $\Delta(\mathcal{C})$ can correct all errors in Δ if and only if $\Delta \uplus \Delta \subseteq \Delta(\mathcal{C})$ ($\uplus$ - element-wise union).*

A link can be established between a perfect general access structure SSS and Error-Set Codes. The following theorems are a generalization of the results by Massey [4] and Van Dijk [9] for the ideal SSS case.

Theorem 3. *[8] Let $\mathcal{M}$ be an MSP program computing Γ, and $\mathcal{M}^{\perp}$ be an MSP computing the dual access structure $\Gamma^{\perp}$. Let code $\mathcal{C}^{\perp}$ have the parity check matrix $H^{\perp} = (\varepsilon \mid (M^{\perp})^T)$ and let code $\mathcal{C}$ have the parity check matrix $H = (\varepsilon \mid M^T)$. Then for any MSP $\mathcal{M}$ there exists an MSP $\mathcal{M}^{\perp}$ such that $\mathcal{C}$ and $\mathcal{C}^{\perp}$ are dual.*

Theorem 4. *[8] Let $\mathcal{M} = (\mathbb{F}, M, \varepsilon, \psi)$ be an MSP computing an access structure Γ. Let $\widetilde{\mathcal{C}}$ be an error-set correcting code, with a set of forbidden distances $\Delta(\widetilde{\mathcal{C}})$ and with a generator matrix $\widetilde{G}$ of the form $\widetilde{G} = (\varepsilon \mid M^T)$. Then the $\mathcal{P}$-minimal codewords for $\widetilde{\mathcal{C}}$ are the vectors of the form $(1, c)$ and $sup_{\mathcal{P}}(c) \in \Gamma^{\perp}$.*

References

[1] A. Shamir. How to share a secret, *Commun. ACM* 22, 1979, pp. 612–613.

[2] G. Blakley. Safeguarding cryptographic keys, *AFIPS* 48, 1979, pp. 313–317.

[3] R. McEliece, D. Sarwate. On sharing secrets and Reed-Solomon codes, *Commun. ACM* 24, 1981, pp. 583–584.

[4] J. Massey. Minimal codewords and secret sharing, *Proc. 6th Joint Swedish-Russian Int. Workshop on Inform. Theory*, 1993, pp. 276–279.

[5] E. Brickell. Some ideal secret sharing schemes, *J. of Comb. Math. and Comb. Computing*

[6] M. Karchmer, A. Wigderson. On Span Programs, *Proc. of 8th Annual Structure in Complexity Theory Conference*, 1993, pp. 102–111.

[7] R. Cramer, I. Damgard, U. Maurer. General Secure Multi-Party Computation from any Linear Secret Sharing Scheme, *EUROCRYPT'00*, LNCS 1807, 2000, pp. 316–334.

[8] S. Nikova, V. Nikov. On a Relation between Verifiable Secret Sharing and a Class of Error-Correcting Codes, *WCC'05*, LNCS 3969, 2005, pp. 275–290, Cryptology ePrint Archive: Report 2003/210.

[9] M. van Dijk. Secret Key Sharing and Secret Key Generation, *Ph.D. Thesis*, TU Eindhoven, 1997.

Integral and Spectral Geometry of Liouville Billiard Tables

Georgi Popov, Peter Topalov

Integral geometry is related to the notion of a Radon transformation. There are two important results obtained in the beginning of the twentieth century which can be considered as a starting point of the modern integral geometry. In 1916 Funk observed that continuous even functions on the sphere are uniquely determined by the integrals on the great circles. In 1917 Radon proved that a continuous even function with a compact support in $\mathbb{R}^2$ is uniquely determined by its integrals on the lines. The main problem of the integral geometry can be stated as follows: Let (X, g) be a smooth manifold and let G be a suitable group of isometries. Given a continuous function f on X, let us define the Radon transform R_f as a map, assigning to each closed geodesic γ the integral $R_f(\gamma)$ of f on γ. Does $R_f \equiv 0$ imply $f \equiv 0$ for any continuous function which is invariant with respect to G?

1 Liouville billiard tables and Radon transform

A billiard table is a smooth compact Riemannian manifold (X, g), $\dim X = n \geq 2$, equipped with a smooth Riemannian metric g and with a C^∞ boundary $\Gamma := \partial X \neq \emptyset$. The elastic reflection of geodesics at Γ determines continuous curves on X called *billiard trajectories* as well as a discontinuous dynamical system on T^*X – the *billiard flow* which induces a discrete dynamical system on an open subset of the coball bundle $B^*\Gamma$ of Γ called *billiard ball map*. Let μ be a positive density on $B^*\Gamma$ (for example $\mu = 1$). We are interested in the following problems.

Problem A. Let K be a continuous function on Γ such the mean value of $K\mu$ on any periodic orbit of the billiard ball map is zero. Does it imply $K \equiv 0$?

Since periodic orbits of the billiard ball map can be regarded as discrete closed geodesics, the analogy with the classical Radon transformation becomes clear. We show below that Problem A holds true for a class of Liouville billiard tables for any K which is invariant with respect to the corresponding group of symmetries. A Liouville billiard table (shortly L.B.T.) of dimension $n \geq 2$ is a completely integrable billiard table admitting n commuting integrals of the billiard flow which are quadratic forms in the momentum and functionally independent a.e. (see [4]). Such a billiard table can be viewed as a 2^{n-1}-folded branched covering of the cylinder $\mathbb{T}^{n-1} \times [-a, a]$. An important subclass of L.B.T.s are those of *classical type* having an additional symmetry and for which the boundary is strictly geodesically convex. The group of isometries of a L.B.T. of classical type is isomorphic to $(\mathbb{Z}/2\mathbb{Z})^n$. Moreover, the group of isometries of (X, g) induces a group of isometries G on Γ which is isomorphic to $(\mathbb{Z}/2\mathbb{Z})^n$. The billiard ball map of a L.B.T. is also completely integrable and its phase space is foliated by invariant tori. Almost any torus Λ of this foliation is regular, which means that Λ is a Lagrangian submanifold of $B^*\Gamma$ diffeomorphic to $\mathbb{T}^{n-1}$ and

it is invariant with respect to the symplectic map $P = B^m$ for some $m \geq 1$. Such tori are also called Liouville and more generally Kronicker tori. An important example of a L.B.T. is the interior of the n-axial ellipsoid.
The map assigning to each periodic orbit of B the mean value of $K\mu$ on it can be considered as a Radon transformation of K. Another Radon transformation of K can be defined as follows. Given a continuous function K on Γ and a regular invariant torus $\Lambda \subset B^*\Gamma$ of the billiard ball map, we denote by $\mathcal{R}_K(\Lambda)$ the mean value of the integral of $K\mu$ on Λ with respect to the Leray form. The map $\Lambda \mapsto \mathcal{R}_K(\Lambda)$ will be called a Radon transform of K as well.

Problem B. Let K be a continuous function on Γ which is invariant with respect to the corresponding group of symmetries and such that $\mathcal{R}_K \equiv 0$. Does it imply $K \equiv 0$?

2 Isospectral deformations

Substantial progress in the inverse spectral problem has been done recently due to the wave-trace formula and the semi-classical trace formulae. The wave-trace formula, known in physics as the Bilian-Bloch formula and treated rigorously by Colin de Verdière and Duistermaat and Guillemin, as well its semi-classical analogue - the Gutzwiller trace formula relate the spectrum of the operator with different invariants of the corresponding closed geodesics such as their lengths and the spectrum of the linear Poincarï¿½ map. The Birkhoff Normal Form (BNF) of certain non-degenerate closed geodesics can be extracted from the singularity expansions of the wave-trace which can be used to reconstruct the boundary of analytic planar domains, as it was shown recently by Zelditch.
Given $K \in C(\Gamma, \mathbb{R})$, denote by Δ_K the Laplace-Beltrami operator in $L^2(X)$ with Robin boundary conditions $\frac{\partial u}{\partial \nu}|_\Gamma = Ku|_\Gamma$, where $\nu(x)$, $x \in \Gamma$, is the inward unit normal to Γ. Let X be the interior of an ellipse Γ in $\mathbb{R}^2$ and let Symm (Γ) be the space of C^∞ real-valued functions on Γ which are invariant with respect to the symmetries of the ellipse. Guillemin and Melrose [1] proved that the map $K \to \text{Spec}\Delta_K$ is one-to-one on Symm (Γ). This result has been generalized in the case of L.B.T.s of dimension 2 by Popov and Topalov [2]. The main tool is again the wave-trace formula. The wave-trace approach to inverse spectral problems works well if we suppose simplicity of the length spectrum (a non-coincidence condition) and non-degeneracy of the corresponding closed geodesic and its iterates.
We propose here another method which avoids the wave-trace formulae and works without assuming any non-coincidence or non-degeneracy conditions. Consider a continuous family of real-valued functions $K_t \in C^\infty(\Gamma, \mathbb{R}), t \in [0,1]$, and set $\Delta_t = \Delta_{K_t}$. Fix $c > 0$ and $d > n/2$, and consider an infinite union of intervals

($\mathbf{H}_1$) $\mathcal{I} := \cup_{k=1}^\infty [a_k, b_k]$, where $a_{k+1} - b_k \geq c b_k^{-d}$, and $\lim a_k = \lim b_k = \infty$, $\lim(b_k - a_k) = 0$.

Impose the following *"weak isospectral assumption"*:

($\mathbf{H}_2$) *There is $a > 0$ such that for any $t \in [0,1]$, $\mathrm{Spec}\,(\Delta_t) \cap [a, +\infty) \subset \mathcal{I}$.*

We suppose also that there is a Kronicker torus of B, which means that

($\mathbf{H}_3$) *There is an embedded submanifold Λ of $B^*\Gamma$ diffeomorphic to $\mathbb{T}^{n-1}$ and invariant with respect to $P = B^m$ for some $m \geq 1$ such that $P|_\Lambda : \Lambda \to \Lambda$ is C^∞ conjugated to the rotation with a Diophantine vector of rotation ω, i.e. $R_{2\pi\omega}(\varphi) = \varphi - 2\pi\omega$ (mod 2π)*

Then Λ is Lagrangian. Moreover, P is uniquely ergodic on Λ, i.e. there is an unique probability measure $d\mu$ on Λ which is invariant under P. Set $\Lambda_j = B^j(\Lambda)$, $j = 0, 1, \ldots, m-1$, and $d\mu_j = (B^{-j})^*(d\mu)$. Then Λ_j is also a Kronicker invariant torus of P with a vector of rotation $2\pi\omega$ and $d\mu_j$ is the unique probability measure on it which is invariant with respect to P. Given $(x, \xi) \in B^*\Gamma$, we denote by $\xi^+ \in T^*_x X$ the corresponding outgoing unit co-vector and by $0 \leq \theta(x, \xi) \leq \pi/2$ the angle defined by the pairing $\cos(\theta(x, \xi)) = \langle \xi^+, \nu(x) \rangle$.

Theorem 1. (Iso-spectral invariants) *Let Λ be an invariant torus of $P = B^m$ satisfying (H_3). Let $[0,1] \ni t \mapsto K_t \in C^\infty(\Gamma, \mathbb{R})$ be a continuous family of real-valued functions on Γ such that Δ_t satisfy the weak isospectral condition $(H_1) - (H_2)$. Then*

$$\phi(t) := \sum_{j=0}^{m-1} \int_{\Lambda_j} \frac{K_t}{\cos\theta}\, d\lambda_j \;\equiv\; \phi(0). \tag{1}$$

The proof of the theorem is based on a quasi-mode construction. In the case of Liouville billiard tables the Kronicker tori Λ are invariant tori either of $P = B$ ($m = 1$) or of $P = B^2$ ($m = 2$). Then (1) means that the Radon transform $\mathcal{R}_{K_t,\mu}(\Lambda)$ is independent of t for any regular torus Λ, where $\mu(x, \xi) = 1/\cos(\theta(x, \xi))$.

3 Injectivity of the Radon transform and spectral rigidity

Let (X, g) be a Liouville billiard table of dimension $n = 2, 3$. Denote by $\mathrm{Symm}^\ell_G(\Gamma)$ the space of C^ℓ real-valued functions on Γ, which are invariant with respect to the group of symmetries G of Γ. Fix the density μ by $\mu \equiv 1$ or by $\mu(x, \xi) = 1/\cos(\theta(x, \xi))$. Our main result is:

Theorem 2.. *Let (X, g), $n = 2, 3$, be a Liouville billiard table of classical type and let $K \in \mathrm{Symm}^0_G(\Gamma)$. Suppose that $R_{K,\mu} \equiv 0$. Then $K = 0$.*

The billiard ball map of a L.B.T. is said to be non-degenerate if the corresponding frequency map is non-degenerate.

Theorem 3.. *Let (X, g), $\dim X = 3$, be a Liouville billiard table of classical type such that the corresponding billiard ball map is non-degenerate. Let K_t, $t \in [0,1]$, be a continuous family of real-valued functions in $C^\infty(\Gamma, \mathbb{R})$ such that Δ_t satisfy $(H_1) - (H_2)$. If $K_0, K_1 \in \mathrm{Symm}^\infty_G(\Gamma)$, then $K_1 \equiv K_0$.*

By Theorem 1, $R_{K,\mu}(\Lambda) = 0$ for any torus Λ with a Diophantine vector of rotation, where $\mu(x,\xi) = 1/\cos(\theta(x,\xi))$. Since the billiard ball map is nondegenerate the Radon transforms of K_1 and K_0 are the same on any regular torus and the claim follows from Theorem 2. In the same way we prove

Theorem 4.. *Let (X,g), $\dim X = 3$, be a Liouville billiard table of classical type such that the corresponding billiard ball map is non-degenerate. Let K be a continuous function on Γ invariant with respect to G and such that the mean value of K on any periodic orbit of the billiard ball map is zero. Then $K \equiv 0$.*

The following result provides sufficient conditions for the non-degeneracy of the billiard ball map.

Theorem 5.. *Let (X,g), $dimX = 3$, be an analytic Liouville billiard table of classical type. Suppose that there exists at least one non-periodic geodesic on its boundary $(\Gamma, g|_\Gamma)$. Then the billiard ball map of (X,g) is non-degenerate.*

For example the interior of the ellipsoid is a non-degenerate Liouville billiard table. The main results are proved in [3-5]. The construction of Liouville billiard tables is given in [4].

References

1. V. Guillemin and R. Melrose: *An inverse spectral result for elliptical regions in* $\mathbf{R}^2$, Advances in Mathematics, **32**(1979), 128-148

2. G. Popov and P. Topalov: *Liouville billiard tables and an inverse spectral result*, Ergod. Th. & Dynam. Sys., **23**(2003), 225-248

3. G. Popov and P. Topalov: *Invariants of isospectral deformations and spectral rigidity*, `http://www.ma.utexas.edu/mp_arc/c/05/05-62.pdf`

4. G. Popov and P. Topalov: *Discrete analog of the projective equivalence and integrable billiard tables*, Ergod. Th. & Dynam. Sys., **28**, 1657-1684 (2008)

5. G. Popov and P. Topalov: *Radon transform and spectral rigidity of Liouville billiard tables*, in preparation

Travelling Waves in Newell-Whitehead Cellular Neural Networks Model

Angela Slavova, Victoria Ivanova

1 Introduction

Reaction-diffusion type of equations are widely used to describe phenomena in different fields, as biology-Fisher model [1], FitzHugh-Nagumo nerve conduction model [1], Vector-disease model, chemistry - Brusselator model, physics - Sine-Gordon model [10], etc.
In his pioneering work, Fisher [1] used a logistic-based reaction-diffusion model to investigate the spread of an advantageous gene in a spatially extended population. The FitzHugh-Nagumo system with two coupled partial differential equations (PDEs) and two diffusion coefficients is a simplification of the Hodgkin-Huxley model and describes the control of the electrical potential accross cell membrane by the change of flow of the ionic channels but also can be used to model electrical waves of the heart [1]. The generalized diffusion equation with a nonlinear source term which encompasses the Fisher, Newell-Whitehead and Fitzhugh-Nagumo equations as particular forms and appears in awide variety of physical and engineering applications. Modulation equations play an essential role in the description of systems which exibit patterns of nearly periodic nature. The so called Newell-Whitehead equation is derived to describe the envelope of modulated roll-slotions with two large extended or unbounded space direction.
In this paper we shall study the Newell-Whitehead equation of the form:

$$\frac{\partial u}{\partial t} = \frac{\partial^2 u}{\partial x^2} + au - bu^3, \tag{1}$$

where a and b are positive parameters. This equation is a second-order parabolic PDE.
Spatial and spatio-temporal patterns occur widely in physics, chemistry and biology. In many cases, they seem to be generated spontaneously. These phenomena have motivated a great deal of mathematical modelling and the analysis of the resultant systems has led to a greater understanding of the underlaying mechanisms. Partial differential equations of diffusion type have long served as models for regulatory feedbacks and pattern formation. Such systems cause some difficulty, since both existence and behavior of the solutions are more difficult to establish. Many aspects of qualitative behavior have to be investigated numericallly. For this purpose we apply the Cellular Neural Networks (CNN) approach for studying such models.

2 Newell-Whitehead CNN model

It is known that some autonomous CNNs represent an excellent approximation to nonlinear partial differential equations (PDEs). In this paper we will present the receptor-based model by a reaction-diffusion CNNs. The intrinsic space distributed topology makes the CNN able to produce real-time solutions of nonlinear PDEs. There are several ways to approximate the Laplacian operator in discrete space by a CNN synaptic law with an appropriate A-template.
We will map $u(x,t)$ into a CNN layer such that the state voltage of a CNN cell $u_j(t)$ at a grid point j is associated with $u(jh,t)$, $h=\Delta x$. Therefore, an one-dimensional Laplacian template will be in the following form:

$$A_1 = (1,-2,1),$$

and the CNN model in this case is:

$$\frac{du_j}{dt} = (u_{j-1} - 2u_j + u_{j+1}) + au_j - bu_j^3, \tag{2}$$

$j=1,\ldots,n$, $n=M.M$, where we have $M\times M$ cells.

3 Travelling waves in the Newell-Whitehead CNN model

Our objective in this section is to study the structure of travelling wave solutions of Newell-Whitehead CNN model.
Let us consider our CNN equation (2). The travelling wave solutions will be presented in the following form:

$$u_j(t) = u(\eta), 1 \le j \le n, \tag{3}$$

where $\eta = t - jh$, $h>0$ is a parameter. Note that η is the coordinate moving along the array with a velocity equal to $c=1/h$. Substituting (3) in (2) we obtain

$$\dot{u} = u(\eta - h) - 2u(\eta) + u(\eta + h) + \mathcal{N}(u),$$

where the dot denotes differentiation with respect to η, $\mathcal{N}(u) = au(\eta) - bu^3(\eta)$. The two difference terms $[u(\eta-h)-u(\eta)]-[u(\eta)-u(\eta+h)]$ can be replaced approximately by the first derivatives: $-\dot{u}/h$ and $+\dot{u}/h$, respectively. Hence, we obtain

$$\dot{u} = \frac{1}{1+2c}\mathcal{N}(u). \tag{4}$$

Clearly, $u\equiv 0$ and $u\equiv \pm\sqrt{\frac{a}{b}}$ are solutions of the stationary problem. So there are three equilibria $E_0=(0,0)$ and $E_1=(\sqrt{\frac{a}{b}},0)$, $E_2=(-\sqrt{\frac{a}{b}},0)$. The following theorem for the travelling waves of the Newell-Whitehead CNN model (2) hold:

Theorem 1. *For the Newell-Whitehead CNN model (2), there exists $c > 0$, such that there is a*
1). heteroclinic orbit connecting the equilbria E_0 and E_1 and the travelling wave $u(\eta)$ is strictly monotonically increasing;
2). heteroclinic orbit connecting the equilbria E_0 and E_2 and the travelling wave $u(\eta)$ is strictly monotonically decreasing.

Remark 1. There are exact solutions of the Newell-Whitehead equation (1) for $a > 0$ and $b > 0$ [8]

$$w(x,t) = \pm\sqrt{\frac{a}{b}}\frac{C_1 exp(\frac{1}{2}\sqrt{2a}x) - C_2 exp(-\frac{1}{2}\sqrt{2a}x)}{C_1 exp(\frac{1}{2}\sqrt{2a}x) + C_2 exp(-\frac{1}{2}\sqrt{2a}x) + C_3 exp(-\frac{3}{2}at)},$$

$$w(x,t) = \pm\sqrt{\frac{a}{b}}[\frac{2C_1 exp(\sqrt{2a}x) + C_2 exp(\frac{1}{2}\sqrt{2a}x - \frac{3}{2}at)}{C_1 exp(\sqrt{2a}x) + C_2 exp(\frac{1}{2}\sqrt{2a}x - \frac{3}{2}at) + C_3} - 1],$$

where C_1, C_2 and C_3 are arbitrary constants.

The following simulations of our CNN model are made for different values of cell parameters.

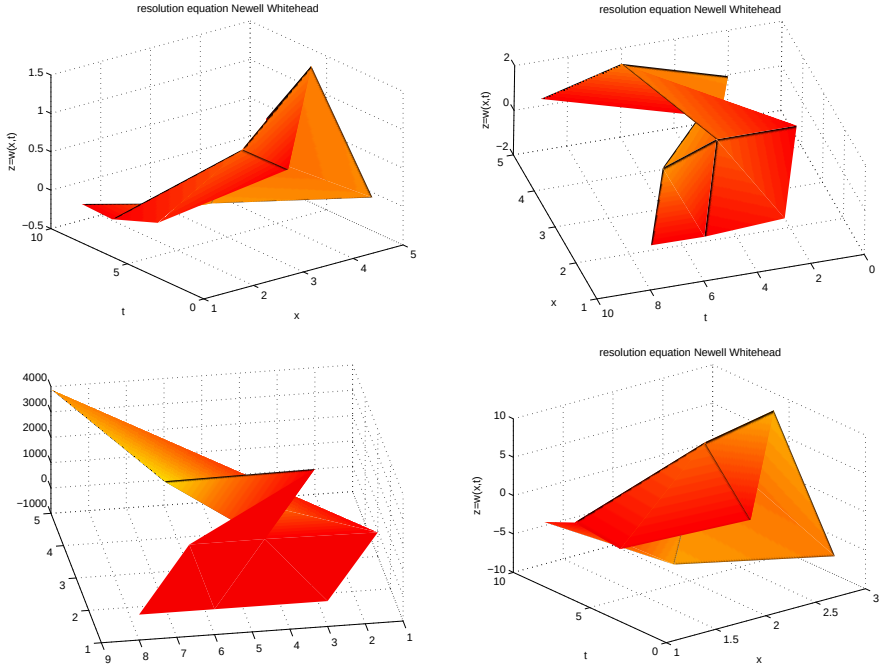

Fig.1. Simulations of our CNN model.

References

[1] N.F.Britton, *Reaction-Diffusion Equations and Their Applications to Biology*, Acad. Press, New York, 1986.

[2] L.O.Chua, L.Yang, Cellular neural networks: Theory, IEEE Trans. Circuits Syst.,35:1257-1272,1988.

[3] Chua L.O., Hasler M., Moschytz G.S., Neirynsk J., Autonomous cellular neural networks: a unified paradigm for pattern formation and active wave propagation, *IEEE Trans. CAS-I*, vol. 42, N 10, pp. 559-577, Oct. 1995.

[4] Genesio R., Tesi A., Villoresi F., A frequency approach for analyzing and controlling chaos in nonlinear circuits, *IEEE Trans. CAS-I*, vol. 40, N 11, pp. 819-827, Nov. 1993.

[5] J.Guckenheimer, Ph.Holmes, *Nonlinear Oscillations, Dynamical Systems, and Bifurcations of Vector Fields*, Springer, 1983.

[6] C.-H.Hsu, S.-S.Lin,W.Shen, Travelling waves in Cellular Neural Networks, Int.J.Bifurcation and Chaos, vol.9,N0.7, pp.1307-1319, 1999.

[7] A.I.Mees, *Dynamics of Feedback Systems*, Wiley, London, 1981.

[8] Polyanin A.D., Zaitsev V.F., Handbook of nonlinear partial differential equations, Chapman & Hall/CRC, Boca Raton, 2004.

[9] Roska T., Chua L.O., Wolf D., Kozek T., Tetzlaff R., Puffer F., Simulating nonlinear waves and partial differential equations via CNN- Part I: Basic techniques, *IEEE Trans. CAS-I*, vol. 42, N 10, pp. 807-815, Oct. 1995.

[10] A.Slavova, Applications of some mathematical methods in the analysis of celullar neural networks, J.Comp.Appl.Math. 114, pp. 387-404, 2000.

On the Solution of the System of ODEs Governing the Polarized Stationary Solutions of CNLSE

Michail D. Todorov, Christo I. Christov

Consider the coupled system of Nonlinear Schrodinger Equations (CNLSE):

$$\begin{aligned} \mathrm{i}\psi_t =& \beta\triangle\psi + [\alpha_1|\psi|^2 + (\alpha_1 + 2\alpha_2)|\phi|^2]\psi \\ \mathrm{i}\phi_t =& \beta\triangle\phi + [\alpha_1|\phi|^2 + (\alpha_1 + 2\alpha_2)\alpha_2|\psi|^2]\phi \end{aligned}$$

where β is the dispersion coefficient, α_1 describes the self-focusing of a signal for pulses in birefringent media, and α_2 governs the nonlinear coupling between the equations. For further convenience we consider the case $\beta = 1$. All other cases can be reduced to this one by means of simple scaling. CNLSE possess solutions that are localized envelopes (see, for example [3, 8]). It is easy to see that if one of the components, say ϕ, is trivially equal to zero, then the system reduces to single scalar NLSE for the other function, ψ. Such a solution of CNLSE is called 'linearly polarized'. The *sech*-solution of the single NLSE, say for ψ-profile, is given by

$$\psi(x,t) = A_\psi \mathrm{sech}[b_\psi(x - X - c_\psi t)] \exp\Big\{\mathrm{i}\Big[\frac{c_\psi}{2\beta}(x - X - c_\psi t) - n_\psi\Big]\Big\} \qquad (1)$$

$$b_\psi^2 = \frac{1}{\beta}\big(n_\psi + \frac{1}{4\beta}c_\psi^2\big); \quad A_\psi = b_\psi\sqrt{2\beta/\alpha_1}; \quad u_c = 2n_\psi\beta/c_\psi,$$

which means that for given phase speed, c_ψ, and carrier frequencies, n_ψ, the solution of the above type is fully specified. The localized solution is identified by the presence of a spatial point, $x = X - c_\psi t$ ('center') which moves with a given phase speed c_ψ. The same initial relationships hold for ϕ-profile when $\psi = 0$. The center is common for both components ψ and ϕ. The above type of analytical initial condition evidently requires the restriction $4\beta\, b_{\psi,\phi} > -c_{\psi,\phi}^2$. It should be noted here, that for the Manakov case [3] when $\alpha_2 = 0$, a solution of type of Eq. (1) can be found for circular polarization of kind $\psi(x,t) = \chi(x,t)\cos\delta,\ \phi(x,t) = \chi(x,t)\sin\delta$, by replacing α_1 by $2\alpha_1$.

The initial conditions play important role in investigation of soliton interaction described by CNLSE. It has been shown in different works of the present authors [1, 4, 6, 7] that linearly polarized initial conditions, after the interaction invariable lead to solitons for which both $\psi, \phi \neq 0$, and have in general elliptic polarizations. This means that a numerical solution for the general case is needed in order to provide initial conditions with elliptic polarization which is the goal of the present work. A numerical solution for elliptic polarized stationary propagating solitons had been provided in [5]. In order to be able to use a numerically computed initial condition, one must have a code that gives the solution. Here we propose a different numerical method to find the solution to be used in our future work on interaction of solitons. Simultaneously, we can verify both our solution and the solution of [5].

The elliptically polarized solution has the form

$$\psi(x,t),\phi(x,t) = A_{\psi,\phi}(x - X - c_{\psi,\phi}t)\exp\left\{\mathrm{i}\big[n_{\psi,\phi} - \frac{c_{\psi,\phi}}{2}(x - X - c_{\psi,\phi}t) + \delta_{\psi,\phi}\big]\right\} \quad (2)$$

where n_ψ, n_ϕ are the carrier frequencies and δ_ψ, δ_ϕ are the phases for the two components. Generally $n_\psi \neq n_\phi$, while $n_\psi = n_\phi$ only for circular polarization. The general polarization angle is defined as $\theta = \arctan(\max\{A_\phi\}/\max\{A_\psi\})$.
After some straightforward manipulations we get the following system of conjugated real ordinary differential equations for the real-valued amplitudes A_ψ, A_ϕ:

$$\vec{F}(\vec{A}) \equiv \begin{pmatrix} A_\psi'' + (n_\psi + \frac{1}{4}c_\psi^2)A_\psi + [\alpha_1 A_\psi^2 + (\alpha_1 + 2\alpha_2)A_\phi^2]A_\psi \\ A_\phi'' + (n_\phi + \frac{1}{4}c_\phi^2)A_\phi + [\alpha_1 A_\phi^2 + (\alpha_1 + 2\alpha_2)A_\psi^2]A_\phi \end{pmatrix} = \begin{pmatrix} 0 \\ 0 \end{pmatrix}, \quad (3)$$

where $\vec{A} = [A_\psi(x - X - c_\psi t), A_\phi(x - X - c_\phi t)]^T$ is the unknown vector function.
The above system has to be solved with the asymptotic boundary conditions

$$\lim_{x\to\pm\infty} A'_{\psi,\phi}(x - X - c_{\psi,\phi}t) = \lim_{x\to\pm\infty} A_{\psi,\phi}(x - X - c_{\psi,\phi}t) = 0. \quad (4)$$

Thus we are faced with solving the bifurcation boundary-value problem (BVP) (3), (4) for the possible nontrivial solution. Introducing a fictitious time $\tau \geq 0$ let assume that the relationship holds

$$\frac{\partial \vec{F}}{\partial \vec{A}}\vec{\alpha} + \frac{\partial \vec{F}}{\partial \vec{A}''}\vec{\alpha}'' + \vec{F} = \vec{0}, \quad \text{with} \quad \vec{\alpha} \equiv \frac{\partial \vec{A}}{\partial \tau}. \quad (5)$$

It is proved in [2] that the iteration

$$\vec{A}^{k+1} = \vec{A}^k + \Delta\tau_k \vec{\alpha}^k, \quad \Delta\tau_k = \frac{||\vec{F}^k||}{||\vec{F}^k|| + ||\vec{F}^{k+1}||}, \quad k = 0, 1, 2, ...$$

is quadratically convergent in the vicinity of the solution of (3),(4). In the last formula $||\cdot||$ stands for the L_2-norm. It is convenient to use cubic Hermitean splines on the uniform mesh

$$x_i = -x_\infty + ih, \qquad h = \frac{2x_\infty}{N}, \qquad i = 0, ..., N,$$

and the Gaussian points $1/2 \pm \sqrt{3}/6$ in $[0, 1]$ to be the the collocation nodes.
We use sech-like function as an initial approximation, i.e., $A^{(0)}_{\psi,\phi} \propto \mathrm{sech}(b_{\psi,\phi}x)$ and solve the above auxiliary BVP for given $n_{\psi,\phi}$, $c_{\psi,\phi}$, α_1 and α_2 with spatial step $h = 10^{-2}$ and "actual" infinity $x_\infty = 15 \div 20$. Taking seven to eight iterations proves to be sufficient to reach the approximate nontrivial solution with L_2-norm of the error lesser than 10^{-12}.
In Fig. 1 we present three cases of elliptic polarization when the carrier frequency of the ψ-component is fixed ($n_\psi = -0.5$) and the carrier frequency of the ϕ-components $n_\phi \in [-0.7, -0.39]$. We were able to generate solutions with all possible angles of

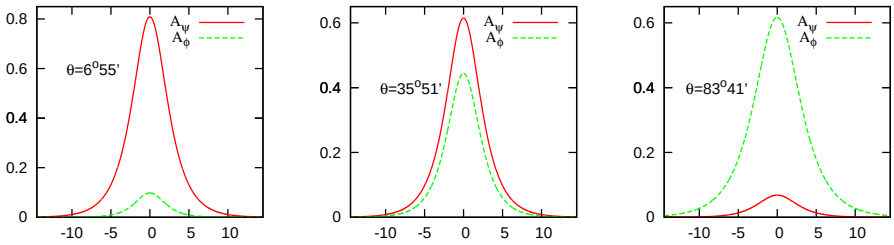

Figure 1: Amplitudes A_ψ and A_ϕ for $c_l = -c_r = 1$, α_1=0.75, $\alpha_2 = 0.2$, $n_\psi = -0.5$. Left: $n_\phi = -0.68$; middle: $n_\phi = -0.55$; right: $n_\phi = -0.395$.

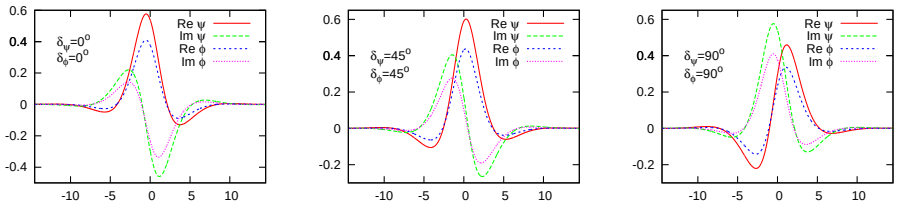

Figure 2: Real and imaginary parts of the amplitudes, $\Re\psi$, $\Im\psi$, $\Re\phi$, $\Im\phi$, from the case shown in the middle panel of Fig. 1 and the dependence on phase angle.

polarization in $\theta \in [0°, 90°]$ including the cases of circular and linear polarization. In this way we found out that the elliptically polarized solitons do exist even for those values of the carrier frequency and phase velocity, for which the linearly polarized sech-solutions do not exist. Note that the latter are limited by the condition $n_{\psi,\phi}+c^2_{\psi,\phi}/4 > 0$. Fig. 1 shows that by varying the carrier frequency one can produce solitons that have different supports. We mention here that as far as it can be judged by the graph, our shapes are in good quantitative agreement with the solution of [5].
Another dimension of complexity is introduced by the phases $\delta_{\psi,\phi}$ of the different components (see Eq. (2)) although these do not affect the amplitudes $A_{\psi,\phi}$. As shown in [7], the initial difference in phases can have a profound influence on the polarizations of the solitons after the interaction. In Fig. 2 we present a case with given amplitudes of envelops but with different phases. Naturally, we present both the real and imaginary parts, because their relative shift is what matters in this case. In the end, we present in Fig. 3 the interaction of two initial solitons with different polarizations. The left one has a circular polarization, while the right one has elliptic polarization. The above mentioned exchange of polarizations is clearly seen. The stability of the computations are ensured by the conservative scheme we employ, but the lack of oscillations and dispersion testifies that the initial conditions are with high accuracy compatible with the equations.

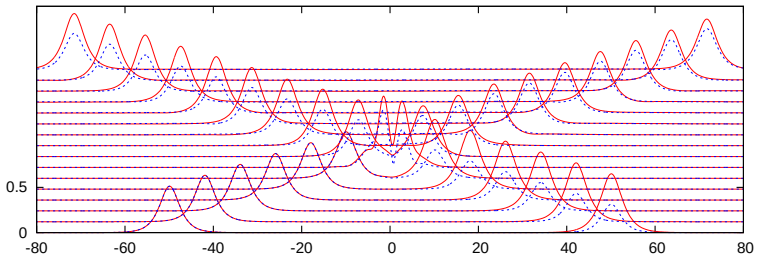

Figure 3: Collision dynamics of quasi-particles or $c_l = -c_r = 1$, α_1=0.75, $\alpha_2 = 0.2$. Left: circular polarization $n_{l\psi} = n_{l\phi} = -0.5$,. Right: elliptic polarization $n_{r\psi} = -0.55$, $n_{r\phi} = -0.46$.

References

[1] C. I. Christov, S. Dost, and G. A. Maugin, *Inelasticity of soliton collisions in system of coupled NLS equations*, Physica Scripta, **50** (1994), 449–454.

[2] V. V. Ermakov and N. N. Kalitkin, *The optimal step and regularization for Newton's method*, Soviet Comp. Phys. and Math. Phys., **21**(2) (1981), 235.

[3] S. V. Manakov, *On the theory of two-dimensional stationary self-focusing of electromagnetic waves*, Soviet Physics JETP, **38** (1974), 248–253.

[4] W. J. Sonnier and C. I. Christov, *Strong coupling of Schr´odinger equations: Conservative scheme approach*, Journal of Mathematics and Computers in Simulation, **69** (2005), 514–525.

[5] C. Sophocleous and D. P. Parker, *Pulse collision and polarization convection for optical fibres*, Optics Commun., **112** (1994), 214–224.

[6] M. D. Todorov and C. I. Christov, *Conservative scheme in complex arithmetic for CNLSE,* in B. Belinskiy et al (Eds) "Dynamical Systems, Differential Equations and Applications," AIMS (2007), 982–992.

[7] M. D. Todorov and C. I. Christov, *Collision dynamics of circularly polarized solitons in nonintegrable coupled nonlinear Schrodinger system*, Supplementary volume of "Discrete and Continuous Dynamical Systems," AIMS (2009), submitted.

[8] V. E. Zakharov and A. B. Shabat, *Exact theory of two-dimensional self-focusing and one-dimensional self-modulation of waves in nonlinear media,* Soviet Physics JETP, **34** (1972), 62–9.

Scalability Tests of Two Parallel PCG Solvers on Blue Gene/P

Yavor Vutov

In this work we study the performance of two PCG solvers on IBM Blue Gene/P massively parallel computer.
Our test problem is μFE (micro finite element) elasticity simulation of human bones. A voxel representation of the bone structure based on micro computer tomography (CT) images is used to formulate the problem. The computational domain is a strongly heterogeneous composition of solid and fluid phases. The structure of the bone is shown on Fig. 1. The solid phase has darker color.
Non-conforming Rannacher-Turek [1] FEs were used for discretization of the problem. The obtained linear system is large, with a sparse, symmetric and positive definite matrix. This implies the use of iterative solvers based on the preconditioned conjugate gradient (PCG) method [2]. The elasticity stiffness matrix has a coupled block structure corresponding to a separable displacement ordering of the unknowns. Here, the performance of the following two basic preconditioning codes, incorporated in a displacement decomposition framework, is studied. The first one is the modified incomplete factorization, MIC(0), and the second is the algebraic multigrid, AMG. The MIC(0) code is developed in IPP-BAS, Sofia, while the AMG one is the BoomerAMG module of the software system Hypre developed at LLNL, Livermore.

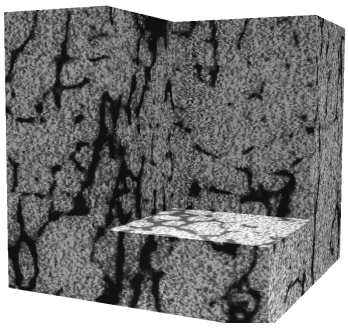

Figure 1: Structure of a human bone

The MIC(0) preconditioner is constructed in two steps. First, displacement decomposition [3] of the stiffness matrix is used. Then MIC(0) factorization is applied to a proper auxiliary M-matrix to get an approximate factorization of the obtained block-diagonal matrix. The auxiliary matrix has a special block structure - its diagonal blocks are diagonal matrices. This allows the solution of the preconditioning system to be performed efficiently in parallel. For more information see [7, 8]
BoomerAMG contains sequential and parallel implementations of algebraic multigrid methods [4]. It can be used as a solver or as a preconditioner. Various different parallel coarsening techniques and relaxation schemes are available. See [5, 6] for a detailed description of the coarsening algorithms, the interpolation and numerical results.
Version 2.4.0 of the Hypre library was used for the performed tests.
The following coarsening techniques are available:

- the Cleary-Luby-Jones-Plassman (CLJP) coarsening;

- various variants of the classical Ruge-Stüben (RS) coarsening algorithm;
- the Falgout coarsening which is a combination of CLJP and the classical RS coarsening algorithm;
- PMIS coarsening - a parallel coarsening algorithm using independent sets, generating lower complexities than CLJP;
- HMIS-coarsening - uses one pass Ruge-Stueben on each processor independently, followed by PMIS using the interior C-points generated as its first independent set;

The following relaxation techniques are available:

- Jacobi relaxation,
- hybrid Gauss-Seidel / Jacobi relaxation scheme,
- symmetric hybrid Gauss-Seidel / Jacobi relaxation scheme, and
- Gauss-Seidel relaxation.

The PMIS coarsening was used in the presented tests. In order to reduce grid and operator complexities (which reduces the RAM consumption) we used an aggressive coarsening at the first two levels. A V(1,1)-cycle with hybrid symmetric Gauss-Seidel smoothing was performed. The related AMG strength threshold is 0.5. Inner PCG iterations with BoomerAMG were used to approximate the DD block-diagonal matrix. The number of inner iterations was fixed to 4.
The compute nodes of Blue Gene/P contain four PowerPC 450 processors with 2 GB of shared RAM and runs a lightweight kernel to execute user-mode applications only. Each compute node has six connections to the torus network at 3.4 Gbps per link, three connections to the global collective network at 6.8 Gbps per link, four connections to the global interrupt network and one connection to the control network (JTAG). The input/output operations from the compute nodes are forwarded to special IO nodes. They run an embedded Linux kernel with minimal packages required to support a Network File System (NFS) client and Ethernet network connections. To achieve a high level of integration and quantity of micro-processors with low power consumption, the system was developed based on a processor with moderate frequency. The system uses system-on-a-chip (SoC) technology to allow a high level of integration, low power, and low design cost. The chip constitutes the Compute Node. The next building blocks are the compute and I/O cards. A single Compute Node attached to a processor card with the memory (RAM) creates the compute and I/O cards. The compute cards and I/O cards are plugged into a node card. There can be up to two I/O cards per node card. A midplane consists of 16 node cards stacked in a rack. A rack holds two midplanes, for a total of 32 node cards. The midplane (512 compute nodes) is the smallest entity for which the torus network topology is available. Only mesh topology is available utilizing less then 512 compute nodes At

our disposal was a Blue Gene/P system at the Bulgarian Supercomputing Center, which consists of two racks 2048 compute nodes or total of 8192 processors.
The compute nodes of a Blue Gene/P system can be utilized in three modes:

- SMP mode - One MPI process per compute node and up to 4 threads (OpenMP or pthread) per MPI process
- DUAL mode - Two MPI processes per compute node and up to 2 threads (OpenMP or pthread) per MPI process
- VN mode - Four MPI processes per compute node - no additional threads allowed.

We used SMP mode for our experiments with OpenMP employed for the parallelism within the compute node. The Hypre library was compiled with OpenMP enabled, and linked to a parallel (SMP) version of the Engineering and Scientific Subroutine Library (ESSL), which provides routines from both BLAS and LAPACK.

Table 1: Parallel Tests

			MIC(0)		AMG	
n	N	p	$T[s]$	n_{it}	$T[s]$	n_{it}
32	2 396 160	8	201	336	271	31
64	19 021 824	64	473	630	312	30
128	151 584 768	512	1 164	894	345	26
64	19 021 824	16	1 485	633	1 045	28
128	151 584 768	128	2 605	893	1 081	26
256	1 210 318 848	1024	4 618	945		

In Table 1 are shown the results from parallel experiments. The complete description of the settings of the tests can be found in [8]. The stopping criterion in all considered tests was $(C^{-1}r^{N_{it}}, r^{N_{it}})/(C^{-1}r^0, r^0) < 10^{-6}$, where r^i is the current residual and C stands for the used preconditioner. In the table, n stands for the number of voxels in each spatial dimension, p for the number of used processors, N is the number of unknowns of the linear system of equations, T is the solution time in seconds and n_{it} - the number of iterations (outer ones in the case of AMG). The tests were performed with the following scheme: Starting with a relatively small problem and given number of processors with each further test the problem sized is increased and the computational resources are increased proportionally to the problem size. Two sets of experiments were performed in this way. The first one starts with a problem of $32 \times 32 \times 32$ voxels on 8 processors, and the other – of $64 \times 64 \times 64$ voxels on 16 processors. The run of the largest problem (n=256) with BoomerAMG preconditioner could not be performed due to insufficient RAM.
What we see is that the number of MIC(0) iterations increases with the problem size, representing the heterogeneous bone structures. Let us remind that for homogeneous

materials $n_{it} = O(\sqrt{n})$. The AMG preconditioner manages to sustain the number of iterations for different problem sizes. The time for the MIC(0) increases with the problem size, while the AMG preconditioner is almost scalable. Some advantage of MIC(0) is the smaller memory requirements. This allows solving the largest problem with 1 210 318 848 degrees of freedom.

Acknowledgements. This work is partly supported by the Bulgarian NSF Grant DO02-115/2008.

References

[1] R. Rannacher, S. Turek: *Simple nonconforming quadrilateral Stokes Element*, Numer. Methods Partial Differential Equations 8(2), 1992, 97-112.

[2] O. Axelsson: *Iterative Solution Methods*. Cambridge University Press, Cambridge, 1994.

[3] R. Blaheta: *Displacement Decomposition - incomplete factorization preconditioning techniques for linear elasticity problems*, Numer. Lin. Alg. Appl., **1** (1994), 107–126

[4] J. W. Ruge and K. Stüben. *Algebraic multigrid (AMG).* In S. F. McCormick, editor, Multigrid Methods, volume 3 of Frontiers in Applied Mathematics, SIAM, Philadelphia, PA, 1987, 73-130.

[5] V. E. Henson and U. M. Yang. *BoomerAMG: a parallel algebraic multigrid solver and preconditioner.* Applied Numerical Mathematics, 41(5), 2002,155-177. Also available as LLNL technical report UCRL-JC-141495.

[6] U. M. Yang. *Parallel algebraic multigrid methods - high performance preconditioners.* In A. M. Bruaset and A. Tveito, editors, Numerical Solution of Partial Differential Equations on Parallel Computers, Springer-Verlag, 2005, 209-236. Also available as LLNL technical report UCRL-BOOK-208032.

[7] P. Arbenz, S. Margenov, Y. Vutov: *Parallel MIC(0) Preconditioning of 3D Elliptic Problems Discretized by Rannacher-Turek Finite Elements*, Comput. Math. Appl. (to appear)

[8] S. Margenov, Y. Vutov: *Preconditioning of Voxel FEM Elliptic Systems*, TASK, Quaterly 11, No 1-2, 2007, 117-128.

Part C

List of participants